Title
Two Approaches to Accelerated Monte Carlo Simulation of Coulomb Collisions

Author
Ricketson, Lee

Publication Date
2014

Peer reviewed|Thesis/dissertation

University of California
Los Angeles

Two Approaches to Accelerated Monte Carlo Simulation of Coulomb Collisions

A dissertation submitted in partial satisfaction
of the requirements for the degree
Doctor of Philosophy in Mathematics

by

Lee Forrest Ricketson

2014

Abstract of the Dissertation

Two Approaches to Accelerated Monte Carlo Simulation of Coulomb Collisions

by

Lee Forrest Ricketson

Doctor of Philosophy in Mathematics

University of California, Los Angeles, 2014

Professor Russel E. Caflisch, Chair

In plasma physics, the direct simulation of inter-particle Coulomb collisions is often necessary to capture the relevant physics, but presents a computational bottleneck because of the complexity of the process. In this thesis, we derive, test and discuss two methods for accelerating the simulation of collisions in plasmas in certain scenarios.

The first is a hybrid fluid-Monte Carlo scheme that reduces the number of collisions that must be simulated. Coupling between the fluid and particle components of the scheme is accomplished by assigning to each particle a passive scalar approximating the *relative entropy* between its distribution of velocities and the fluid distribution. When this quantity is sufficiently small, the particle is moved into the fluid so its associated collisions need not be simulated.

The second method is an adaptation of the multilevel Monte Carlo method. Instead of a single time step, this method introduces a hierarchy of time steps - i.e. levels - and uses the interplay between adjacent levels for variance reduction. We present new applications to plasmas, a method for eliminating the cost of the coarsest level calculation, and an alternative method for achieving the optimal overall computational complexity.

Throughout, we discuss applications beyond plasma physics, including rarefied gases and chemical reaction networks.

The dissertation of Lee Forrest Ricketson is approved.

George Morales

Marcus Roper

Christopher Anderson

Russel E. Caflisch, Committee Chair

University of California, Los Angeles

2014

To my parents, as well as J.N. Davidson ...

each of whom believed in me

when I didn't believe in myself.

Table of Contents

1 Introduction **1**

1.1 Context and Motivation 1

1.2 Introductory Kinetic Theory 4

1.2.1 Thermodynamic Equilibrium and Maxwellian Distributions 8

1.2.2 Boltzmann's H-theorem 11

1.2.3 Moment Equations and Fluid Mechanics 12

1.2.4 Collisional Closure 14

1.3 Kinetic Theory of Plamsas 17

1.3.1 Debye Shielding 18

1.3.2 Plasma Parameter and Weak Coupling 20

1.3.3 The Landau-Fokker-Planck Collision Operator 22

1.4 Numerical Methods for LFP Equation 25

1.4.1 Survey of existing methods 25

1.4.2 Monte Carlo and Particle in Cell 26

1.4.3 Binary Collision Algorithms 28

1.4.4 Langevin/SDE-Based Algorithms 30

1.5 Summary 32

2 Hybrid Fluid-Monte Carlo Scheme **34**

2.1 Introduction 34

2.2 Hybrid Fluid-Monte Carlo Schemes 36

2.2.1 Velocity-based Schemes 38

2.2.2 Scattering Angle-based Schemes . . . 39
2.3 Paradigm and Theoretical Background . . . 40
2.3.1 Relative Entropy . . . 42
2.3.2 Idea for Thermalization Scheme . . . 43
2.4 Approximating Relative Entropy . . . 43
2.4.1 Toward a uniformly valid approximation of relative entropy . . . 45
2.4.2 Monte Carlo Implementation . . . 46
2.5 Algorithm Summary and Error Scalings . . . 47
2.5.1 Choice of $\mathcal{H}_c$ . . . 49
2.5.2 Error Analysis . . . 50
2.5.3 Dethermalization Error . . . 52
2.6 Numerical Results . . . 53
2.6.1 Testing Relative Entropy Approximations . . . 53
2.6.2 Full Numerical Tests . . . 55
2.7 Discussion and Conclusions . . . 61

3 Multi-Level Monte Carlo - Improvements . . . 66
3.1 Introduction . . . 66
3.2 Background . . . 69
3.2.1 MLMC Review . . . 70
3.2.2 Milstein and Lévy Areas . . . 72
3.3 Variance Reduction via Ito's Lemma . . . 74
3.4 Approximate Milstein for MLMC . . . 77
3.4.1 Review of Antithetic Method . . . 78
3.4.2 Approximate Milstein for $M = 2$ . . . 79

3.4.3 Generalization to $M > 2$ . . . 84
3.5 Generalization of Antithetic Method to $M > 2$ . . . 86
3.6 Summary and Implementation . . . 88
3.7 Numerical Results . . . 90
3.7.1 Generalized antithetic test . . . 91
3.7.2 Ito linearization and approximate Milstein test . . . 92
3.7.3 Discussion . . . 94
3.8 Conclusions . . . 95

4 Conclusions and Future Work . . . 96
4.1 Hybrid Fluid-Monte Carlo Scheme . . . 97
4.2 Multilevel Monte Carlo . . . 98
4.3 Concluding Remarks . . . 99

A Proof of Relative Entropy Theorem . . . 100

B Results on Collisional Moments . . . 103
B.1 Approximating $\mathbf{u}_j$ . . . 103
B.2 Approximating T . . . 104

C Numerical Integration of Collisional Moments . . . 107
C.1 Simplifying W' . . . 107
C.2 Simplifying $\mathbf{F}$ . . . 108

D Proof of Lemma 3.1 . . . 110

E Proof of Theorem 3.2 . . . 112

F Proof of Lemma 3.4 . . . . . **114**

References **117**

List of Figures

2.1 Comparison of scaled temperature (T), mean velocity (u), and relative entropy (H) of the distribution of a test particle in a Maxwellian background computed by three different methods: direct Monte Carlo collision simulation (solid blue), evolution via numerical integration of $\mathbf{F}$ and W (dash-dot black), and evolution according to the asymptotic expressions (2.31) and (2.32) (dashed red). The left-most column has $v_0 = 0$, the middle $v_0 = v_{tM}$, and the right-most $v_0 = 2v_{tM}$ 55

2.2 The temperature anisotropy in a two temperature Maxwellian as a function of time. Computation compares the linearized analytic result (solid black), pure Monte Carlo using Takizuka-Abe (dash-dot red), and the hybrid scheme proposed herein (dashed blue). 57

2.3 Six time snapshots of the velocity distribution in the x dimension for the bump-on-tail problem. Monte Carlo solution: solid red; hybrid solution: black "x". 58

2.4 A comparison of accuracy Γ_{acc} and efficiency $\mathcal{S}$, $\mathcal{S}_H$ for four different realizations of a hybrid scheme: the entropy-based and scattering angle-based schemes, each with and without dethermalization. The entropy scheme is plotted against both $\mathcal{S}$ (green '+') and $\mathcal{S}_H$ (blue and magenta dots). The scattering angle scheme is plotted both with thermalization (dashed black) and without (solid red). Comparing the green '+' curve to the solid red and dashed black compares the entropy and scattering angle schemes when the number of simulated particles is equal. Comparing the dotted blue to the solid red compares the two schemes when the total computational load is equal and when there is no dethermalization. Comparing the dotted magenta to the dashed black compares the two schemes for equal computational load when thermalization is present. A sixth possible curve - Entropy scheme without dethermalization vs. $\mathcal{S}$ - is not plotted, because it falls directly on top of the green '+' curve. 64

2.5 A comparison of the errors incurred by pure Monte Carlo and hybrid schemes. 65

2.6 The systematic L^1 dethermalization error as a function of time for three different initial conditions. 65

3.1 The fraction of the computational work exerted at each level in a sample MLMC computation. The Heston model - see (3.84) and proceeding text for specification - is solved with a sinusoidal payoff function, and $M = 2$. 75

3.2 Left: A plot of $V_l/\Delta t$ against Δt for the Euler, standard antithetic, and generalized antithetic methods. As expected, the Euler curve is constant, while both antithetic methods demonstrate the same scaling. Right: A comparison of the computational cost of the Euler method to the antithetic method for various refinement factors M as a function of the error tolerance ε. As expected, an M of 4 or 5 is optimal. 92

3.3 Computational cost of MLMC variants with sinusoidal payoff as a function of error tolerance. Euler (red), antithetic (blue), and approximate Milstein (black) discretizations are shown, each with Ito linearization (solid) and without (dashed). All results in this plot use $M = 4$. 93

Acknowledgments

I will begin by acknowledging those who have had a direct impact on the research presented in this thesis. First, I thank my thesis advisor, Professor Russel Caflisch. His insights are pervasive in all of the work presented here, and his passion for discovery is infectious. Moreover, while many students leave their graduate work embittered and jaded, I leave inspired and eager, a state of affairs which is due almost entirely to Professor Caflisch's guidance. He has given me great freedom to pursue my interests rather than any agenda of his own. I could not imagine a better advisor. I also wish to thank the members of my thesis committee: Chris Anderson, Marcus Roper, and George Morales.

Mark Rosin's impact on this thesis is second only to Professor Caflisch's. Throughout the last four years, Mark has been an invaluable mentor to me, both scientifically and professionally. I also wish to acknowledge the contributions and mentoring of collaborators at Lawrence Livermore National Laboratory, Bruce Cohen and Andris Dimits. Further scientific insight was provided by Antoine Cerfon of the Courant Institute at New York University and David Levermore of the University of Maryland. I have also been taught courses at UCLA by Christopher Anderson, Andrea Bertozzi, Joseph Teran and Marcus Roper that have been valuable in the development of this thesis.

On a personal level, I of course thank my mother, Mary Ricketson, and father, Emory Ricketson. Without the constant love, encouragement, and support of either, this thesis would have been inconceivable. Many children spend a lifetime seeking their parents' approval, and I am eternally grateful that my parents have always granted theirs willingly, eagerly, and vociferously.

There are many teachers from my secondary and undergraduate education to whom I am forever indebted for inspiring in me an interest in learning, often in environments in which such a thing was not widely promoted. In particular, it is important that I acknowledge Lisa Skomp of Murphy Elementary School, Julie Curtis of Murphy Middle School, Ms. Snow, Caesar Campana, David Wilson, and Lonnie Oliver of Murphy High School, and Jonathan

Bennett, John Kolena, Peggy Craft, Daniel Teague, and Elizabeth Moose of the North Carolina School of Science and Mathematics. Particular thanks is due to Dr. Bennett, whose guidance taught me a great deal about how to be a scientist, and Dr. Kolena, from whom I learned much more than I could possibly summarize here. I am also indebted to a number of professors, lecturers, and research mentors from my time at MIT. These include Sunghwan Jung, John Bush, Pedro Reis, Ruben Rosales, and Alar Toomre.

I have also been the beneficiary of a tremendous number of friendships throughout my life. It would be impossible to acknowledge them all, but I would be particularly remiss in failing to mention Walker Owen, who has been a dear and caring friend ever since I could read, and the entire Bryce family, who for several years treated me as one of their own. I must also mention John Neil Davidson, to whose memory this thesis is partially dedicated. I think of him often.

Last, but most certainly not least, I thank Kate Leary. While her presence in my life is a more recent occurrence than the others listed here, it is one I no longer feel I can live without. Thanks for everything.

Vita

1986	Born, Murphy, North Carolina, USA.
2007–2009	Research Assistant, Mathematics Department, Massachusetts Institute of Technology, Cambridge, Massachusetts.
2009	B.S. (Mathematics), Massachusetts Institute of Technology, Cambridge, Massachusetts.
2009–2011	Teaching Assistant, Mathematics Department, UCLA. Taught sections of Mathematics 32A/B (Multivariable Calculus), 134 (Systems of Differential Equations), 142 (Mathematical Modeling), and 146 (Methods of Applied Mathematics).
2011	M.A. (Mathematics), UCLA, Los Angeles, California.
2011–present	Research Assistant, Mathematics Department, UCLA.

Publications

M.S. Rosin, L.F. Ricketson, R.E. Caflisch, A.M. Dimits, B.I. Cohen, Multilevel Monte Carlo simulation of Coulomb collisions, *submitted to Journal of Computational Physics*

L.F. Ricketson, Three improvements to multi-level Monte Carlo simulation of SDE systems, *submitted to SIAM MM&S*

L.F. Ricketson, M.S. Rosin, R.E. Caflisch, A.M. Dimits, An entropy based thermalization

scheme for hybrid simulations of Coulomb collisions, *in revision of Journal of Computational Physics*

A.M. Dimits, B.I. Cohen, R.E. Caflisch, M.S. Rosin, L.F. Ricketson, Higher order time integration of Coulomb collisions in a plasma using Langevin equations, *Journal of Computational Physics*

CHAPTER 1

Introduction

1.1 Context and Motivation

The field of statistical physics is born out of the realization that a full microscopic description of any system of many particles is intractable, both analytically and numerically. The goal thus becomes the characterization of the relevant macroscopic properties of the system - density, flow velocity, temperature, viscosity, etc. - while retaining as little information about the states of the individual particles as possible. This may be accomplished in many ways, prominent among which is asymptotic expansion in terms of mean free path.

When the mean free path is much smaller than other length scales of interest, local thermodynamic equilibrium may be assumed. This assumption gives rise to the Euler and Navier-Stokes equations of classical fluid dynamics [CC70], and to analogous equations in the case of plasmas [Bra65, Fre07, HW04]. In the opposite case, when the mean free path is long, collisions between individual particles may be neglected, and the system evolves through only the action of the comparatively smooth mean fields and body forces. This regime primarily appears in plasmas [Vla68].

In the intermediate regime, inter-particle collisions play a direct and important role in the system's dynamics, and there can be no avoiding accounting for them in some way. Because exact specification of particle positions and velocities is impossible, collisions are an essentially random process in the statistical physics framework. Moreover, collisional processes are functions of both particle position and velocity, so the problem is high dimensional. The combination of these two factors has led many to utilize Monte Carlo methods in the

direct simulation of particle systems, for they are well suited to deal with both randomness and high dimensionality. Standard Monte Carlo methods exist for both neutral fluids [Bir76] and plasmas [TA77, Nan97]. Such methods have been applied to the simulation of a wide variety of systems in both neutral fluids [LWW07, NHH98, SF03, WL04] and plasmas [BBD02, JNS06, KPV04, SMK00].

Though successful in these contexts, the Monte Carlo simulation of collisions is a computationally intensive process. At present, quantitatively accurate, fully three-dimensional simulations require massively parallel supercomputers [CW03, CRG96, FVF13, IKV11]. This is due to the slow convergence of Monte Carlo methods, which itself is a direct result of the central limit theorem. That is, for a number of simulated particles N, there is an error due to random sampling which scales as $N^{-1/2}$.

This slow convergence is fundamental to Monte Carlo methods. The tradeoff is that the computational requirements of Monte Carlo schemes scale very favorably with the dimension of the problem, making them attractive for collision simulation in spite of their drawbacks. Any circumvention of the drawbacks inherent in Monte Carlo methods would make the continuation and expansion of their application to collision simulation even more attractive, and possibly make feasible simulations which are currently beyond our computational reach. There is thus great interest in accelerated Monte Carlo collision methods in the context of many particle systems. In that vein, we pose several questions, each of which is addressed in this thesis:

- Because the simulation of fluid systems is relatively cheap, can we combine a fluid description with a Monte Carlo collision algorithm to obtain a scheme with the speed of a fluid simulation but with the ability to capture non-equilibrium behavior of a Monte Carlo method?
- Can we give a mathematical characterization of the errors present in such a scheme?
- In Monte Carlo schemes applied to time dependent systems, there is typically a time stepping error as well as the random sampling error. Can the interplay between these

two sources of error be leveraged to improve the performance of the scheme in the plasma context?

The research presented here provides an affirmative answer to each of these questions in the context of spatially homogeneous plasmas. In chapter 2, we present a hybrid fluid-Monte Carlo scheme along the lines of [CWD08, DCC10]. In contrast to these and other prior efforts, we are able to understand the various sources of error in our scheme and their respective scalings. The key to this analysis is the use of *relative entropy* as a passive scalar that measures each particle's proximity to thermal equilibrium. In the process of presenting these results, we will also discuss potential applications to rarefied gases.

In chapter 3, we discuss the application of the Multilevel Monte Carlo (MLMC) method to plasmas, the key to which is the interplay between time-stepping and sampling errors, as in the final question above. Aside from adapting this existing method to a new application, we present improvements to the method in general. These improvements have the effect of further accelerating computations in a wide array of applications.

In this introductory chapter, we establish the background necessary to understand the results in subsequent chapters. We begin in section 1.2 by introducing kinetic theory, initially developed by Maxwell and Boltzmann. This is the mathematical theory of non-equilibrium, many-particle systems, and is useful in the context of both neutral fluids and plasmas. A foundational result - both of the theory in general and for the work in chapter 2 of this thesis - is Boltzmann's H-theorem. This theorem is proved and its importance discussed. We also cover the relationship between kinetic theory and fluid dynamics. In particular, we derive the Euler equations of fluid mechanics from kinetic theory in the asymptotic limit of high collisionality.

We then proceed, in 1.3, to the particularities of the treatment of plasmas in the kinetic theory framework. We will see that a special treatment of collisions is necessary, due to the long range nature of the Coulomb force. This treatment will lead us to the Landau-Fokker-Planck equation, the standard kinetic model of collisional plasma behavior.

In 1.4, we discuss standard numerical methods for the Landau-Fokker-Planck equation. After a brief survey, we focus on the so called Particle in Cell (PIC) methods. These have as a component some Monte Carlo method for Coulomb collisions. The collision methods fall into two categories - binary collisions and Langevin-based methods. Improvements to each of these methods are the subjects of chapters 2 and 3, respectively.

We conclude the chapter in 1.5 with a summary and a discussion of the background material's relationship to the results in subsquent chapters.

1.2 Introductory Kinetic Theory

For our purposes, the object of study in kinetic theory is a system of N identical particles, the states of which are specified by their positions $\mathbf{x}_j$ and velocities $\mathbf{v}_j$ for $j = 1, 2, ...N$. For N comparable to Avogadro's number - as is the case when discussing gases and plasmas - the full specification of the state of the system is clearly intractable. Kinetic theory's approach to this problem is to introduce the phase-space density $f(\mathbf{x}, \mathbf{v}, t)$. Let us denote by $N_{U\cap V}$ the number of particles with $\mathbf{x} \in U$ and $\mathbf{v} \in V$. Then f is defined by the following relation:

$$N_{U\cap V}(t) = \int_V \int_U f(\mathbf{x}, \mathbf{v}, t)\, d\mathbf{x}\, d\mathbf{v} \tag{1.1}$$

for every U and V.

Under reasonable assumptions, f may be shown to satisfy a partial differential equation (PDE) of the form

$$f_t + \mathbf{v} \cdot \nabla_x f + \mathbf{a} \cdot \nabla_v f = \mathcal{C}(f, f), \tag{1.2}$$

where ∇_x and ∇_v denote the gradients in position and velocity space respectively, $\mathbf{a}$ is the macroscopic force on the system, and $\mathcal{C}(f, f)$ is a bilinear operator describing inter-particle collisions. $\mathcal{C}$ is often called the *collision operator*.

Two forms of the collision operator are relevant to the work presented in this thesis. The first is named for Boltzmann and is discussed presently. The second is the Fokker-Planck form, which is relevant to plasmas. This is discussed in section 1.3.

The expression for the Boltzmann collision operator is rather cumbersome, so we begin by introducing some notation and briefly discussing inter-particle collisions in general. Suppose two particles approach each other with velocities $\mathbf{v}$ and $\mathbf{v}_*$, and define their relative velocity $\mathbf{w} = \mathbf{v} - \mathbf{v}_*$. After they collide, the particles have respective velocities

$$\mathbf{v}' = \mathbf{v} + \mathbf{n}(\mathbf{n} \cdot \mathbf{w}), \qquad \mathbf{v}'_* = \mathbf{v}_* - \mathbf{n}(\mathbf{n} \cdot \mathbf{w}), \tag{1.3}$$

where $\mathbf{n}$ is an arbitrary unit vector. The post-collision velocities are just defined so as to conserve momentum ($\mathbf{v} + \mathbf{v}_* = \mathbf{v}' + \mathbf{v}'_*$) and energy ($v^2 + v_*^2 = v'^2 + v'^2_*$). Here and in the rest of this thesis, for any vector quantity $\mathbf{u}$, we let $u = |\mathbf{u}|$. Additionally, for any subscript or superscript on $\mathbf{v}$, we denote f evaluated at that velocity by using the same superscript or subscript. For example, $f'_* = f(\mathbf{x}, \mathbf{v}'_*, t)$. With this notation in hand, we may define the Boltzmann collision operator as

$$\mathcal{C}_B(f, f) = \int_{\mathbb{R}^3} \int_{S^2} B\left(\mathbf{w}, \frac{\mathbf{n} \cdot \mathbf{w}}{w}\right) (f' f'_* - f f_*) \, d\mathbf{n} \, d\mathbf{v}_*, \tag{1.4}$$

where $B(\mathbf{w}, \cos\theta)$ is the rate at which particles are scattered through angle θ and S^2 is the set of all unit vectors in $\mathbb{R}^3$.

At an intuitive level, (1.4) is relatively simple to understand. The number of pairs of particles at position $\mathbf{x}$ with respective velocities $\mathbf{v}$ and $\mathbf{v}_*$ is $f f_*$, so the total rate at which these particle pairs are scattered through angle θ is $B(\mathbf{w}, \cos\theta) f f_*$. The integral of this quantity over all possible collision partners (i.e. velocities $\mathbf{v}_*$) and scattering angles (i.e. $\mathbf{n}$) gives the total rate at which particles are scattered *out* of the velocity state $\mathbf{v}$. Since particles are leaving the velocity $\mathbf{v}$, this represents a negative contribution to the collision operator. Similarly, the quantity $B(\mathbf{w}, \cos\theta) f' f'_*$ is the rate at which particles are scattered *into* $\mathbf{v}$.

There are a number of assumptions which this intuitive argument glosses over. A full derivation begins with Liouville's theorem for the N-particle phase space density (which has $6N$ space/velocity arguments, for the position and velocity of each individual particle) and proceeds by integrating out successive arguments. This leads to what is known as the BBGKY hierarchy [BG46a, BG46b, Kir46, Yvo35] - a sequence of equations for the n-particle

phase space distributions ($n = 1, 2, ..., N-1$), each of which depends on the $(n+1)$-particle distribution. The Boltzmann equation is arrived at by truncating this hierarchy at the first term. While a full reprinting of this derivation is beyond the scope of this thesis - the interested reader may see any of the original papers cited above - it is important to understand the assumptions that go into deriving (1.4). Some of the more important assumptions and descriptions of their roles in the derivation are listed below.

- Pairwise collisions are time-reversible - a direct consequence of Newtonian mechanics. This allows us to think of $\mathbf{v}'$ and $\mathbf{v}'_*$ as either post-collisional or pre-collisional velocities at our whim. In particular, they were defined as post-collisional, but are treated as pre-collisional in (1.4).

- The sphere of influence of a given particle is much smaller than the typical distance between particles. This allows us to neglect events in which more than two particles collide simultaneously, for such events are rare when a small fraction of space is occupied by particles. This is the reason (1.4) involves products of f evaluated at two different velocities, but not at three or more.

- The length scales of interest are considerably larger than the distance between two colliding particles. This allows us to assume that two colliding particles are essentially at the same position $\mathbf{x}$, so that f is evaluated at multiple velocities but only at a single position.

- To good approximation, the incoming velocities of two colliding particles are independent. This is commonly referred to as the *molecular chaos assumption*. It bears some elaboration, since immediately after a collision the outgoing velocities of the colliding particles are certainly correlated. The assumption is that before those two particles interact again, they will undergo a large number of collisions with other particles that randomize their respective velocities to the point of being essentially independent. This assumption is what allows us to write the distribution of velocity pairs (i.e. the two-particle distribution in the BBGKY hierarchy) as the product of the distribution of

individual velocities (i.e. the single-particle distribution f), which truncates the hierarchy and gives rise to the products ff_* and $f'f'_*$ in (1.4). The assumption of molecular chaos is both particularly fundamental and particularly controversial.

There is also the question of the functional form of $B(\mathbf{w}, \theta)$. It is given by

$$B(\mathbf{w}, \cos\theta) = w\frac{d\sigma}{d\Omega}(w, \theta), \tag{1.5}$$

where $d\Omega = \sin\theta d\theta d\phi$ is the solid angle element, and $d\sigma/d\Omega$ is the differential cross section associated with the inter-particle force law. The differential cross section may be derived directly from the force law, but closed forms do not exist in all cases. Three particularly important cross sections are:

- Coulomb/Rutherford: For the Coulomb force - the force between charged particles, which scales as the inverse-square of their separation - the differential cross section is given by

$$\frac{d\sigma}{d\Omega}(w, \theta) = \left[\frac{Z_1 Z_2 e^2}{8\pi\epsilon_0 \mu w^2}\right]^2 \frac{1}{\sin^4\theta/2}, \tag{1.6}$$

  where e is the elementary charge unit (the magnitude of the electron charge), Z_1 and Z_2 are the charge-numbers of the respective particles, $\mu = m_1 m_2/(m_1 + m_2)$ is the reduced mass of the particle pair, and ϵ_0 is the permittivity of free space. This is the relevant cross section in plasma simulation.

- Hard Spheres: For hard (impenetrable) spheres of radius R which exert no force on each other when not in contact, the differential cross section is given by

$$\frac{d\sigma}{d\Omega}(w, \theta) = \frac{R^2}{4}. \tag{1.7}$$

  This cross section and some of its generalizations are popular in Monte Carlo simulations of neutral fluids [Bir76].

- Maxwell Molecules: For a central force that decays as one over the sixth power of the particle separation, the differential cross section has the general form

$$\frac{d\sigma}{d\Omega}(w, \theta) = \frac{1}{w} f(\theta). \tag{1.8}$$

Particles interacting through this force law and thus having this differential cross section are often called *Maxwell molecules*. They are particularly important because they give a collision rate $B(w, \theta)$ that is independent of w. This property is useful in analysis of the Boltzmann equation, so many analytic results are restricted to this case. It is also useful in deriving binary collision algorithms for plasma simulation, as we shall see in section 1.4.

Later in this introduction, we will also discuss the *total cross section* σ, which is defined by

$$\sigma = \int_{S^2} \frac{d\sigma}{d\Omega}\, d\Omega = 2\pi \int_0^\pi \frac{d\sigma}{d\Omega} \sin\theta\, d\theta. \tag{1.9}$$

Note that $w\sigma$ is the rate at which a pair of particles is scattered through *any* angle.

For any cross section, the kinetic equation

$$f_t + \mathbf{v} \cdot \nabla_x f = \mathcal{C}_B(f, f) \tag{1.10}$$

is called the Boltzmann equation. It is an excellent model of many-particle interacting systems. The remainder of this section is devoted to a discussion of its most important properties and its connection to the Euler and Navier-Stokes equations. More detailed discussions of this material may be found in [Cer69, CC91], among others.

1.2.1 Thermodynamic Equilibrium and Maxwellian Distributions

Equilibrium, or steady-state, is just the statement that the distribution function is constant in time:

$$\frac{\partial f}{\partial t} = 0. \tag{1.11}$$

If we assume no variation in space, then the Boltzmann equation at steady state reduces to

$$\mathcal{C}_B(f, f) = 0. \tag{1.12}$$

To find the solutions of this equation, it is helpful to consider the weak form of $\mathcal{C}_B$ -

$$C_W[\varphi] = \int_{\mathbb{R}^3} \mathcal{C}_B(f, f)\varphi(\mathbf{v})\, d\mathbf{v}, \tag{1.13}$$

for arbitrary smooth functions $\varphi(\mathbf{v})$ - which has useful symmetry properties. Note first that the above integral is symmetric with respect to the exchange of $\mathbf{v}$ and $\mathbf{v}_*$, and antisymmetric with respect to exchange of the primed and unprimed variables. As such, we have the following identity:

$$C_W[\varphi] = \frac{1}{4}\int B\left(\mathbf{w}, \frac{\mathbf{n}\cdot\mathbf{w}}{w}\right)(f'f'_* - ff_*)(\varphi + \varphi_* - \varphi' - \varphi'_*)\, d\mathbf{n}\, d\mathbf{v}\, d\mathbf{v}_*, \tag{1.14}$$

where the limits of integration are understood. The above is zero independent of f if

$$\varphi + \varphi_* = \varphi' + \varphi'_*. \tag{1.15}$$

A function φ satisfying (1.15) is called a *collision invariant*, since (1.14) represents the rate of change in a φ's expectation due to collisions (to see this, multiply through by φ in (1.10) and integrate). Momentum and energy are two simple examples of collision invariants.

In fact, they are the only two examples, aside from constant functions. That is, $C_W[\varphi] = 0$ if and only if

$$\varphi(\mathbf{v}) = a + \mathbf{b}\cdot\mathbf{v} + cv^2, \tag{1.16}$$

with a and c scalars and $\mathbf{b}$ a vector, none of which depend on $\mathbf{v}$. In proving this claim, one direction is easy (just plug this form of φ into (1.15) and confirm that it works). The other direction - showing that there are no other collision invariants - is lengthy, so we will omit it here. It makes sense physically, however, because if there were another linearly independent invariant, that would impose another constraint on the relationship between the pre- and post-collision velocities, and we already have the right number by just considering momentum and energy.

This leads to a solution of (1.12) in the following way: we notice that if

$$f'f'_* = ff_*, \tag{1.17}$$

then the collision integral is certainly zero. Taking the logarithm of this equation, it follows that $\log f$ is a collision invariant of the form in (1.16). In fact, this is the only such f that results in $\mathcal{C}_B(f, f) = 0$, a fact that we now show.

Notice first that $\mathcal{C}_B(f,f)=0$ implies that $C_W[\phi]=0$ for every ϕ. Next, set $\phi=\log f$ in (1.14), finding

$$C_W[\log f]=\frac{1}{4}\int B\left(\mathbf{w},\frac{\mathbf{n}\cdot\mathbf{w}}{w}\right)(f'f'_*-ff_*)\log\left(\frac{ff_*}{f'f'_*}\right)\,d\mathbf{n}\,d\mathbf{v}\,d\mathbf{v_1}. \tag{1.18}$$

It is easy to see that

$$(x-y)\log\left(\frac{y}{x}\right)\leq 0 \tag{1.19}$$

with equality only achieved if $x=y$. Using $x=f'f'_*$ and $y=ff_*$, and recalling that $B\geq 0$, we see that $C_W[\log f]=0$ if and only if (1.17) is satisfied. Therefore, this is a necessary condition for $\mathcal{C}_B(f,f)=0$ to hold. Thus, a collision invariant $\log f$, i.e.

$$f(\mathbf{v})=\exp(a+\mathbf{b}\cdot\mathbf{v}+cv^2) \tag{1.20}$$

characterizes all solutions of $\mathcal{C}_B(f,f)=0$. Note that we've also shown that

$$C_W[\log f]\leq 0 \tag{1.21}$$

for any f, which will be crucial in the next subsection.

We have just shown that all solutions of (1.12) have the form (1.20). Only a subset of these solutions are physically relevant. In particular, we require $c<0$ so that each point in space contains a finite mass. We may then complete the square and rename constants to arrive at

$$f(\mathbf{v})=A\exp(-\alpha|\mathbf{v}-\mathbf{u}|^2). \tag{1.22}$$

The velocity integral of f should give the spatial mass density ρ, so we set $A=\rho(\pi/\alpha)^{-3/2}$. Using the well known fact that the mean energy in an ideal gas is $(3/2)kT$, we arrive at the *Maxwellian distribution* for particle velocity in an ideal gas moving at net velocity $\mathbf{u}$:

$$f_M(\mathbf{v})=\rho\left(\frac{m}{2\pi kT}\right)^{\frac{3}{2}}\exp\left(-\frac{m|\mathbf{v}-\mathbf{u}|^2}{2kT}\right). \tag{1.23}$$

It is important to note that $\mathcal{C}_B(f_M,f_M)=0$ even if ρ, $\mathbf{u}$, and T depend on space and time. Such a distribution function is often called a *local Maxwellian*. It does not solve the Boltzmann equation, but will be of great importance in the remainder of this thesis.

Distributions f that are local Maxwellians at every point in space are said to be in *local thermodynamic equilibrium*. A global Maxwellian has the form above with constant ρ, $\mathbf{u}$, and T, and is a solution to the Boltzmann equation. Such solutions are said to be in *global thermodynamic equilibrium*.

1.2.2 Boltzmann's H-theorem

As mentioned above, in the course of finding solutions to $\mathcal{C}_B(f, f) = 0$, we found (1.21). This is one of the key components in proving the famous Boltzmann H-theorem. For this section, let's assume that all our particles exist in some bounded region U, which may be moving with velocity $\mathbf{v_0}$. That is, f is zero outside U. Consider the quantity

$$\mathcal{H} = \int_{\mathbb{R}^3} f \log f \, d\mathbf{v}. \tag{1.24}$$

In particular, let's consider it's time derivative:

$$\frac{\partial \mathcal{H}}{\partial t} = \int_{\mathbb{R}^3} \frac{\partial f}{\partial t}(1 + \log f) \, d\mathbf{v}. \tag{1.25}$$

We may eliminate the time derivative of f using (1.10) to get

$$\frac{\partial \mathcal{H}}{\partial t} = \int_{\mathbb{R}^3} C(f, f) \log f \, d\mathbf{v} - \nabla_x \cdot \int_{\mathbb{R}^3} \mathbf{v}(f \log f) \, d\mathbf{v}, \tag{1.26}$$

where we have noted that 1 is a collision invariant, integrated by parts and applied the divergence theorem with the fact that $f \log f \to 0$ as v diverges.

The last term on the right side is the divergence of the flow of $\mathcal{H}$. We will call this flow $\mathcal{F}_{\mathcal{H}}$. We also know from (1.21) that the other term on the right side is non-positive. Let us now integrate this last equation over U in position space and find, after application of the divergence theorem,

$$\frac{dH}{dt} - \int_{\partial U} (\mathcal{F}_{\mathcal{H}} \cdot \mathbf{n} - \mathcal{H}\mathbf{v_0} \cdot \mathbf{n}) \, dS \leq 0, \tag{1.27}$$

where $\mathbf{n}$ is the inward normal to ∂U, and

$$H = \int_U \mathcal{H} \, d\mathbf{x} \tag{1.28}$$

is the volume integral of $\mathcal{H}$.

We have just shown the following:

Theorem 1.1 (Boltzmann H-theorem)**.** *If*

$$\int_{\partial U} \left(\mathcal{F}_{\mathcal{H}} \cdot \mathbf{n} - \mathcal{H}\mathbf{v_0} \cdot \mathbf{n}\right) \, dS \leq 0,$$

then H is non-increasing in time. H is constant in time if and only if equality is achieved in the above inequality and f is a Maxwellian.

The left side of the inequality in the theorem represents the flow of $\mathcal{H}$ into U, so we may rephrase the theorem to say that if there is no net flux of $\mathcal{H}$ into the system, then H may never increase. H is related to the macroscopic entropy S as follows:

$$S = -NkH, \tag{1.29}$$

where N is the total number of particles as before and k is Boltzmann's constant. Thus, the H-theorem implies that entropy is non-decreasing so long as entropy is not flowing out of the system. In this sense, the H-theorem is the mathematical formalization of the second law of thermodynamics in physics.

1.2.3 Moment Equations and Fluid Mechanics

In applications, one is often uninterested in the full distribution function f; of far greater interest are macroscopically observable quantities like density ρ, flow velocity $\mathbf{u}$, temperature T, pressure p, and so forth. Each of these quantities is defined as a *moment* of f. We denote the r^{th} moment of f by $\mathbf{M}_r$, and define it as

$$\mathbf{M}_r = \int_{\mathbb{R}^3} \mathbf{v}^r f \, d\mathbf{v}, \tag{1.30}$$

where $\mathbf{v}^r$ denotes the rank-r tensor composed of all possible r-fold products of the components of $\mathbf{v}$. $\mathbf{M}_r$ is thus also a rank-r tensor. The macroscopic quantities above are written as

$$\rho = \mathbf{M}_0, \quad \mathbf{u} = \frac{1}{\rho}\mathbf{M}_1, \quad T = \frac{1}{3}\frac{m}{\rho k}\left\{\text{tr}(\mathbf{M}_2) - \rho u^2\right\}, \quad p = \frac{\rho}{m}kT, \tag{1.31}$$

where $\mathrm{tr}(\cdot)$ denotes the trace operator.

In the course of our discussion, it will sometimes be easier to work with the moments in different coordinates. In particular, it will be useful to separate the bulk motion of the system $\mathbf{u}$ from the random fluctuations about that motion. With that in mind, we define

$$\mathbf{m}_r = \int_{\mathbb{R}^3} (\mathbf{v} - \mathbf{u})^r f \, d\mathbf{v}, \tag{1.32}$$

the moments in coordinates in which the mean velocity vanishes. Notice that $\mathbf{m}_0 = \mathbf{M}_0 = \rho$ and $\mathbf{m}_1 = 0$. It is clear that $\mathbf{m}_r$ may be written in terms of the $\mathbf{M}_s$, $s = 0, 1, ..., r$. Using the lower-case moments makes the expression for temperature especially simple:

$$T = \frac{1}{3}\frac{m}{\rho k}\mathrm{tr}(\mathbf{m}_2). \tag{1.33}$$

Because these moments of f are the physically relevant quantities, one is inclined to seek equations for them directly. These are obtained by multiplying the relevant kinetic equation - we will work with Boltzmann equation here - by $\mathbf{v}^r$ and integrating over all velocities. One obtains

$$\frac{\partial \mathbf{M}_r}{\partial t} + \nabla_x \cdot \mathbf{M}_{r+1} = C_W[\mathbf{v}^r]. \tag{1.34}$$

The key point here is that the time derivative of the r^{th} moment depends on the $(r+1)^{\text{st}}$ moment. We thus have a hierarchy of infinitely-many moment equations.

Nevertheless, these equations are attractive because they are independent of the particle velocity $\mathbf{v}$ - we have thus reduced the dimension of the problem by three. However, a tractable solution procedure must rely on an appropriate truncation of the hierarchy. This is analogous to the procedure of obtaining the Boltzmann equation from Liouville's theorem. There, the BBGKY hierarchy of equations for the n-particle distribution functions - each of which depended on the $(n+1)$-particle distribution - was truncated at the first term by the molecular chaos assumption, which enabled us to write the two-particle distribution in terms of the one-particle distribution.

In the case of the moment hierarchy, the goal is the same: to write some moment in terms of lower moments, thereby avoiding the infinite, coupled hierarchy of moment equations - this

general procedure is referred to as *closure*, for it yields a finite, *closed* system of equations. This requires some *a priori* knowledge of the system, beyond what has already been set out here. Typically, this takes the form of an asymptotic expansion in terms of some small parameter. To carry further the analogy with the BBGKY hierarchy, the molecular chaos assumption may be viewed as an asymptotic expansion with the correlation between the velocities of colliding particles as the small parameter, and we obtain the Boltzmann equation by truncating at the zero-th order term.

However, in contrast to the BBGKY closure procedure, there are many small parameters that may be used in closing the moment hierarchy. We will focus on a single choice which is particularly important and relevant to this thesis, but the reader should bear in mind the existence of a plethora of alternative closure procedures, e.g. [CFP13, HR88, Lev96, Lev97]. The small parameter we focus on is the ratio of collisional mean free path λ_{mfp} to the characteristic length scale L over which f varies. In the rarefied gas dynamics literature, this ratio is commonly called the Knudsen number, so we will denote it by Kn. That is,

$$\mathrm{Kn} = \frac{\lambda_{mfp}}{L}. \tag{1.35}$$

In neutral fluids near standard temperature and pressure, the Knudsen number is typically very small. The relevant analog of the Knudsen number can also be very small in relatively quiescent plasmas. In both contexts, systems with small Knudsen number are said to be *highly collisional*, while systems with large Knudsen number are said to be *collisionless*. In the following subsection, we derive the Euler equations of fluid mechanics under the assumption of high collisionallity (small Knudsen number).

1.2.4 Collisional Closure

Upon non-dimensionalization, the Boltzmann equation may be rewritten as

$$f_t + \mathbf{v} \cdot \nabla_x f = \frac{1}{\mathrm{Kn}} \mathcal{C}_B(f, f). \tag{1.36}$$

By expanding f in powers of the Knudsen number,

$$f = \sum_{p=0}^{\infty} f_p \mathrm{Kn}^p, \tag{1.37}$$

and solving order by order in Kn we find that

$$\mathcal{C}_B(f_0, f_0) = 0 \tag{1.38}$$

to leading order. From section 1.2.1, we know this implies that f_0 is a local Maxwellian. We are, however, free to choose any local Maxwellian we like. We mean to truncate the expansion after the first term, so it behooves us to choose the local Maxwellian with the same ρ, $\mathbf{u}$, and T as the full distribution f - in general, this choice leads to the so-called Chapman-Enskog expansion [CC70].

Closure is achieved by truncating the asymptotic expansion. The simplest option is to truncate it at that first term - that is, we assume $f \approx f_0$. By virtue of being a local Maxwellian, f_0 has arbitrary M_0 (i.e. ρ), $\mathbf{M}_1$ (i.e. $\mathbf{u}$), and $\mathrm{tr}(\mathbf{m}_2)$ (i.e. T). The hierarchy is closed by noting the restriction placed on $\mathbf{m}_3$ by the constraint the f_0 is a local Maxwellian. In particular, it is not difficult to show that

$$(\mathbf{m}_2)_{ij} = \delta_{ij} \frac{\rho}{m} kT = \delta_{ij} p, \quad \mathbf{m}_3 = 0, \tag{1.39}$$

where δ_{ij} is the Kronecker delta function, taking the value 1 when $i = j$, and 0 otherwise. The results that $\mathbf{m}_3 = 0$ and that the off-diagonal components of $\mathbf{m}_2$ vanish are simple consequences of symmetry.

With these facts in hand, we can begin to write down a closed system of moment equations. We begin with the 0^{th} moment by simply setting $r = 0$ in (1.34). We find

$$\rho_t + \nabla \cdot (\rho \mathbf{u}) = 0, \tag{1.40}$$

where we've used the fact that 1 is a collision invariant to show that the right-hand side vanishes. Here, and in the rest of this section, all gradients in moment equations are assumed to be over $\mathbf{x}$. This equation is referred to as the *conservation of mass* or sometimes *continuity* equation. It should be familiar to many readers.

The equation for the first moment is more commonly written in terms of $\mathbf{m}_1$. To find it, we multiply the Boltzmann equation by $(\mathbf{v} - \mathbf{u})$ and integrate over all $\mathbf{v}$. Assuming all functions are sufficiently smooth that derivatives and integrals may be commuted, we have, after some algebra,

$$\rho \left(\frac{\partial}{\partial t} + \mathbf{u} \cdot \nabla \right) \mathbf{u} + \nabla \cdot \mathbf{m}_2 = 0, \tag{1.41}$$

where we've again used our knowledge of collision invariants to eliminate the right side. Recalling (1.39), we can rewrite $\mathbf{m}_2$ and find

$$\rho \left(\frac{\partial}{\partial t} + \mathbf{u} \cdot \nabla \right) \mathbf{u} + \nabla p = 0. \tag{1.42}$$

This is often called the *conservation of momentum* equation, and will be familiar to readers with a background in fluid theory as the most famous of the Euler equations.

Similarly, to obtain the equation for the second moment (more precisely, its trace) we multiply the Boltzmann equation by $|\mathbf{v} - \mathbf{u}|^2$ and integrate over all $\mathbf{v}$. After some algebra, we obtain

$$\frac{\partial}{\partial t} \left\{ \mathrm{tr}(\mathbf{m}_2) \right\} + \nabla \cdot (\mathrm{tr}(\mathbf{m}_3) + \mathbf{u}\mathrm{tr}(\mathbf{m}_2)) + 2\nabla \mathbf{u} \colon \mathbf{m}_2 = 0. \tag{1.43}$$

We again make use of our asymptotic assumption that f is a local Maxwellian, so that we may use (1.39) to simplify (1.43). Doing so, we find

$$\frac{\partial p}{\partial t} + \nabla \cdot (\mathbf{u}p) + \frac{2}{3} p \, (\nabla \cdot \mathbf{u}) = 0. \tag{1.44}$$

This is commonly referred to as the *conservation of energy* equation.

Together, (1.40), (1.42), and (1.44) form a closed system of equations for the variables ρ, $\mathbf{u}$, and p (or, equivalently, T). These are the Euler equations for an ideal gas. The reader should be cautioned that while the notation used here for the first two equations is typical, the notation for the third (energy conservation) is not. A plethora of different notations exist in the literature. This one has been chosen to emphasize the fact that the system of equations is closed.

While no one would claim that the Euler equations are particularly simple to solve, they are much more amenable to numerical solution than the Boltzmann equation because they do

not involve $\mathbf{v}$, thus reducing the dimensionality of the problem dramatically. Indeed, many reasonably efficient schemes exist for the Euler equations in both two- and three-dimensions, e.g. [JST81, Roe86, TT99, Van82].

Since the contents of this and the previous section are rather technical, let us summarize: because f, the solution of the Boltzmann equation, contains more information than is actually of interest, it is often desirable to derive equations for the moments of f. A closed system of such equations is only possible through some additional assumption. While many are possible, we've described the equations that result under the assumption of extremely small Knudsen number, which is equivalent to high collisionality. We've shown that, to leading order, this assumption forces f to be a local Maxwellian, which in turn leads us to the Euler equations of fluid dynamics. By carrying the asymptotic expansion one term further (i.e. including f_1 as well as f_0), it is possible to derive the Navier-Stokes equations as well, under the assumption the the collision operator is that of the Maxwell molecules [CC70]. However, such a derivation is beyond the scope of this thesis.

From the perspective of this thesis, the key point is this: Fluid equations are *only valid* in some asymptotic limit. In particular, the Euler equations are only valid when f is (at least approximately) a local Maxwellian. However, fluid equations are much easier to solve than the Boltzmann equation because of their reduced dimensionality.

1.3 Kinetic Theory of Plamsas

The preceding introduction to kinetic theory is directly applicable to neutral fluids. However, in the case of plasmas, some changes are necessary. Firstly, in the study of plasmas the acceleration term $\mathbf{a} \cdot \nabla_v f$ - which was largely ignored above - plays a much more important role. In particular, $\mathbf{a}$ is the Lorentz force,

$$\mathbf{a} = \frac{e}{m}\left(\mathbf{E} + \frac{\mathbf{v}}{c} \times \mathbf{B}\right), \tag{1.45}$$

where $\mathbf{E}$ and $\mathbf{B}$ are the electric and magnetic fields and c is the speed of light. The fields depend on charge density $e\rho$ and current density $\mathbf{J} = e\rho\mathbf{u}$ through Maxwell's equations.

Second, and of much more direct importance to the work in this thesis, is the peculiar nature of the Rutherford cross-section that describes Coulomb collisions. We reprint that cross-section here in the case of $Z_1 = Z_2 = 1$ for clarity:

$$\frac{d\sigma}{d\Omega}(w, \theta) = \left[\frac{e^2}{8\pi\epsilon_0\mu w^2}\right]^2 \frac{1}{\sin^4\theta/2}. \tag{1.46}$$

This differential cross-section has divergent total cross section, since

$$\sigma = 2\pi \int_0^\pi \frac{d\sigma}{d\Omega} \sin\theta \, d\theta \sim \int_0^\pi \frac{\sin\theta}{\sin^4\theta/2} \, d\theta \to \infty. \tag{1.47}$$

This begins to hint that the Boltzmann collision operator (1.4) may not even make sense for this cross-section. Worse yet, the mean momentum transfer due to Coulomb collisions, given by

$$\langle \Delta p \rangle = 2\pi m \int_0^\pi \frac{d\sigma}{d\Omega}(\mathbf{v}' - \mathbf{v}) \, d\theta \tag{1.48}$$

is logarithmically divergent [AV04]. Heuristically speaking, the Coulomb force between charged particles is so long-range - that is, that each particle experiences a force from so many others - that the collective effect diverges.

How are we to make any sense of a collision operator in this case? The standard answer of plasma physicists is a phenomenon known as Debye shielding. We discuss this effect in the following subsection, then discuss the Landau collision operator, which is the standard one used in plasma simulations.

1.3.1 Debye Shielding

The Rutherford cross section arises from the electrostatic force between two point particles, whose magnitude is given by

$$F = \frac{Z_1 Z_2 e^2}{4\pi\varepsilon_0} \frac{1}{r^2}, \tag{1.49}$$

where r is the distance between the particles. However, in a plasma, two point particles do not exist in a vacuum, but rather in a sea of many other particles. Gauss's law gives the electric field for a distribution of particles with charge e having number density ρ as

$$\nabla \cdot \mathbf{E} = \frac{e\rho}{\varepsilon_0}. \tag{1.50}$$

In the electrostatic case, $\mathbf{E}$ is curl-free and may thus be written in the equivalent potential form

$$\Delta\phi = -\frac{e\rho}{\varepsilon_0}, \qquad \mathbf{E} = -\nabla\phi, \tag{1.51}$$

where ϕ is the *electrostatic potential*.

Even this equation, though, is not the whole story. Under no other forces but the electrostatic, particles will tend to flow toward lower values of $e\phi$. In fact, at equilibrium, the charge density obeys the Boltzmann distribution:

$$e\rho = \langle e\rho \rangle \exp\left\{\frac{-e\phi}{kT}\right\}, \tag{1.52}$$

where $\langle e\rho \rangle$ is some constant, reference charge density, and T is the plasma temperature. This charge distribution is a classical result in equilibrium statistical mechanics, but the validity of its application may not be obvious in this context. However, it is simple to show that it is a steady state ($\partial_t f = 0$) solution to the kinetic equation - one assumes f to be a local Maxwellian, shows that $\mathbf{u}$ and T must be constant at steady state, and the result follows immediately.

When the electrostatic energies are small compared to the kinetic energies of the particles - this is called a *weakly coupled* plasma and will be the case we're concerned with - the Boltzmann distribution is approximately

$$e\rho \approx \langle e\rho \rangle \left(1 - \frac{e\phi}{kT}\right). \tag{1.53}$$

Substituting (1.53) into (1.51), we find

$$\Delta\phi + \left(\frac{e^2\langle\rho\rangle}{\varepsilon_0 kT}\right)\phi = e\langle\rho\rangle. \tag{1.54}$$

The Debye length is defined by

$$\lambda_D = \sqrt{\frac{\epsilon_0 kT}{e^2\langle\rho\rangle}}, \tag{1.55}$$

so the above equation may be rewritten as

$$\Delta\phi + \frac{\phi}{\lambda_D^2} = \frac{e\langle\rho\rangle}{\varepsilon_0}. \tag{1.56}$$

This equation admits exponentially decaying solutions. In particular the response to adding a point charge to an otherwise quiescent system is

$$\phi = \frac{1}{4\pi\varepsilon_0}\frac{e^{-r/\lambda_D}}{r}, \tag{1.57}$$

in contrast to $\phi \sim 1/r$ as would be the case for a point charge in a vacuum.

Physically, this has an intuitive explanation. The force due to any given charged particle on its neighbors tends to move those particles in such a way as to *shield* the more distant neighbors from that particle's influence. This phenomenon is called *Debye shielding*, and has characteristic length scale λ_D. The result is an effective potential that decays exponentially in r, which leads to a finite total cross section and finite momentum transfer.

Ideally, one would derive the differential cross section associated with the potential (1.57) and use that in the Boltzmann collision operator in place of the Rutherford cross section. Unfortunately, no explicit form of the cross section is known, and the implicit form is complex [AV04]. In practice, the following cruder approximation is used:

$$\frac{d\sigma}{d\Omega}(w,\theta) = \left[\frac{e^2}{8\pi\epsilon_0\mu w^2}\right]^2 \frac{1}{\sin^4\frac{\theta}{2}}\mathbb{1}_{\theta\geq\theta_{min}}, \tag{1.58}$$

where $\mathbb{1}$ is the indicator function - i.e. one if $\theta \geq \theta_{min}$, and zero otherwise. The variable θ_{min} is some small scattering angle below which Debye shielding takes over and no collision is assumed to take place. The computation of an appropriate value for θ_{min} is the subject of the next subsection. In the process of doing so, we will discover the range of validity of the approximate cross section (1.58).

1.3.2 Plasma Parameter and Weak Coupling

We begin the computation of θ_{min} by noting that in the course of the derivation of the Rutherford cross section - see e.g. [GPS02] - one arrives at

$$b = \frac{e^2}{4\pi\varepsilon_0\mu v_0^2}\cot\frac{\theta}{2}, \tag{1.59}$$

where b is the so called *impact parameter* - the distance of closest approach for the two colliding particles if there were no force between them - μ the reduced mass, v_0 the relative

velocity between the collision partners, and θ the scattering angle in the center of mass frame. The minimum angle clearly results from the largest impact parameter for which a substantial force is still present. Since we have exponential decay on the Debye length scale, a reasonable choice is $b = \lambda_D$. Typical particle kinetic energies are on the order kT, so we set $\mu v_0^2 = kT$. As we expect the minimum angle to be small, we approximate $\cot \theta/2 \approx (\theta/2)^{-1}$. Substituting each of these assumptions into (1.59), we find

$$\frac{2}{\theta_{min}} \approx 4\pi\rho\lambda_D^3, \tag{1.60}$$

where we've dropped the angle brackets on ρ. The quantity on the right is called the *plasma parameter*, typically denoted by Λ. It is (to within a factor of 3) the number of particles within a sphere of radius λ_D - such a sphere is often called a *Debye sphere*.

Plasmas with $\Lambda \gg 1$ (and thus $\theta_{min} \ll 1$) are called *weakly coupled*. Earlier, in our discussion of Debye shielding, we used the term 'weakly coupled' to mean a plasma in which typical kinetic energies far exceed electrostatic energies. In fact, the two characterizations are equivalent. To see this, define r_c as the classical distance of closest approach, at which particle kinetic energies and electrostatic potential energies are equal. That is, r_c satisfies

$$\frac{e^2}{4\pi\varepsilon_0 r_c} = kT. \tag{1.61}$$

Additionally, we define the typical distance between particles r_d, given by $r_d = \rho^{-1/3}$. With some simple algebra, we find $r_c = 1/4\pi\rho\lambda_D^2$, which implies that

$$\Lambda = \frac{\lambda_D}{r_c} = \frac{1}{\sqrt{4\pi}} \left(\frac{r_d}{r_c}\right)^{3/2}. \tag{1.62}$$

Thus, $\Lambda \gg 1$ is equivalent to $r_d \gg r_c$. That is, the distance between particles is much greater than the distance at which kinetic and electrostatic energies are comparable, so that electrostatic energies are typically much smaller than kinetic energies.

In general, weakly coupled plasmas are characterized by high temperature (since this gives small r_c) and low density (since this gives large r_d). When discussing plasmas in this thesis, they will always be assumed to be weakly coupled. Some examples of weakly coupled

plasmas include interstellar and ionospheric plasmas, the solar wind, and both magnetic and inertial confinement fusion plasmas [HW04].

Most significantly for our purposes, in weakly coupled plasmas a particle rarely experiences significant electrostatic forces from two particles simultaneously. This allows us to continue to treat collisions as essentially binary. Moreover, while the Rutherford cross-section's rapid divergence at small scattering angles already makes it clear that small angle collisions dominate the dynamics, this point is further emphasized in the weakly coupled case. Indeed, in the weakly coupled case it is extremely rare that particles pass close enough to each other to experience a large angle collision.

1.3.3 The Landau-Fokker-Planck Collision Operator

The last two points in the previous subsection - that weakly coupled plasmas experience essentially binary collisions, and that the effects of those collisions are dominated by small scattering angle events - form the underpinnings of the derivation of the standard collision operator in the kinetic theory of plasmas.

That operator was originally derived by Landau [Lan36], and takes the general form of a Fokker-Planck operator. It is in various places referred to as the Landau operator, Fokker-Planck operator, and Landau-Fokker-Planck operator. In this thesis, we will use the last of these names, often abbreviating it to LFP.

A full reprinting of Landau's original derivation is beyond the scope of this thesis, but it has two key elements that warrant exposition. The first is that, since collisions may be thought of as binary, we may begin from the Boltzmann operator with the cutoff Coulomb potential (1.58). Second, since only small angle collisions are relevant, $f(\mathbf{v}')$ and $f(\mathbf{v}'_*)$ are well approximated by Taylor expansions of f about $\mathbf{v}$ and $\mathbf{v}_*$, respectively.

Using these two assumptions, Landau arrived at

$$\mathcal{C}_{LFP}(f,f) \equiv \left(\frac{e^4 \log\Lambda}{8\pi\varepsilon_0^2 m^2}\right) \nabla_v \cdot \int_{\mathbb{R}^3} \left(\frac{w^2\mathbf{I} - \mathbf{ww}}{w^3}\right) \cdot (f_*\nabla_v f - f\nabla_{v_*} f_*)\, d\mathbf{v}_*. \tag{1.63}$$

In fact, it was shown in [Bob75] that this is only the lowest order term in an infinite series

expansion of the Boltzmann collision operator. However, the higher order terms are complex and rarely used. An equivalent expression to (1.63), which we will find more convenient to work with, was derived in [RMJ57] and is given by

$$\mathcal{C}_{LFP}(f,f) = -\left(\frac{e^4 \log\Lambda}{8\pi\varepsilon_0^2 m^2}\right)\frac{\partial}{\partial \mathbf{v}}\cdot\left(2\frac{\partial H}{\partial \mathbf{v}}f - \frac{\partial^2 G}{\partial \mathbf{v}\partial \mathbf{v}}\cdot\frac{\partial f}{\partial \mathbf{v}}\right), \tag{1.64}$$

where the so-called Rosenbluth potentials H and G satisfy

$$\Delta_v H = -4\pi f, \qquad \Delta_v G = 2H. \tag{1.65}$$

For a demonstration of the equivalence of (1.63) and (1.64), see [HW04].

Notice that, in both forms, the operator is proportional to $\log\Lambda$. This is a direct consequence of the choice of θ_{min} in (1.60), for in the course of the derivation, integrals related to the mean momentum transfer arise, which we recall scale like θ^{-1} as $\theta \to 0$. The result is that the integral is proportional to $\log 1/\theta_{min} \sim \log\Lambda$.

In reality, the value of Λ varies in space - after all, Λ depends on both density ρ and temperature T. However, because the LFP operator's dependence on Λ is only logarithmic - i.e. very weak - Λ may be regarded as a constant in most circumstances.

Throughout, a kinetic equation using the LFP collision operator, i.e.

$$f_t + \mathbf{v}\cdot\nabla_x f + \mathbf{a}\cdot\nabla_v f = \mathcal{C}_{LFP}(f,f), \tag{1.66}$$

will be referred to as a Landau-Fokker-Planck (LFP) equation. Much of this thesis is devoted to this equation in the special case in which f does not depend on $\mathbf{x}$ - that is, the spatially homogeneous case. In this case, we have

$$f_t = \mathcal{C}_{LFP}(f,f). \tag{1.67}$$

Chapter 2 of this thesis is dedicated to the derivation and testing of an accelerated Monte Carlo method for the treatment of the LFP collision operator (1.64) that is particularly applicable in the moderate to high collisionality regime. We characterize these regimes here. We first note that the collision operator (1.64) has an associated frequency

$$\nu_{FP} \sim \frac{e^4 n}{4\pi\varepsilon_0^2 m^2 v_t^3}\log\Lambda = \frac{1}{2\sqrt{2}}\,\omega_p\frac{\log\Lambda}{\Lambda}, \tag{1.68}$$

where $v_t = \sqrt{2T/m}$ is the magnitude of the typical relative velocity between two colliding particles and $\omega_p = v_t/\sqrt{2}\lambda_D$ is the plasma frequency [HW04]. Since $\Lambda \gg 1$ is required for the LFP equation to be valid, the existence of a moderately to highly collisional regime may appear questionable since $\nu_{FP} \ll \omega_p$. However, one can see otherwise in - for instance - the case of an electrostatic, single component, fully ionized plasma. In this case, $\mathbf{a} = e\mathbf{E}/m$, with the electric field $\mathbf{E}$ given - as before - by Gauss's law,

$$-\Delta\phi = \frac{e}{\varepsilon_0}(Zn_i - n_e), \qquad -\nabla\phi = \mathbf{E}, \tag{1.69}$$

where n_i and n_e are the ion and electron densities, respectively, and Z is the ion atomic number. A commonly accepted assumption (so long as high frequency oscillations are not present in the system) is that the electron density - to good approximation - obeys a Boltzmann response to the electrostatic potential [1]:

$$n_e = n_0 \exp\left\{\frac{e\phi}{kT}\right\}, \tag{1.70}$$

where n_0 is a constant reference density. This is the same assumption used in deriving the Debye screening potential in 1.3.1. Substituting (1.70) into (1.69) and performing a simple perturbation analysis, we find the convection and mean field terms have associated frequencies

$$\nu_C \sim \nu_{MF} \sim \frac{v_t}{L}, \tag{1.71}$$

where L is a characteristic length scale. We see by comparing (1.68) to (1.71), we see that for plasmas varying over large length scales - in particular, $L \gg \lambda_D$ - it is indeed possible that $\nu_{FP} \gg \nu_C, \nu_{MF}$, leading to a highly collisional system. Indeed, the collision term dominates if

$$\frac{L}{\lambda_D} \gg \frac{\Lambda}{\log\Lambda}. \tag{1.72}$$

[1] This assumption is commonly referred to as 'quasineutrality', or 'the plasma approximation'. See e.g. [CL84], among many other standard texts, for a discussion.

1.4 Numerical Methods for LFP Equation

The LFP equation, like most kinetic equations, has very few known exact solutions. However, being a quite general model of plasma behavior, its solutions can provide invaluable information in the design, testing, and interpretation of physical experiments and engineering projects. One is thus motivated to seek numerical solutions for problems of interest. Such simulations play an important and growing role in plasmas [KK09, VKB09] and a great many other fields.

Kinetic equations, and in particular the LFP equation, pose particular challenges for numerical simulations. They are high-dimensional, nonlocal, nonlinear, and often feature a wide range of spatial and/or temporal scales that must be resolved. As a consequence of the problem having so many challenges, the optimal numerical method is problem dependent.

1.4.1 Survey of existing methods

The existing methods may be divided into three categories. The first category consists of fluid-based methods, e.g. [CDW99, DUX09, KHY02]. These methods are based on some asymptotic or *ad hoc* closure of the moment hierarchy of section 1.2.3. In plasmas, a commonly used closure is that of Braginskii [Bra65]. The resulting equations are solved using any of a wide variety of applicable finite difference, finite element, or spectral methods (we will collectively refer to these as *continuum methods*). When applicable, these methods are usually the most efficient option available because of the reduced dimension of the fluid equations. Their main drawback is in their limited range of applicability. As noted in 1.2.5, fluid equations can only be valid in some asymptotic limit, and there is certainly no universally valid limit for all plasma systems. In fact, there are many circumstances in which no natural small parameter can be identified. Fluid methods are thus efficient but of limited applicability.

The second category consists of continuum methods applied to the LFP equation - or some linearization of it - directly, e.g. [FP02, GH13, PRT00, PG11, TTT13]. These methods

have the advantage over fluid methods of being much more generally applicable, but the disadvantage of solving an equation in higher dimension - a considerable disadvantage, since the complexity of continuum methods scales exponentially with dimension. Many applications of this class of methods are to systems with some sort of symmetry that can be used to reduce the spatial and/or velocity dimension of the problem [FP02, TTT13], thereby making the computation more tractable.

The third category is the particle based, Monte Carlo methods. These methods will be the focus of this thesis. Their primary advantage is their excellent scaling with dimension, making them a good choice for high dimensional kinetic equations. In contrast to the exponential scaling of continuum methods, Monte Carlo methods (often) scale linearly with dimension[2]. On the other hand, Monte Carlo methods converge much more slowly than continuum methods, being subject to statistical noise that is absent from continuum methods.

Additional qualitative discussion of the relative advantages of these different methods may be found in [TTR12]. We proceed with a more detailed discussion of Monte Carlo and particle methods, as all the methods in this thesis fall into this category.

1.4.2 Monte Carlo and Particle in Cell

In very general terms, Monte Carlo methods work by formulating a problem in terms of the computation of the expectation of a random variable. Then, many samples of that random variable are generated and averaged to arrive at a solution. The price of Monte Carlo's excellent scaling with dimension is its slow convergence. As mentioned in 1.1, this is because the error is governed by the central limit theorem, meaning that if N samples are generated, the root mean square error (i.e. standard deviation of the sample mean) scales like $N^{-1/2}$. The computational cost K of achieving an RMS error ε is thus

$$K = O(\varepsilon^{-2} K_s) \tag{1.73}$$

[2]We will see examples in chapter 3 in which, for dimension D, the complexity is actually proportional to D^2 and D^4. Each of these, however, is still preferable to e^D.

where K_s is the complexity of generating a single sample. For example, if a single sample consists of the solution of an ODE using Euler's method, the complexity scales with the number of time steps taken, which scales with $\Delta t^{-1} \sim \varepsilon^{-1}$, for the error ε scales like Δt. We would thus say that a such a Monte Carlo method has overall complexity $O(\varepsilon^{-3})$.

Throughout this thesis, and especially in chapter 3, we will find the scaling of K with dimension D and error ε a useful metric for evaluating the performance of a numerical scheme. Since D is typically fixed in plasma applications, we will often speak only of the scaling of K with ε, but we will revisit the issue of dimension near the end of chapter 3.

A typical Monte Carlo method for the LFP equation proceeds as follows. First, the spatial domain is partitioned into cells which are sufficiently small that the distribution function can be considered roughly independent of position within a given cell. Second, 'particles' are placed into each cell, with velocities randomly sampled so as to be representative of the initial distribution at that point. That is, if $f_0(\mathbf{x}, \mathbf{v})$ is the initial distribution and the j^{th} cell is centered at $\mathbf{x}_j$, then a histogram of the velocities of the particles within the j^{th} cell should approximate $f_0(\mathbf{x}_j, \mathbf{v})$.

Time is discretized into steps of size Δt. The general structure of the time-stepping loop may be characterized as follows.

- **Compuation of mean fields**:
  - Compute $\mathbf{a}$, if it's present, by some appropriate method, depending on its dependence on f. For example, in the electrostatic plasma case, one would solve Poisson's equation (1.51) on the grid formed by the cells, with the density ρ computed from the number of particles in each cell.
- **Convection Step**:
  - For each particle position $\mathbf{x}_i$ and velocity $\mathbf{v}_i$, update them to be

$$\mathbf{x}_i^{new} = \mathbf{x}_i + \Delta t\, \mathbf{v}_i, \tag{1.74}$$

$$\mathbf{v}_i^{new} = \mathbf{v}_i + \Delta t\, \mathbf{a}(\mathbf{x}_i, \mathbf{v}_i). \tag{1.75}$$

- **Collision Step**:
  - Alter the velocity of each particle in a manner consistent with the collision operator.

The rough outline above describes the Particle-In-Cell (PIC) method [Bir91]. There are of course numerous variations on this general structure. The mean field may, for example, include a magnetic field. A more advanced time-stepping scheme may be used in the convection step, including implicit schemes [Fri05]. Variations in the collision step are especially large, with dramatically different methods in use for neutral fluids [Bir76, AG97] and for plasmas.

In the remainder of this section, we discuss two standard Monte Carlo approaches to simulation of LFP collisions.

1.4.3 Binary Collision Algorithms

In the *binary collision* approach, the particles within a given cell are first grouped into random pairs. These particles are then 'collided' according to some algorithm which is meant to approximate the effect of LFP operator. Two standard methods exist, due to Takizuka & Abe [TA77] and Nanbu [Nan97].

The Takizuka-Abe method (henceforth TA) is more commonly used, and is the only binary collision algorithm used in this thesis, so we will focus on its summary. Let $\mathbf{v}_\alpha$ and $\mathbf{v}_\beta$ be the velocities of the particles in a given collision pair, with masses m_α and m_β, charges e_α and e_β. The algorithm proceeds as follows:

- Generate two random variables ζ and ϕ, with ζ normally distributed with mean zero and
$$\mathrm{Var}[\zeta] = \frac{1}{2}\frac{e_\alpha^2 e_\beta^2 n_L \log\Lambda}{8\pi\varepsilon_0^2 m_{\alpha\beta}^2 u^3}\Delta t, \tag{1.76}$$
where $\mathbf{u} = \mathbf{v}_\alpha - \mathbf{v}_\beta$, $m_{\alpha\beta} = m_\alpha m_\beta/(m_\alpha + m_\beta)$, and n_L is the smaller of the densities of the two particle species. Meanwhile, ϕ is uniformly distributed in 0 to 2π.

- Set $\theta = 2 \arctan \zeta$.

- Set the updated particle velocities to

$$\begin{aligned} \mathbf{v}'_\alpha &= \mathbf{v}_\alpha + \frac{m_{\alpha\beta}}{m_\alpha} \Delta \mathbf{u}, \\ \mathbf{v}'_\beta &= \mathbf{v}_\beta - \frac{m_{\alpha\beta}}{m_\beta} \Delta \mathbf{u}, \end{aligned} \tag{1.77}$$

  where $\Delta \mathbf{u}$ is defined by

$$\begin{aligned} \Delta u_x &= [(u_x/u_\perp)u_z - (u_y/u_\perp)u] \sin\theta \cos\phi - u_x(1 - \cos\theta) \\ \Delta u_y &= [(u_y/u_\perp)u_z + (u_x/u_\perp)u] \sin\theta \cos\phi - u_y(1 - \cos\theta) \\ \Delta u_z &= -u_\perp \sin\theta \cos\phi - u_z(1 - \cos\theta), \end{aligned} \tag{1.78}$$

  with $u_\perp = \sqrt{u_x^2 + u_y^2}$.

The complex formula (1.78) just translates a scattering through angle θ with azimuthal angle ϕ in the center-of-mass frame into the observer's frame.

The method of Nanbu has the same general structure, but with a different probability density for the scattering angle. As noted in [BP13], the similarity of the methods comes from their common origin - each takes advantage of the fact that there are many cross-sections which give rise to the same LFP collision operator as a leading order approximation of the Boltzmann operator. It is computationally convenient to choose a cross section with total collision rate independent of $\mathbf{v}$ - these are called *Maxwellian-type*, since this property is shared with the Maxwellian cross section. This is what allows the algorithms to pair particles at random, rather than having to perform a weighted pairing dependent on the velocities of all the particles.

The issue of the accuracy of these algorithms is a subtle one, and not entirely resolved. In [BN00], there appeared a formal argument that the error is $O(\Delta t)$ for Nanbu, and in [CWD08] it was shown that the same result holds for TA. However, an empirical study [WLC08] appeared to show that TA and Nanbu each converge as $O(\sqrt{\Delta t})$. However, this data was not entirely conclusive. As a side note in this thesis, we will find data in support of

the hypothesis that TA in fact converges as $O(\Delta t)$. Finally, a rigorous proof that the error is *no worse than* $O(\sqrt{\Delta t})$ appears in [BP13].

In the error analysis contained in this thesis, we will simply assume that the error due to binary collision algorithms scales as $O(\Delta t^\alpha)$, for some $1/2 \leq \alpha \leq 1$. The methods we develop are useful regardless of the particular value α takes within this range.

As a final comment, we note that for these time-stepping Monte Carlo methods, the complexity K_s of generating a single sample[3] scales as $\Delta t^{-1} \sim \varepsilon^{-1/\alpha}$, so that the total complexity is

$$K = O\left(\varepsilon^{-(2+1/\alpha)}\right). \tag{1.79}$$

The total complexity of binary collision methods is thus between $O(\varepsilon^{-3})$ and $O(\varepsilon^{-4})$.

1.4.4 Langevin/SDE-Based Algorithms

An alternative Monte Carlo approach takes advantage of the equivalence between convection-diffusion operators of the type seen in (1.64) and stochastic differential equations. This relation is known as the *forward Kolmogorov equation* in mathematics, and as the Fokker-Planck equation in other fields. It states that if a random variable $\mathbf{S}$ obeys the stochastic differential equation (often called a *Langevin* equation in physics contexts)

$$dS_i = \alpha_i(t, \mathbf{S})\, dt + \beta_{ij}(t, \mathbf{S})\, dW_j,$$

where the W_j are independent, standard Brownian motions, and summation over repeated indices is implied, then the the probability density p of $\mathbf{S}$ obeys the PDE

$$\frac{\partial}{\partial t} p(t,x) = -\frac{\partial}{\partial x_i}\left(\alpha_i(t,x)p\right) + \frac{1}{2}\frac{\partial^2}{\partial v_i \partial v_j}\left(\beta_{ij}^2(t,x)p\right). \tag{1.80}$$

A sketch of the proof of this result can be found in [Shr04], exercise 6.9.

Since f may be interpreted as a rescaling of the probability density of $\mathbf{v}$, we may use this result on (1.64) along with some integration by parts to find that $\mathbf{v}$ obeys

$$dv_i = F_i\, dt + D_{ij}\, dW_j \tag{1.81}$$

[3] In this case a sample is the full time evolution of the velocity of a single particle, the complexity of which scales like the total number of time steps.

with F_i and D_{ij} given by

$$F_i = \left(\frac{e^4 \log\Lambda}{2\pi\varepsilon_0^2 m^2}\right)\frac{\partial H}{\partial v_i}, \qquad D_{ij} = \left[\left(\frac{e^4 \log\Lambda}{4\pi\varepsilon_0^2 m^2}\right)\frac{\partial^2 G}{\partial v_i \partial v_j}\right]^{1/2}. \tag{1.82}$$

In a particle method, we may thus think of the collision step as the evolution the SDE (1.81) for each simulated particle through a single time step. This is done using a finite difference time-stepping method for SDEs, the simplest of which is the Euler-Maruyama method:

$$v_{i,n+1} = v_{i,n} + F_i(\mathbf{v}_n)\,\Delta t + D_{ij}(\mathbf{v}_n)\,\Delta W_{j,n}, \tag{1.83}$$

where the $\Delta W_{j,n}$ are independent normal random variables with mean zero and variance Δt. Many other advanced methods are discussed in [KP11]. All the methods we will discuss in this thesis have time-stepping error[4] $O(\Delta t)$.

It is worth emphasizing the two distinct roles of f and $\mathbf{v}$ in the two different formulations. In the Langevin formulation, the distribution f is the (rescaled) probability density of the *dependent* variable $\mathbf{v}$ of (1.81). It may be reconstructed from a histogram of many different solutions of (1.81) for different Brownian paths W_j. This is to be contrasted with the original LFP formulation, where $\mathbf{v}$ was an *independent* variable, and the dependent variable is f itself.

Langevin-based collision methods of this type for LFP collisions have been used in e.g. [AV94, JLM96, MLJ97]. They have the advantage over binary collision algorithms of provably having computational complexity

$$K = O\left(\varepsilon^{-3}\right) \tag{1.84}$$

in the case of fixed F_i and D_{ij}, while binary collision algorithms may be as bad as $O(\varepsilon^{-4})$. On the other hand, when F_i and D_{ij} vary, Langevin methods have the disadvantage of needing to re-compute F_i and D_{ij} in every cell at every time step. This is not a simple task - in general, it involves the solution of the two Poisson equations (1.65) with f as input - and is one that is not faced in binary collision algorithms. There do, however, exist scenarios

[4]There are two senses of 'error' in SDEs, *strong* and *weak*. Here, we mean the weak sense, which is the more relevant in this context. The distinction between the two will be discussed in detail in chapter 3.

in which a linearized collision operator suffices - see e.g. [TTT13, RRD13]. In these cases, the SDE coefficients do not couple to the solutions $\mathbf{v}$, and the solution procedure is much simpler.

There are thus advantages and disadvantages to both binary collision methods and Langevin methods. As such, it is worthwhile to pursue the improvement of both methods, as we do in this thesis.

1.5 Summary

In the introduction to this thesis, we have argued that while Monte Carlo methods are effective, general simulation procedures for collisions in many-particle physical systems, the simulation of such systems remains computationally onerous. Therefore, accelerated Monte Carlo methods would be a great boon to simulation efforts.

We have focused on plasma physical applications of these methods, starting from fundamental kinetic theory and then deriving the Landau-Fokker-Planck collision operator as an approximation of the Boltzmann operator in the case of charged particles. We discussed two classes of Monte Carlo methods for approximating this operator - binary collision methods and SDE-based methods.

In chapter 2 we present the first of two accelerated Monte Carlo methods for the spatially homogeneous LFP equation. This method builds on binary collision methods, but relies on the assumption that the distribution function is relatively close to a Maxwellian. It then leverages the fact that collisions within a Maxwellian have no impact to reduce the computational burden. The concept of 'closeness' to a Maxwellian is made precise by the use of *relative entropy*. We analyze and test the new scheme, finding results in agreement with out analysis.

In chapter 3, we discuss the application of the Multilevel Monte Carlo (MLMC) method to the LFP operator through its reformulation as an SDE. We then proceed to develop several variants of and improvements to the MLMC algorithm. These methods are not restricted to

plasma applications, so they will be introduced in a more general mathematical setting. We analyze and test each new method, comparing their performance to the existing state of the art.

Finally, in chapter 4, we conclude by discussing avenues for future work. We discuss the possibilities for extending both new methods to spatially inhomogeneous problems, as well as to rarefied neutral fluids. Other applications for the novel MLMC variants are discussed as well.

CHAPTER 2

Hybrid Fluid-Monte Carlo Scheme

2.1 Introduction

Any model equation of a system of kinetic particles necessarily contains a degree of error. The challenge, in the applied mathematics sense, is to control this error. For example, in the introduction to this thesis we discussed the fluid equations of Euler and Navier-Stokes, whose errors are bounded to the degree that collisions dominate the dynamics. Other examples include the Vlasov equation [Vla68], whose errors are bounded to the degree that collisions may be ignored; the Braginskii equations [Bra65], to the degree that collisions and magnetic fields jointly dominate; the kinetic MHD equations, to the degree the gyrofrequency exceeds other frequencies. Each of these may be regarded as a perturbation expansion of the Boltzmann or LFP equation.

Each of these expansions has the benefit of considerably simplifying the numerical simulation of the system in question, usually by virtue of dimension reduction. Of obvious interest is the extension of such computational simplifications to regimes in which these expansions are not directly applicable. In one such regime - that of intermediate collisionality - the idea of combining Monte Carlo methods with fluid solvers to get accurate and efficient simulations has gained popularity in the last 15 years or so [CWD08, DL93, Hew03, HH07, HK94, JLM96, Lar03, PC99, She08], with applications to both plasmas and rarefied gases. While useful in practice, the modeling considerations inherent in many of these schemes prevent a mathematical account of the size and scaling of the associated errors.

In this chapter, we take a step toward a scheme applicable to this regime whose errors

may be bounded in the same sense as in the perturbation expansions above. The scheme we present is a modification of those developed in [CWD08, DCC10] that is more mathematically justified than either and more accurate than the scheme in [CWD08]. While we treat the case of Coulomb collisions in a plasma - that is, the method generates approximate solutions to the spatially homogeneous LFP equation - an advantage of the present scheme over those in [CWD08, DCC10] is that the core ideas may be applied to any elastic collision process described by the Boltzmann equation. The present work focuses on the spatially homogeneous case, while its extension to the full LFP equation is a topic of active research. We also treat only single component plasmas, but the extension to multiple species is straightforward.

Moderately collisional plasmas appear in a variety of applications, including the tokamak edge plasma [KCK12, PCJ10], inertial confinement fusion [CDL06], and counter-streaming astrophysical plasmas [BBF92]. Generically, any system characterized by large variations in temperature and/or density is likely to feature a region in space where collisionality is moderate. Moreover, even in largely collisionless systems, collisional simulation may be necessary to model turbulence due to the small-scale structure developed [ABC08].

Typically, simulation of the full LFP equation is required when plasma collisionality is moderate. While some continuum methods for the LFP equations were mentioned in the introduction, and some simplified model collision operators [ABC08, BGK54, HS76] that simplify the numerics have been used, we will focus here on the binary collision method of Takizuka and Abe, outlined in section 1.4.1.

In this and other Monte Carlo methods, the simulation of Coulomb collisions frequently represents a computational bottleneck in LFP simulations. Not only can the smallness of the collisional time scale restrict the time step size, but there may be multiple disparate collisional time scales in a single system [CWD08]. The necessity of capturing the shortest scale makes the observation of long time scale effects - sometimes the more important ones - very inefficient. To see this, we consider a simple example. Let $f_m(\mathbf{v}; n, \mathbf{u}, T)$ denote a

Maxwellian distribution with density n, mean velocity $\mathbf{u}$, and temperature T. Consider

$$f = f_m(\mathbf{v}; n_1, \mathbf{0}, T_1) + f_m(\mathbf{v}; n_2, \mathbf{u}_B, T_2) \tag{2.1}$$

with $u_B \gg \max_i \sqrt{T_i}$. The time scale $t_{FP} = \nu_{FP}^{-1}$, where ν_{FP} is as defined in (1.68), for intra-Maxwellian collisions is much shorter than that for inter-Maxwellian collisions, since ν_{FP} scales like one over the typical relative velocity cubed. Thus, the former dominate the computational effort, but they don't change the distribution because the collision operator vanishes on Maxwellians. This makes direct Monte Carlo methods very inefficient for this and similar problems.

The scheme we present here accelerates LFP collisional simulation by assigning time-dependent passive scalars to each simulated particle. The scheme has commonalities with those presented in [FS01, Hew03, Lar03, SB02], but the development here is independent and less heuristic. The mathematical nature of the derivation makes it possible to perform a formal error analysis of the scheme, a property not shared by previous efforts.

The remainder of this chapter is structured as follows: Section 2.2 summarizes previous results on hybrid schemes of the type introduced in [CWD08]. Section 2.3 motivates and outlines the steps in our new scheme. Section 2.4 details our methodology for tracking the values of the passive scalars assigned to each particle. Section 2.5 summarizes and presents an error analysis of the complete algorithm. Section 2.6 presents numerical results for two test initial conditions: a slightly anisotropic Maxwellian and a bump-on-tail distribution. Finally, Section 2.7 presents conclusions and indicates directions for future work. Some details are left to appendices.

2.2 Hybrid Fluid-Monte Carlo Schemes

Hybrid schemes of the type we consider arise from a splitting of the distribution f into $f = f_M + f_k$, where f_M is some initially Maxwellian distribution satisfying $f_M \leq f$. If f_M

and f_k satisfy

$$\partial_t f_M = C(f_M, f_M) + C(f_M, f_k) + S \tag{2.2}$$

$$\partial_t f_k = C(f_k, f_k) + C(f_k, f_M) - S \tag{2.3}$$

where S is some arbitrary function of $(\mathbf{v}, t)$, then the spatially homogeneous LFP equation (1.67) is satisfied by $f = f_M + f_k$. We let C denote the LFP collision operator, since this is the only collision operator with which we will be concerned in this chapter.

Since we choose our splitting such that f_M is initially Maxwellian, $C(f_M, f_M) = 0$ initially. If f_M happens to remain close to a Maxwellian throughout the evolution, we are justified in ignoring $C(f_M, f_M)$ completely. In this way, this splitting generates a computational savings over traditional Monte Carlo by avoiding the necessity of simulating collisions between particles within f_M. If f_M constitutes a large fraction of the system's mass, then this saving will be significant. The scheme also gains accuracy over a pure fluid scheme, because such schemes treat only perturbative deviations from a Maxwellian, while the split kinetic system (2.2)-(2.3) does not assume f_k is asymptotically small.

The problem, then, becomes choosing S in such a way that f_M remains - at least approximately - a Maxwellian for all future times, while at the same time maximizing the fraction of the system's mass residing in f_M. The closer S keeps f_M to a Maxwellian, the more accurate the scheme. The more positive S is, the faster the scheme.

Previous efforts resort to model equations for S [CWD08, DCC10]. These models are more easily summarized if we rewrite

$$S = f_k r_T - f_M r_D \tag{2.4}$$

for some positive r_T and r_D representing distribution normalized $\mathbf{v}$-dependent exchange rates into and out of f_M, respectively.

In the presence only of collisions, the system tends toward a Maxwellian distribution. The quantity r_T represents the transfer of particles from f_k to f_M to reflect this. Increasing r_T makes the scheme more efficient but less accurate. The movement of kinetic particles into f_M will be referred to as *thermalization*.

Similarly, collisions between particles in f_M and f_k drive f_M away from its current equilibrium state. The quantity r_D represents the transfer of particles from f_M to f_k to reflect this. Decreasing r_D makes the scheme more efficient but less accurate. The movement of particles from f_M into f_k will be referred to as *dethermalization*.

We shall refer to any method that prescribes r_T and r_D - and therefore the number and variety of particles to be thermalized and dethermalized at each time step - as a thermalization scheme. The derivation and testing of an improved thermalization scheme is the subject of this paper.

We first discuss previous thermalization schemes used in hybrid methods of the type described here. Since these methods require finite time steps, we choose to write our statements in terms of

$$p_T = r_T \Delta t, \qquad p_D = r_D \Delta t, \tag{2.5}$$

the probabilities of a given particle being thermalized or dethermalized in a given time step of length Δt. The variables on which p_T and p_D depend characterize previous thermalization schemes.

2.2.1 Velocity-based Schemes

Introduced in [CWD08], velocity-based schemes have p_T, p_D dependent only on $|\mathbf{u}_M - \mathbf{v}_p|$, where $\mathbf{v}_p$ is the particle's present velocity and $\mathbf{u}_M$ is the mean velocity of f_M. p_T is a decreasing function of this quantity, while p_D is increasing.

This scheme is intuitively sensible, but has numerous drawbacks. Firstly, there are many choices for p_T and p_D, and it is unclear if an optimal choice even exists. In [CWD08], choices were made to reduce this to two free parameters, but we will find that the scheme presented here has only one free parameter. An equally serious drawback, we claim, is the conflation of "similar velocity" with "many collisions". It is true that if a particle undergoes many collisions with particles from a given Maxwellian, its mean velocity will tend toward that of the Maxwellian. However, the converse is most certainly false. To illustrate this, consider

the following initial distribution

$$f = f_m(\mathbf{v}; n_1, \mathbf{0}, T) + f_m(\mathbf{v}; n_2, \mathbf{0}, \varepsilon T) \tag{2.6}$$

for $\varepsilon \ll 1$ and $n_2 < n_1$. A hybrid method might divide this distribution into a Maxwellian component (f_M) given by the first Maxwellian and kinetic component (f_k) given by the second Maxwellian.

If a velocity based scheme is to be efficient then for the example (2.6), it should immediately thermalize every kinetic particle, because their velocities are very near the center of f_M. On the other hand, this is not possible since if a velocity based scheme is to be accurate, p_T must be relatively small, even at f_M's mean velocity, thereby sacrificing efficiency for other initial conditions. We conclude that the velocity of a particle alone is not enough information to decide whether or not it should be thermalized.

Moreover, in [CWD08], the number of particles in f_k does not tend to zero as a Maxwellian distribution is approached, but instead approaches some constant fraction of the total distribution. This is clearly undesirable, for it greatly diminishes the possible speed-up of the hybrid scheme. In contrast, in the method presented here number of particles in f_k *does* converge to zero as a Maxwellian is approached.

2.2.2 Scattering Angle-based Schemes

The thermalization scheme developed by Dimits et. al. [DCC10] is such that p_T depends only on θ, the scattering angle the particle subtended in its most recent collision, and one additional (overall multiplier) parameter. In its current form, this scheme sets $p_D = 0$. p_T is typically an increasing function of θ.

This scheme is intuitively sensible for the case of Coulomb collisions in which small angle collisions dominate the dynamics. The applicability of this scheme to other potentials, for which small angle collisions do not dominate, is questionable.

Like velocity based schemes, scattering angle schemes use only velocity information from the most recent time step in making decisions about thermalization. We argue that it is

desirable for a scheme to make use of additional variables, which better capture the long-term collisional history of the kinetic particles.

2.3 Paradigm and Theoretical Background

As discussed in the previous section, we claim that a particle's velocity is not enough information to determine whether it should be thermalized, nor is any information dependent on only the most recent time step. We claim that one should look at the distribution of velocities that particle might have had, given its collisional history. This point merits elaboration.

A Monte Carlo scheme represents f as a sum of particles with known velocities. Each particle undergoes a sequence of random collisions throughout the simulation, so that after any given number of time steps, the velocity of a single simulated particle may be regarded as a random variable. Let us denote by $f_j(\mathbf{v}, t)$ the probability density function of the velocity $\mathbf{v}$ of the jth simulation particle's velocity at time t, rescaled so that the total mass of the f_j's matches that of f. Notice that this is initially a delta function at the particle's designated velocity. In a Monte Carlo scheme, f is realized - conceptually - as

$$f = \sum_j f_j, \tag{2.7}$$

where the sum is taken over all simulated particles.

The analogous equation for the hybrid scheme is

$$f = f_M + \sum_j f_j. \tag{2.8}$$

Moreover, we may apply a splitting analogous to that in (2.2)-(16):

$$\partial_t f_M = C(f_M, f_M) + \sum_j C(f_M, f_j) + \sum_j S_j \tag{2.9}$$

$$\partial_t f_j = \sum_i C(f_j, f_i) + C(f_j, f_M) - S_j, \tag{2.10}$$

where the indices j and i run over all the simulated particles. We will often write $f_k = \sum_j f_j$.

In this framework, once (2.9)-(2.10) are discretized with time step Δt, the thermalization of the jth particle amounts to setting

$$f_M(t+\Delta t) = \Pi_M(f_M(t) + f_j), \tag{2.11}$$

where Π_M is the projection operator onto a Maxwellian - that is, $\Pi_M f$ is a Maxwellian with the same $(n, \mathbf{u}, T)$ as f. The goal of the scheme we propose is to thermalize particles in such a way as to introduce as little error as possible into the overall scheme. That is, the decision to thermalize a particle should have little effect on the overall distribution. This is achieved by thermalizing the jth particle only if

$$\frac{1}{n_j} \left\| f_M + f_j - \Pi_M(f_M + f_j) \right\|_{L^1_v} \leq \varepsilon \tag{2.12}$$

for some $\varepsilon > 0$, where n_j is the density associated with f_j. The choice of norm is somewhat arbitrary, but L^1 will prove convenient later. By the triangle inequality, (2.12) is implied by

$$\left\| \hat{f}_M - f_j \right\|_{L^1_v} + \left\| \left(1 + \frac{n_j}{n_M}\right) f_M - \Pi_M(f_M + f_j) \right\|_{L^1_v} \leq n_j \varepsilon, \tag{2.13}$$

where $\hat{f}_M = (n_j/n_M) f_M$. The second norm is small if $f_j \approx \hat{f}_M$, which it must be for the first norm to be small. It's even smaller if $n_j \ll n_M$, which is the case in the parameter regimes we consider. We therefore find it sufficient to enforce

$$\frac{1}{n_j} \left\| \hat{f}_M - f_j \right\|_{L^1_v} \leq \varepsilon \tag{2.14}$$

as a condition for thermalization.

We propose to thermalize the jth particle whenever (2.14) is satisfied and to dethermalize it when (2.14) is violated. In order to implement this, we need a way of computing the L^1 norm in (2.14). This is not a simple task. We instead compute a quantity called relative entropy, which bounds the L^1 norm from above, and thermalize particles when this quantity is sufficiently small and dethermalize them when it is sufficiently large. Relative entropy has the added advantage of evolving monotonically through the action of collisions with a Maxwellian background, as we show below.

2.3.1 Relative Entropy

Define the relative entropy (sometimes called the Kullback-Leibler divergence) $\mathcal{H}(f|g)$ by

$$\mathcal{H}(f|g) = \int_{\mathbb{R}^3} \log\left(\frac{f}{g}\right) f \, d\mathbf{v}. \tag{2.15}$$

for any two non-negative functions f, g depending on $\mathbf{v}$. This quantity has its origins in information theory, where it is used in the context of coding information sources [CT06]. Here, we need only cite four properties: for any non-negative f and g satisfying $\langle f\rangle = \langle g\rangle$, where $\langle\cdot\rangle$ denotes the integral over all velocity space,

$$\mathcal{H}(f|g) \geq 0 \tag{2.16}$$

$$\mathcal{H}(f|g) = 0 \quad \text{iff} \quad f \equiv g \tag{2.17}$$

$$\|f - g\|_{L^1}^2 \leq 2\langle f\rangle^2 \mathcal{H}(\bar{f}|\bar{g}) \tag{2.18}$$

$$\int_{\mathbb{R}^3} C(f, f_m) \log\left(\frac{f}{\hat{f}_m}\right) d\mathbf{v} \leq 0 \tag{2.19}$$

where f_m is a Maxwellian, $\hat{f}_m = (\langle f\rangle/\langle f_m\rangle) f_m$, $\bar{f} = f/\langle f\rangle$ and similarly for $\bar{g}$.

The first two properties are standard (e.g. [CT06]). The third is a straightforward generalization of the CKP inequality [DV05, Kul67] to distributions with non-unit mass. The fourth is a modification of Boltzmann's H-theorem whose proof we present in appendix A.

The inequality (2.18) allows us to impose (2.14) by bounding $\mathcal{H}(\bar{f}_j|\bar{f}_M)$, since (2.18) implies

$$\mathcal{H}(\bar{f}_j|\bar{f}_M) \leq \frac{\varepsilon^2}{2} \implies \frac{1}{n_j}\left\|\hat{f}_M - f_j\right\|_{L^1_v} \leq \varepsilon. \tag{2.20}$$

The result (2.19) states that the role of the term $C(f_j, f_M)$ in (19) is to drive f_j irreversibly toward $\hat{f}_M$. Moreover, (2.19) shows that collisions between f and f_M tighten the L^1 bound monotonically in time. We have not shown that $C(f_j, f_M)$ drives f_j toward $\hat{f}_M$ at any particular rate. However, numerical experiments in section 7 suggest the rate is comparable to ν_{FP}. The final thermalization criterion is

$$\mathcal{H}(\bar{f}_j|\bar{f}_M) \leq \mathcal{H}_c, \tag{2.21}$$

where $\mathcal{H}_c$ is a parameter of the scheme. We specify the scale of this parameter in section 2.6.1.

2.3.2 Idea for Thermalization Scheme

This leads us to a more precise formulation of the thermalization scheme previously proposed: To the jth kinetic particle f_j, assign a passive scalar representing its relative entropy, $\mathcal{H}(\bar{f}_j|\bar{f}_M)$. Whenever it undergoes a collision in a given time-step with a particle whose distribution is given by f_i, we evolve this passive scalar in a way that is consistent with (2.10). If at the end of any time step the particle's relative entropy has dipped below the threshold $\mathcal{H}_c$, we thermalize it.

Similarly, whenever a particle's velocity must be sampled from the Maxwellian component in order to perform a collision, we assign it a relative entropy of zero (corresponding to $f_j \equiv \hat{f}_M$), and evolve it one time step according to the same kinetic equation. If at the end of the time step, the particle's relative entropy exceeds $\mathcal{H}_c$, we dethermalize it, and it carries with it this relative entropy value.

It remains to specify the details of evolving the relative entropy of f_j according to collisional terms in (2.10). The following section is devoted to doing this for the case of Coulomb interactions.

2.4 Approximating Relative Entropy

Toward evaluating $\mathcal{H}(\bar{f}_j|\bar{f}_M)$, we note from (23) that its rate of change due to collisions with f_M during a single time step is

$$(\partial_t \mathcal{H})_M = \int_{\mathbb{R}^3} \log\left(\frac{f_j}{\hat{f}_M}\right) C(\bar{f}_j, f_M)\, d\mathbf{v}, \tag{2.22}$$

where the subscript M indicates that we're only treating collisions with f_M. In 5.3, we show how to extend this treatment to the other terms in (20).

The right hand side of (2.22) is, in general, difficult to evaluate. In particular, evaluating

the right side exactly requires knowledge of the full distribution f_j for each kinetic particle, which is not computationally feasible. We approximate the integral by approximating f_j by a finite-moment truncation of a tensor expansion (see [Cer88], chapter 7). The more moments we keep, the better the approximation of f_j, but the more quantities we have to evolve at each time step for each kinetic particle. We make the compromise of keeping the standard five moments ρ, $\mathbf{u}$, T that define a Maxwellian, corresponding to the assumption that f_j is in fact Maxwellian. This is justified both early in the simulation - when $f_j \approx \delta^3(\mathbf{v} - \mathbf{u}_j)$ - and late - when $f_j \approx \hat{f}_M$.

We will say that f_M has temperature T_M and mean velocity $\mathbf{u}_M$, while f_j has mean velocity $\mathbf{u}_j$ and temperature T_j. Algebraic manipulation of (2.15) reveals that

$$\mathcal{H}(\bar{f}_j|\bar{f}_M) = \frac{3}{2}\left(\frac{T_j - T_M}{T_M} + \log\left(\frac{T_M}{T_j}\right)\right) + \frac{mu_{jM}^2}{2T_M}, \tag{2.23}$$

where m is the common mass of all the particles under consideration and $\mathbf{u}_{jM} = \mathbf{u}_j - \mathbf{u}_M$. Notice that here, in in the remainder of this thesis, we let $kT \to T$, as is common in physical kinetic theoretic literature. To specify the relative entropy in this case, it is thus enough to specify $\mathbf{u}_j$ and T_j, so instead of having to compute the integral in (2.22), we can work with the comparatively simple collisional rates of change of mean velocity and temperature:

$$(\partial_t \mathbf{u}_j)_M = \int_{\mathbb{R}^3} \mathbf{v} C_{FP}(\bar{f}_j, f_M)\, d\mathbf{v}, \tag{2.24}$$

$$(\partial_t T_j)_M = \frac{1}{3} m \int_{\mathbb{R}^3} |\mathbf{v} - \mathbf{u}_j|^2 C_{FP}(\bar{f}_j, f_M)\, d\mathbf{v}. \tag{2.25}$$

This approach has the additional advantage of avoiding the direct approximation of $\partial_t \mathcal{H}$, which can be arbitrarily large, as indeed can $\mathcal{H}$ itself (consider $T_j \to 0$ in (2.23)). Derivatives of $\mathbf{u}_j$ and T_j are much more well behaved.

Some results on the integrals in (2.24) and (2.25) are derived in [HW04], and some others are attributed to Decoster in [JLM96, Lar03]. Here, we make use of both results as well as deriving some that are new to the best knowledge of the authors. Because the derivations are lengthy and the results partially known, we leave the details to appendix B and present only the results here.

Define $\mathbf{F}_{jM}$ as the right hand side of (2.24), and $2W_{jM}/3$ the right side of (2.25). When $T_j \ll T_M$, we show in appendix B that

$$\mathbf{F}_{jM} \approx \mathbf{F}^{\delta}_{jM} \equiv \frac{4\gamma n_M}{m^2 v_{tM}^2} \frac{\mathbf{U}_{jM}}{U_{jM}^3} \left[U_{jM} \frac{d\ \mathrm{erf}(U_{jM})}{dx} - \mathrm{erf}(U_{jM}) \right], \tag{2.26}$$

$$W_{jM} \approx W^{\delta}_{jM} \equiv \frac{2\gamma n_M}{m v_{tM}} \frac{\mathrm{erf}(U_{jM})}{U_{jM}}. \tag{2.27}$$

where $\mathbf{U}_{jM} = \mathbf{u}_{jM}/v_{tM}$, with $v_{tM} = \sqrt{2T_M/m}$ denoting the thermal velocity of f_M. For the definition of the constant γ, see (B.3). Equation (2.26) is equivalent to the analogous result in [JLM96, Lar03].

When $u_{jM} \ll v_{tj}$, with v_{tj} denoting the thermal velocity of f_j, we show in appendix B that

$$\mathbf{F}_{jM} \approx \mathbf{F}^{m}_{jM} \equiv -\frac{1}{\tau_{jM}} \mathbf{u}_{jM}, \tag{2.28}$$

$$W_{jM} \approx W^{m}_{jM} \equiv \frac{1}{\tau_{jM}} \left[\frac{3}{2} \left(1 - \frac{u_{jM}^2}{v_{tj}^2} \right) (T_M - T_j) + m u_{jM}^2 \right], \tag{2.29}$$

where

$$\tau_{jM} = \frac{3\sqrt{\pi} m^2}{16} \frac{\left(v_{tj}^2 + v_{tM}^2 \right)^{3/2}}{\gamma n_M}. \tag{2.30}$$

Note that (2.28) is equivalent to the analogous result in [HW04], while (2.29) is a generalization of the analogous result in same.

2.4.1 Toward a uniformly valid approximation of relative entropy

While the above asymptotic expressions are interesting in their own right, we require expressions that are uniformly valid throughout parameter space. The integrals in (2.24) and (2.25) can be calculated numerically, but the inline evaluation of multi-dimensional integrals is computationally prohibitive in this context. It is possible to reduce the problem to one dimensional integrals dependent on only two non-dimensional parameters (see appendix C), from which a look-up table can be generated. However, numerical experiments presented in section 7.1 show that the majority of the error in our relative entropy estimation comes from

the assumption that f_j is Maxwellian, rather than from the asymptotic assumptions used to derive (2.26)-(2.29). We will therefore find it satisfactory to set

$$(\partial_t \mathbf{u}_j)_M = \begin{cases} \mathbf{F}^{\delta}_{jM} & : u_{jM} \geq \alpha v_{tj} \\ \mathbf{F}^{m}_{jM} & : u_{jM} < \alpha v_{tj} \end{cases} \tag{2.31}$$

$$(\partial_t T_j)_M = \frac{2}{3} \cdot \begin{cases} W^{\delta}_{jM} & : u_{jM} \geq \alpha v_{tj} \\ W^{m}_{jM} & : u_{jM} < \alpha v_{tj} \end{cases} \tag{2.32}$$

where $\alpha \in (0, 1)$. This clearly recovers the correct behavior when $u_{jM} \ll v_{tj}$. To see the recovery of the other limit, we rely on numerical experiments to confirm that when $u_{jM} \gg v_{tj}$, it is also the case that $T_j \ll T_M$, making (2.26)-(2.27) valid. All tests indicate that the properties of the scheme are not sensitive to the choice of α. In all results that follow, we use $\alpha = 0.9$.

2.4.2 Monte Carlo Implementation

Thus far, we have discussed the role of the term $C(f_j, f_M)$ in (2.9)-(20) in the evolution of T_j and $\mathbf{u}_j$. There are two other collisional effects that must be taken into account.

Firstly, we must also evolve T_j and $\mathbf{u}_j$ through collisions with other kinetic particles. That is, we must account for the term $\sum_i C(f_j, f_i)$. This is done by retaining our assumption that each of the particle distributions is a Maxwellian. Then, the difference between treating collisions with f_M and with f_i is merely a matter of changing parameters, since both satisfy the assumptions in previous subsections. For instance, if we were to rewrite (2.29) to give the rate of change of T_j due to collisions with the ith particle, we would have

$$W_{ji} \approx W^{m}_{ji} \equiv \frac{1}{\tau_{ji}} \left[\frac{3}{2} \left(1 - \frac{u^2_{ji}}{v^2_{tj}} \right) (T_i - T_j) + m u^2_{ji} \right], \tag{2.33}$$

where $\mathbf{u}_{ji} = \mathbf{u}_j - \mathbf{u}_i$, and

$$\tau_{ji} = \frac{3\sqrt{\pi} m^2}{16} \frac{\left(v^2_{tj} + v^2_{ti} \right)^{3/2}}{\gamma n_i}. \tag{2.34}$$

The expression (2.33) is then valid when $u_{ji} \ll v_{tj}$. Analogous changes are made to (2.26)-(2.28), and when the jth kinetic particle collides with the ith kinetic particle, we evolve $\mathbf{u}_j$

and T_j according to

$$(\partial_t \mathbf{u}_j)_i = \begin{cases} \mathbf{F}^{\delta}_{ji} & : u_{ji} \geq \alpha v_{tj} \\ \mathbf{F}^{m}_{ji} & : u_{ji} < \alpha v_{tj} \end{cases} \tag{2.35}$$

$$(\partial_t T_j)_i = \frac{2}{3} \cdot \begin{cases} W^{\delta}_{ji} & : u_{ji} \geq \alpha v_{tj} \\ W^{m}_{ji} & : u_{ji} < \alpha v_{tj} \end{cases} \tag{2.36}$$

where the i subscript denotes change due to ith particle.

Secondly, we have so far only looked at the rate of change in $\mathbf{u}_j$ and T_j for one of the two collision partners. The collision also affects the moments of the other distribution. These effects are captured by recalling that collisions conserve momentum and energy. That is,

$$\langle \mathbf{v} \left[C(f,g) + C(g,f) \right] \rangle = 0, \tag{2.37}$$

$$\left\langle v^2 \left[C(f,g) + C(g,f) \right] \right\rangle = 0, \tag{2.38}$$

for any f and g. Therefore, we have

$$\mathbf{F}_{ji} \equiv \langle \mathbf{v} C_{FP}(\bar{f}_j, f_i) \rangle = -\langle \mathbf{v} C_{FP}(\bar{f}_i, f_j) \rangle \equiv -\mathbf{F}_{ij}, \tag{2.39}$$

and

$$2m^{-1} W_{ji} = 2m^{-1} W_{ij} - 2\mathbf{u}_{ji} \cdot \mathbf{F}_{ij}. \tag{2.40}$$

In this way, our treatment of the terms $C(f_j, f_M)$ and $C(f_j, f_i)$ implicitly generates the analogous formulas for $C(f_M, f_j)$ and $C(f_i, f_j)$.

2.5 Algorithm Summary and Error Scalings

Denote the number of simulated particles constituting f_k by N_k, and that constituting f_M by N_m. To generate a numerical solution of the spatially homogeneous LFP equation, at each time step the following substeps are taken.

1. Determine the number of collisions of each type to perform. In the algorithms of Nanbu and TA, each particle undergoes exactly one collision with a randomly selected partner:

(a) $N_{kk} = N_k^2/2(N_k + N_m)$ is the number of collisions between two kinetic particles.

(b) $N_{mk} = N_m N_k/(N_m + N_k)$ is the number of collisions between a kinetic and a Maxwellian particle.

(c) Collisions between Maxwellian particles do not affect the distribution and are thus not simulated.

2. Perform collisions:

   (a) Randomly select N_{kk} kinetic particles, and assign each a partner from among those not already selected. Perform collisions between each pair by altering their actual velocities according to the collision algorithm as well as their mean velocities and temperatures according to (2.35) and (2.36), respectively.

   (b) For each kinetic particle unused in (a), generate a particle with velocity sampled from f_M, and with mean velocity and temperature equal to those of f_M. Perform a collision between this and the kinetic particle as in (a), but evolve the mean velocity and temperature of each particle according to (2.31) and (2.32), respectively.

3. Thermalization/Dethermalization:

   (a) For each kinetic particle, compute $\mathcal{H}(\bar{f}_j|\bar{f}_M)$ from $\mathbf{u}_j, T_j$ using (2.23). If this quantity is less than $\mathcal{H}_c$, remove the particle from the kinetic component, increment N_m and decrement N_k.

   (b) For each particle sampled from f_M, compute $\mathcal{H}(\bar{f}_j|\bar{f}_M)$ as in (a). If this number exceeds $\mathcal{H}_c$, add the particle to the kinetic component, decrement N_m and increment N_k.

4. Enforce conservation:

   (a) Adjust u_M so that the total momentum in the system is the same as before the collisions.

(b) Adjust T_M so that the total energy in the system is the same as before the collisions.

If there exists spatial dependence in the problem, fluid equations which adjust n_M, $\mathbf{u}_M$, and T_M must also be evolved.

2.5.1 Choice of $\mathcal{H}_c$

The algorithm outlined above has one free parameter: $\mathcal{H}_c$, the value of relative entropy below which a particle is thermalized and above which it is dethermalized. We now present an argument that specifies the scale of this quantity, although not its precise value.

Notice that, unlike the thermalization process, the dethermalization process occurs over a single time step. That is, if the scheme doesn't dethermalize a given particle, that particle is inserted back into the Maxwellian and its interaction with the kinetic component of the scheme is forgotten. Accuracy demands that this does not happen to *every* particle sampled from the Maxwellian, so that some particles get dethermalized. Thus, $\mathcal{H}_c$ should not be much larger than the change in relative entropy experienced by a Maxwellian particle in a single time step.

Similarly, efficiency demands that not every sampled particle be dethermalized. Therefore, $\mathcal{H}_c$ should not be much smaller than the aforementioned change in relative entropy. We conclude that $\mathcal{H}_c$ should be comparable to the typical change in relative entropy experienced by a particle sampled from the Maxwellian. It remains only to specify this scale.

Denote the change in temperature a Maxwellian particle undergoes during a collision with a kinetic particle by ΔT and the change in u by Δu. If we assume $\Delta T/T_M \ll 1$, then to leading order in (2.23), the change in relative entropy is

$$\Delta\mathcal{H} \approx \frac{3}{4}\left(\frac{\Delta T}{T_M}\right)^2 + \left(\frac{\Delta u}{v_{tM}}\right)^2. \tag{2.41}$$

From (2.29) and (2.40), we can estimate ΔT.

$$\Delta T \approx \frac{8}{\sqrt{\pi}}\frac{\gamma}{m^2 v_{tM}^3} T_M \Delta t. \tag{2.42}$$

Similarly, by using (2.28), we can estimate

$$\Delta u \approx \frac{3}{4\sqrt{\pi}} \frac{\gamma}{m^2 v_{tM}^3} u \Delta t \tag{2.43}$$

By rewriting the above in terms of $t_{FP} = \nu_{FP}^{-1}$ using (1.68) and (B.3), then plugging into (2.41), we have

$$\mathcal{H}_c \approx \Delta\mathcal{H} \approx \frac{12}{\pi}\left(1 + \frac{3}{256}\left(\frac{u}{v_{tM}}\right)^2\right)\left(\frac{\Delta t}{t_{FP}}\right)^2 \approx 3.8\left(\frac{\Delta t}{t_{FP}}\right)^2. \tag{2.44}$$

In the last approximation, we've assumed that u is not so large as to make the second term significant, which is valid so long as $u \lesssim 9 v_{tM}$. In general, we set

$$\mathcal{H}_c = c\left(\frac{\Delta t}{t_{FP}}\right)^2 \tag{2.45}$$

for some c we choose. Unless otherwise specified, we use $c = 12.9$ henceforth. This choice makes the errors more visible, although the fidelity of the results is not sensitive to this choice.

This scaling for $\mathcal{H}_c$ implies that the (de-)thermalization error scales like Δt, since by (2.20) we have

$$\mathcal{H}(\bar{f}_j | \bar{f}_M) \leq O\left(\frac{\Delta t^2}{t_{FP}^2}\right) \implies \frac{1}{n_j}\left\| f_j - \hat{f}_M \right\|_{L_v^1} \leq O\left(\frac{\Delta t}{t_{FP}}\right). \tag{2.46}$$

In numerical experiments to follow, we find that the accuracy and efficiency of the scheme are each insensitive to changes in $\mathcal{H}_c$ within a factor of 10 to 100 around the value in (2.44).

2.5.2 Error Analysis

For a spatially homogeneous scheme using the collision algorithm of TA or Nanbu, we have

$$\| f_{true} - f_{MC} \|_{L_v^1} = O\left((\Delta t / t_{FP})^q\right) + O(N^{-1/2}), \tag{2.47}$$

where f_{true} is the analytic solution and f_{MC} its approximation by a standard Monte Carlo method with N particles and time step Δt. The exponent q is between $1/2$ and 1, but is left

unspecified to account for the fact that the temporal convergence rate of the TA and Nanbu schemes remains a subtle issue [BP13].

A hybrid method which never thermalizes particles and dethermalizes every particle sampled from the Maxwellian component reproduces the result of the Monte Carlo scheme in expectation. Moreover, because each simulated particle carries equal weight, we have $n_j = n/N$. Thus, each thermalization or failed dethermalization event introduces an $O(\Delta t/t_{FP}N)$ error by (2.46). There are $O(N)$ failed dethermalizations at each time step, and $O(1/\Delta t)$ total time steps, so there are $O(N/\Delta t)$ failed dethermalizations over the course of the simulation.

Contrast this with the scaling of the number of thermalization events. This number may be said to be $\mathcal{F}(\mathcal{H}_c)O(N)$, where $\mathcal{F}$ is the fraction of the simulated particles that are thermalized during a simulation, which is clearly an increasing function of $\mathcal{H}_c$. Since, in addition, $\mathcal{H}_c$ is an increasing function of Δt, we may say that $\mathcal{F} = O(\Delta t^\beta)$ for some $\beta > 0$. This gives the overall scaling

$$\|f_{MC} - f_{hybrid}\|_{L^1_v} = O\left(\frac{\Delta t}{t_{FP}N}\right)\left(O\left(\frac{N}{\Delta t}\right) + O\left(N\Delta t^\beta\right)\right) = O\left(t_{FP}^{-1}\right) + O\left(\frac{\Delta t^{1+\beta}}{t_{FP}}\right). \tag{2.48}$$

Combining (2.47) and (2.48) gives the error scaling for the hybrid scheme proposed here:

$$\|f_{true} - f_{hybrid}\|_{L^1_v} = O\left(\left(\frac{\Delta t}{t_{FP}}\right)^q\right) + O\left(N^{-1/2}\right) + O\left(t_{FP}^{-1}\right) + O\left(\frac{\Delta t^{1+\beta}}{t_{FP}}\right), \tag{2.49}$$

where the first term is the finite time step error, the second the sampling error, the third the (failed) dethermalization error, and the fourth the thermalization error.

The formal derivation of (2.49) is hardly rigorous, and in particular has the following weakness: it assumes that we know the *actual* value of the relative entropy for each f_j, when in fact we only have an estimate of it based on the assumption that f_j is Maxwellian. The derivation of (2.49) remains unchanged if we have

$$\mathcal{H}^{true} \leq k\mathcal{H}^{est} \tag{2.50}$$

for some $k > 0$, where the superscript *true* indicates the actual relative entropy for a given particle, and *est* indicates our estimate of that quantity.

However, for any $\mathcal{H}^{est}$ computed using a finite moment truncation of f_j, there exist pathological cases in which $\mathcal{H}^{est} = 0$ while $\mathcal{H}^{true}$ is strictly positive, so (2.50) cannot hold in general. However, for many problems these pathological conditions may not be achieved, giving hope that (2.49) may be realized. Indeed, results in the following section are consistent with the scaling relations presented here.

2.5.3 Dethermalization Error

Since failed dethermalizations are shown in (2.49) to be the dominant error source, it warrants more discussion. In particular, having seen that this error doesn't scale with Δt or N, we seek to understand what sets the size of this error.

By (2.18) and (2.44), we have a bound on the error incurred by each failed dethermalization event, which we denote by ε_e:

$$\varepsilon_e \leq \sqrt{2c}\frac{n}{N}\frac{\Delta t}{t_{FP}} \tag{2.51}$$

for some constant c. The growth rate of this error, denoted by ε_t, is thus given by

$$\varepsilon_t = \varepsilon_e \mathcal{R}, \tag{2.52}$$

where $\mathcal{R}$ is the number of failed dethermalization events per unit time, which may be written as

$$\mathcal{R} = \frac{n_k}{n}\frac{N}{\Delta t} \tag{2.53}$$

when n_k/n is small. Combining (2.51)-(2.53), we have

$$\frac{\varepsilon_t}{n} \leq \frac{\sqrt{2c}}{t_{FP}}\frac{n_k}{n}, \tag{2.54}$$

where we divide through by n so that the right side may be thought of as a fractional error.

The t_{FP} above is the characteristic time for collisions between f_M and f_k, which will change throughout the simulation. We find it instructive to express the same statement in terms of the characteristic time for collisions within f_M, denoted by t_{FP}^M.

$$\frac{\varepsilon_t}{n} \leq \frac{\sqrt{2c}}{t_{FP}^M}\frac{n_k}{n}\left(\frac{v_{tM}}{u_{kM}}\right)^3, \tag{2.55}$$

where u_{kM} is the characteristic relative velocity between a particle sampled from f_k and one from f_M.

The inequality (2.55) highlights two ways in which the dethermalization error can be made small: the kinetic component can be small - i.e. $n_k \ll n$ - and/or the kinetic component can have velocity very different from the maxwellian component - $u_{kM} \gg v_{tM}$. Moreover, the case in which neither of these conditions is realized is short lived, as a kinetic component with $u_{kM} \lesssim v_{tM}$ will be rapidly thermalized.

We compare results from numerical tests to the predictions of (2.55) in the following section.

2.6 Numerical Results

We perform two types of numerical test. First, we check that the approximations (2.23), (2.31), and (2.32) capture the actual evolution of relative entropy through collisions with a Maxwellian background. Second, we test the entire algorithm's accuracy and efficiency against pure Monte Carlo simulations in two test cases: the relaxation of a slightly anisotropic Maxwellian and a bump-on-tail distribution.

2.6.1 Testing Relative Entropy Approximations

We are interested in the following problem: given a distribution $f(\mathbf{v}, t)$ solving

$$\partial_t f = C_{FP}(f, f_m), \qquad f(\mathbf{v}, 0) = \delta(\mathbf{v} - \mathbf{v_0}), \tag{2.56}$$

where f_m is Maxwellian and constant in time, what is the time evolution of $\mathcal{H}(f|f_m)$?

We attack the problem in three different ways. First, we represent f by a single test particle with initial velocity $\mathbf{v_0}$, and evolve its velocity according to the algorithm of TA, where each collision partner has velocity sampled from f_m. The test particle's velocity is then a random variable $\mathbf{v_p}(t)$ whose distribution is given by $f(\mathbf{v}, t)$. By simulating the evolution of $\mathbf{v}_p$ repeatedly, we may generate - at each t - a histogram that, by definition,

approximates f at that time. We then evaluate $\mathcal{H}(f|f_m)$ by direct numerical integration of (2.15). This will be thought of as the true value of the relative entropy, as it is subject only to the errors in the Monte Carlo scheme and the numerical integration, each of which can be made arbitrarily small. Results from this method are plotted in solid blue in fig. 1.

Second, we evolve the mean velocity and temperature of f according to the collisional moments $\mathbf{F}$ and W under the assumption that f is a Maxwellian. $\mathbf{F}$ and W are numerically integrated (refer to (C.5) and (C.11) in appendix C) to find the rates of change of $\mathbf{u}$ and T, which are then evolved by forward Euler and plugged into (2.23) to find $\mathcal{H}$. This method is designed to test the validity of the assumption that f is Maxwellian, since this is the only assumption made here that was not used in the direct simulation of collisions outlined above. Results from this method are plotted in dash-dot black in fig. 1.

Third, we evolve $\mathbf{u}$ and T according to the numerical solution of the ODEs (2.31) and (2.32), then evaluate $\mathcal{H}$ using (2.23). This tests the validity of our asymptotic expressions, since this is the only assumption used here but not in the previous method. Results from this method are plotted in dashed red in fig. 1.

Fig. 2.6.1 shows the values of u, T, and $\mathcal{H}(\bar{f}_j|\bar{f}_M)$ computed from each of the three methods above for three different values of v_0. From this, we conclude that the approximations (2.23), (2.31), (2.32) are a satisfactory framework for the approximation of relative entropy evolution. In particular, the approximation captures the monotonicity and overall rate of relative entropy decay, and is especially accurate when the relative entropy is small, which is of particular importance for our application.

Increased accuracy in the evolution of T and $\mathbf{u}$ may be obtained through numerical integration of (B.5), (B.14), which may be of independent interest, but this does little to improve the relative entropy approximation, and in fact even degrades the quality of the approximation in some regimes (see bottom right plot in fig. 1). The numerical evaluation also greatly increases the complexity of the scheme in practice, so we use the asymptotic approximations (2.23), (2.31), and (2.32) in all numerical tests that follow.

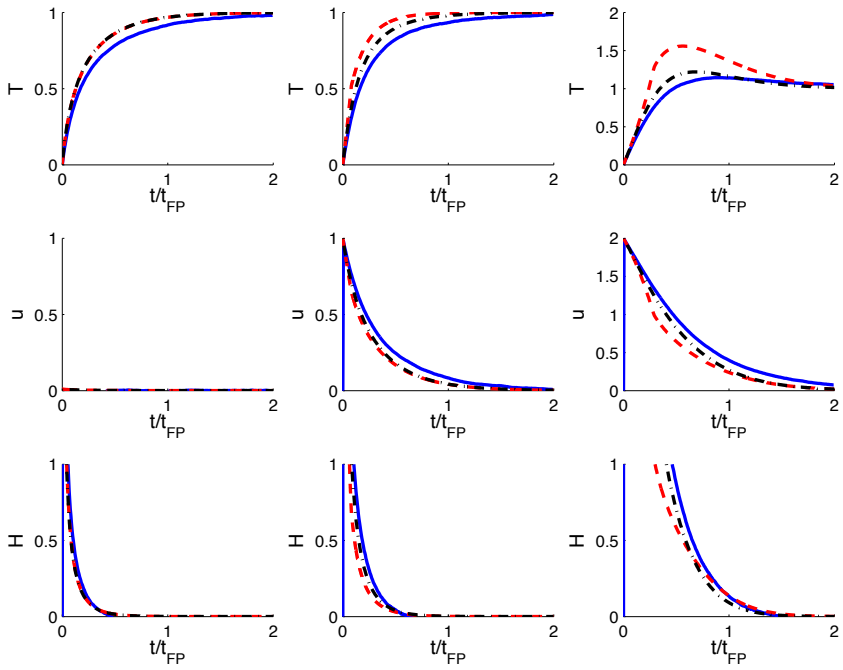

Figure 2.1: Comparison of scaled temperature (T), mean velocity (u), and relative entropy (H) of the distribution of a test particle in a Maxwellian background computed by three different methods: direct Monte Carlo collision simulation (solid blue), evolution via numerical integration of $\mathbf{F}$ and W (dash-dot black), and evolution according to the asymptotic expressions (2.31) and (2.32) (dashed red). The left-most column has $v_0 = 0$, the middle $v_0 = v_{tM}$, and the right-most $v_0 = 2v_{tM}$

2.6.2 Full Numerical Tests

We now present numerical results for the full algorithm outlined in section 6 when applied to two test problems: a slightly anisotropic Maxwellian, and a bump-on-tail distribution.

As the goal of this algorithm is to accelerate the simulation of collisions, a discussion of computational cost is warranted. To leading order, the computational cost of collisional simulation is proportional to the number of collisions simulated during the scheme, which is proportional to the number of simulated particles, averaged over the full run. Therefore, a

hybrid scheme of the type we discuss is faster than a pure Monte Carlo scheme by a factor of roughly

$$\mathcal{S} = \left\langle \frac{N}{N_k} \right\rangle = \left\langle \frac{N_m + N_k}{N_k} \right\rangle, \tag{2.57}$$

where the angle brackets now represent an average over all time steps. This is the measure of efficiency we use when testing schemes of the types outlined in sections 3.1 and 3.2.

However, the entropy based scheme proposed here incurs an additional computational load for each collision due to the passive scalars that must be evolved. The cost of the simulation of any given collision is roughly proportional to the number of scalar quantities that must be evolved. This implies that the analogous efficiency measure for the entropy based scheme is

$$\mathcal{S}_H = \frac{3}{4 + d_u} \left\langle \frac{N_m + N_k}{N_k} \right\rangle, \tag{2.58}$$

where d_u is the number of components of $\mathbf{u}$ that we track, which will be problem dependent. In most cases, d_u is the number of spatial dimensions in the problem since velocities in other dimensions are assumed to vanish on average. However, in problems with no spatial dependence but non-Maxwellian initial data, we will require $d_u \neq 0$. In the bump-on-tail problem in 7.2.2, for instance, we set $d_u = 1$.

All of the following results were performed in a dimensionless formulation with $m = 1$, $t_{FP}^M = 5.348275$, $T = 0.05065776$, and $n = 0.1$ (consistent with parameters in [CWD08]).

2.6.2.1 Two-temperature Maxwellian Relaxation

We first test the fidelity of our implementation in a scenario with a known approximate solution. Consider the initial distribution

$$f = \frac{n m^{3/2}}{(2\pi)^{3/2} T \sqrt{T + \delta T}} \exp\left(-\frac{m(v_x^2 + v_y^2)}{2T} \right) \exp\left(-\frac{m v_z^2}{2(T + \delta T)} \right) \tag{2.59}$$

with $\delta T \ll T$. In [Tru65], Trubnikov showed that the temperature difference δT - to leading order - decays exponentially in time:

$$\delta T(t) = \delta T(0) e^{-t/\tau}, \tag{2.60}$$

with τ given in Gaussian units by

$$\tau = \frac{5}{8\sqrt{\pi}} \frac{\sqrt{m} T^{3/2}}{n e^4 \log \Lambda}. \tag{2.61}$$

In fig. 2, we compare this approximate solution to the method of TA and the entropy-based hybrid method proposed here. We use $\delta T(0)/T = 1/10$, $\Delta t = t_{FP}^M/20$, and $N = 1.024 \times 10^6$ with the other parameters as described above. We find agreement between all

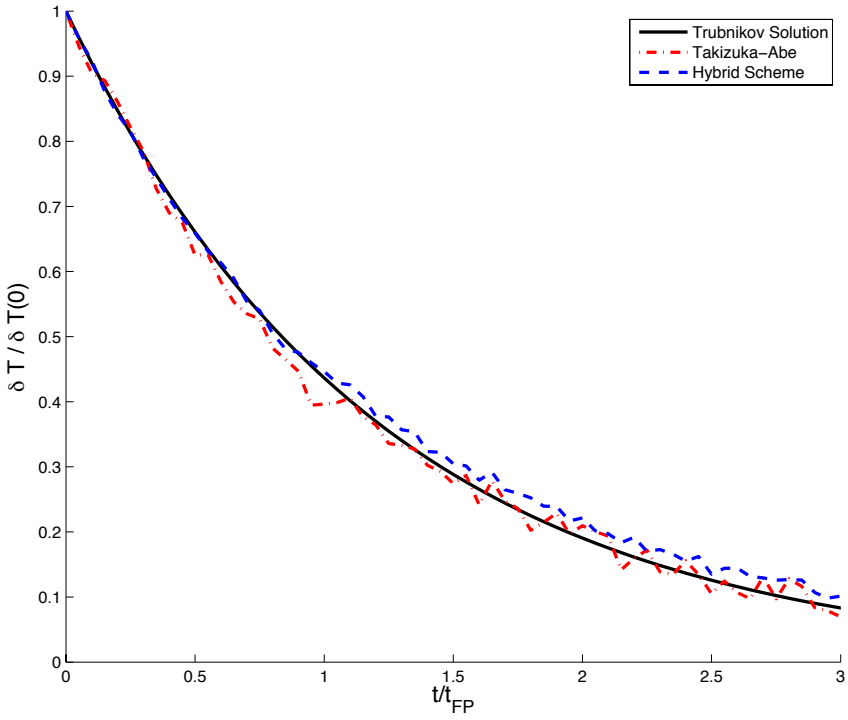

Figure 2.2: The temperature anisotropy in a two temperature Maxwellian as a function of time. Computation compares the linearized analytic result (solid black), pure Monte Carlo using Takizuka-Abe (dash-dot red), and the hybrid scheme proposed herein (dashed blue).

three solutions up to the level of statistical fluctuations in the numerical solutions.

2.6.2.2 Accuracy and Efficiency Tests

The bump-on-tail initial distribution we treat is given by

$$f(t=0) = f_m(\mathbf{v}; \beta n, \mathbf{0}, T) + f_m(\mathbf{v}; (1-\beta)n, \mathbf{u}_k, T_k) \tag{2.62}$$

with $\beta \in (0,1)$ corresponding to the fraction of the total mass in each Maxwellian. We set the initial f_M equal to the first Maxwellian term and f_k equal to the second, and display plots for $\beta = 0.9$, $\mathbf{u}_k = 2.83 v_{tM} \widehat{\mathbf{x}}$, and $T_k = 10^{-4}$.

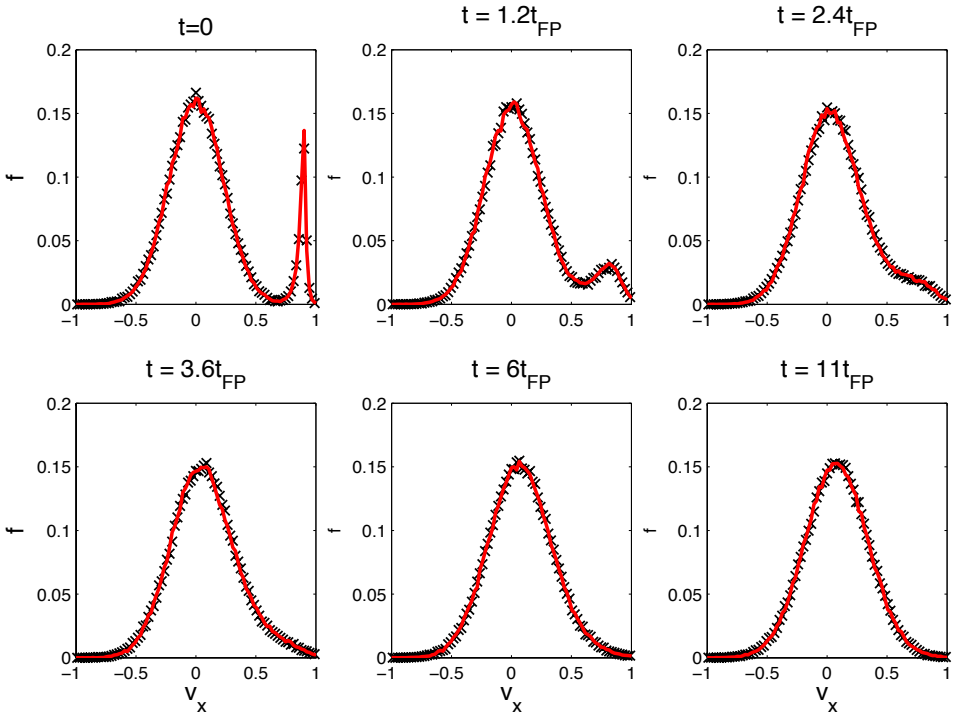

Figure 2.3: Six time snapshots of the velocity distribution in the x dimension for the bump-on-tail problem. Monte Carlo solution: solid red; hybrid solution: black "x".

In fig. 3, we plot a time series of the hybrid solution compared to the Takizuka-Abe solution using $\Delta t = t_{FP}^M/20$ and $N = 256,000$ total particles. The plots show excellent qualitative agreement between the pure Monte Carlo solution and the hybrid solution with $S_H \approx 10$.

In fig. 4, we compare the efficiency and accuracy of the entropy-based scheme proposed

here to the scattering angle-based scheme outlined in section 3.2. Analogous results for the velocity-based scheme described in section 3.1 may be found in [CWD08], showing inferior performance compared to both schemes tested here. For each scheme, the accuracy is measured by

$$\Gamma_{acc} = \frac{1}{t_{max} n} \int_0^{t_{max}} \| f_{MC}(t) - f_{hybrid}(t) \|_{L^1_v} \, dt, \tag{2.63}$$

the same measure used in [CWD08]. We set $t_{max} = 11 t_{FP}$ to capture most of the progress toward equilibrium shown in fig. 3, although the results we present are not sensitive to this choice.

For the scattering angle-based scheme, we set

$$p_T = \min \left\{ k \sin \frac{\theta}{2}, 1 \right\}, \tag{2.64}$$

where θ is the scattering angle in the two-particle center of mass frame, and vary k to change the efficiency - $\mathcal{S}$ - of the scheme. For the entropy based scheme, we vary the efficiency $\mathcal{S}_H$ by varying $\mathcal{H}_c$ about the value prescribed in (2.44).

We test each scheme in two cases. In the first, no particle is ever dethermalized. In the second, we dethermalize particles according to $p_D = p_T/2$ for the scattering angle based scheme and as described in section 6 for the entropy based scheme. This is intended to test whether collisionally driven dethermalization plays a significant role in the evolution of the distribution and how efficiently each scheme handles the dethermalization process. Results for $\Delta t = t^M_{FP}/20$ and $N = 256,000$ are shown in fig. 4. The sampling error is estimated at 0.015 by comparing multiple independent Monte Carlo simulations.

We see immediately the improved accuracy effected by the entropy-based scheme for a fixed number of simulated collisions by comparing the green and red curves. However, the additional computational load incurred by the entropy scheme effectively cancels this gain in the absence of dethermalization, as seen by comparing the blue and red curves. However, in the presence of dethermalization the advantage is restored - seen by comparing magenta and black.

Moreover, we notice that adding dethermalization has no effect on the efficiency of the

entropy scheme (compare blue and magenta curves in fig. 4), while it degrades that of the scattering angle scheme (compare red and black curves). Dethermalization slows the scattering-angle scheme because dethermalized particles are slow to be re-thermalized. In the entropy scheme, on the other hand, recently dethermalized particles are re-thermalized quickly because they have particle temperature and mean velocity very close to those of the Maxwellian. We discuss the consequences of these observations in more detail in section 8.

2.6.2.3 Convergence Study

In fig. 5 we present a numerical convergence study comparing the various sources of error in (2.49), again using the bump-on-tail initial distribution. In an effort to isolate the systematic errors, we increase the number of simulated particles to $N = 2.5398 \times 10^6$. We use time steps $\Delta t = t_{FP}^M 2^{-k}$ for $k = 2, ..., 7$. The sampling error is of course not completely eliminated, and is thus subtracted from each curve in fig 5. For each curve, the sampling error is estimated by comparing multiple independent simulations.

The red, unmarked curve in fig. 5 shows the errors between Monte Carlo schemes at the various time steps and the Monte Carlo scheme at the finest time. The black, x-marked curve shows errors for the entropy-based hybrid scheme with no thermalization (we simply skip step 3a in section 6), i.e. it shows the dethermalization error. As expected, this curve is asymptotically constant, and begins to show the time-stepping error only to the right of the plot when time-stepping error becomes comparable to the dethermalization error.

The blue, square-marked curve shows errors for the entropy based hybrid scheme exactly as summarized in section 6. The difference between the blue and black curves is the thermalization error, shown in the green, triangle-marked curve, and is found to scale like $o(\Delta t)$, as predicted in (2.49). All hybrid simulations presented in the plot have $\mathcal{S}_H \geq 5.9$, with the full hybrid simulations (blue) having efficiency as high as $\mathcal{S}_H \approx 8.6$.

We notice that the time stepping error appears to be smaller by a constant factor for the hybrid scheme as compared to the Monte Carlo simulations - i.e. at the right edge of fig. 5,

the blue, square marked curve lies slightly below the red, unmarked curve. We hypothesize that this is because only a small portion of the distribution is subject to the time stepping error in the hybrid scheme, while the whole of the distribution is subject to it for Monte Carlo schemes.

Moreover, we note that the slope of the red, unmarked curve may be of interest independent of the hybrid scheme, for we find $O(\Delta t)$ convergence, consistent with formal arguments in [BN00, CWD08], but at odds previous empirical results [WLC08] and improved relative to the rigorous argument in [BP13].

2.6.2.4 Dethermalization Error Study

Lastly, we test some of the predictions of (2.55) using the bump-on-tail distribution. We investigate the rate of error generation by plotting the L^1 difference between the hybrid and Monte Carlo solutions as a function of time, using only dethermalization. We vary u_k in (2.62), which is analogous to u_{kM} in (2.55), and display the results in fig. 6.

Notice that, as expected, increasing u_k decreases the error generation rate, while decreasing u_k shortens the time to equilibration. Moreover, the scale of the error generation rate is correctly predicted by (2.55). For instance, with $u_k = 2.83 v_{tM}$, (2.55) sets an upper bound on the error generation near two percent per t_{FP}^M, while the plot shows a maximum rate of approximately one percent per t_{FP}^M.

2.7 Discussion and Conclusions

A hybrid algorithm for the accelerated simulation of Coulomb collisions has been presented. The algorithm is derived directly from the LFP equation without appealing to the ad hoc modeling used in other hybrid particle methods [CWD08, Hew03, Lar03], permitting quantification of error sources and scalings, at least at a formal level. The accuracy and efficiency of the method are confirmed by the results of numerical simulations. Moreover, for this method the number of kinetic particles tends to zero as equilibrium is approached, thus re-

covering the efficiency of a fluid scheme for Maxwellian distributions, which is not a feature of the scheme in [CWD08].

It is an unfortunate - but not unexpected - consequence of the approximations used to accelerate the algorithm that the hybrid scheme does not converge as $\Delta t \to 0$. It bears noting that one could make the hybrid scheme presented here formally convergent by taking the relative entropy cutoff $\mathcal{H}_c = O(\Delta t^k)$ for any $k > 2$. However, such a scheme inevitably has the property that the speed-up factor $\mathcal{S} \to 1$ as $\Delta t \to 0$, thus recovering the computational efficiency of a Monte Carlo scheme in the limit. The choice of $k = 2$ made in the preceding results is the unique choice that bounds the computational gain from below and the error from above. Moreover, we demonstrate in sections 6.3 and 7.2.4 the ability to predict the scale of the dominant error and find it to be small for the intended applications.

For a given number of simulated particles, the entropy based scheme has been shown to be more accurate than the particle- and scattering angle-based schemes. However, the additional computational load incurred by the tracking of the passive scalars assigned to each particle is seen to effectively cancel this gain in the case of a spatially homogeneous relaxation process. However, in the application of the hybrid scheme to problems with other potentially destabilizing agents - e.g. spatial inhomogeneity or electromagnetic fields - we expect that the dethermalization error will become more significant, and it is reasonable to expect the entropy scheme's improved treatment of dethermalization to yield dividends.

There are a number of directions in which the present work could be extended. The first is the treatment of spatially inhomogeneous problems, which is of obvious importance for application to real world scenarios, and may reveal more benefits of the entropy scheme, as just mentioned. A second is the extension to other collision operators, which only requires modification of the expressions for W and $\mathbf{F}$. Thirdly, one might incorporate unequal weighting of the simulated particles [HK94], potentially including negative weights as in [HH07]. The incorporation of negative weights is of particular interest because it would allow the scheme to efficiently capture small negative deviations from Maxwellian distributions. A fourth is to use the numerical evaluation of the expressions in appendix C to evolve the rel-

evant passive scalars, which may yield a more robust scheme. Other directions include the potential for adaptively choosing the number of moments used to approximate the particle distributions and the possibility of fusing multiple kinetic particles when the relative entropy between them is small so as to further reduce computational cost, an approach similar to [Hew03, Lar03]. Each of these is a topic of current research of the authors.

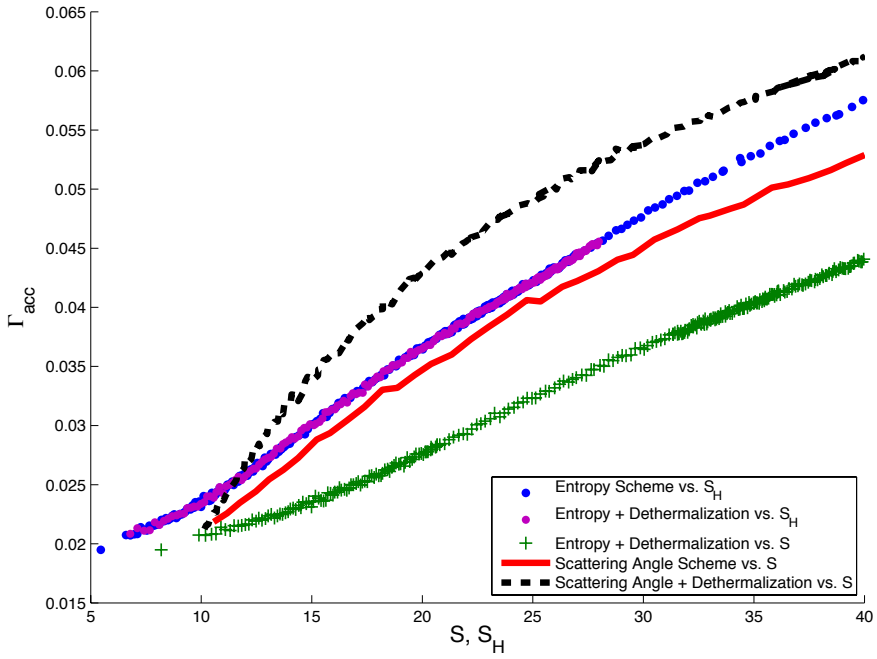

Figure 2.4: A comparison of accuracy Γ_{acc} and efficiency $\mathcal{S}$, $\mathcal{S}_H$ for four different realizations of a hybrid scheme: the entropy-based and scattering angle-based schemes, each with and without dethermalization. The entropy scheme is plotted against both $\mathcal{S}$ (green '+') and $\mathcal{S}_H$ (blue and magenta dots). The scattering angle scheme is plotted both with thermalization (dashed black) and without (solid red). Comparing the green '+' curve to the solid red and dashed black compares the entropy and scattering angle schemes when the number of simulated particles is equal. Comparing the dotted blue to the solid red compares the two schemes when the total computational load is equal and when there is no dethermalization. Comparing the dotted magenta to the dashed black compares the two schemes for equal computational load when thermalization is present. A sixth possible curve - Entropy scheme without dethermalization vs. $\mathcal{S}$ - is not plotted, because it falls directly on top of the green '+' curve.

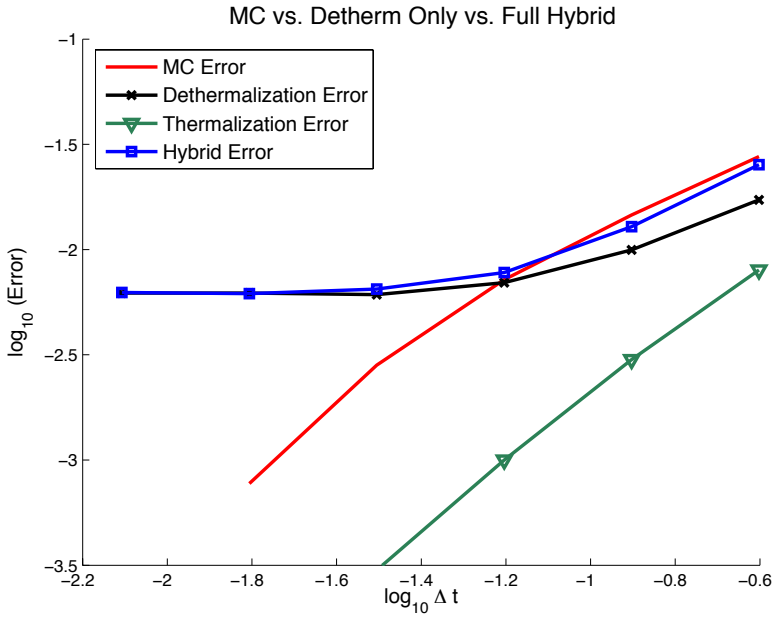

Figure 2.5: A comparison of the errors incurred by pure Monte Carlo and hybrid schemes.

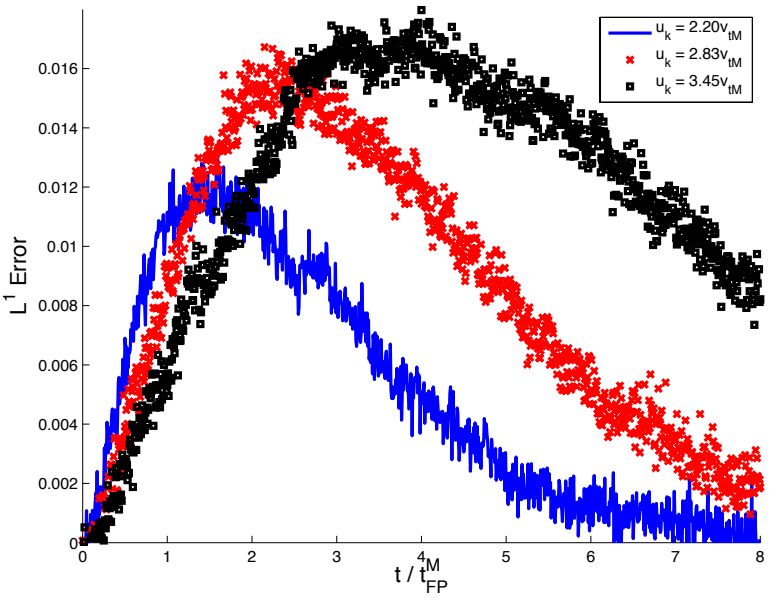

Figure 2.6: The systematic L^1 dethermalization error as a function of time for three different initial conditions.

CHAPTER 3

Multi-Level Monte Carlo - Improvements

3.1 Introduction

Stochastic differential equations (SDEs) have numerous applications: neuroscience [Bur06, KW87], chemical kinetics [Gil00], civil engineering [HFU88, Har77], biological fluid dynamics [KPA08], plasma physics [LWD09, MT04], particle physics [Lee94], polymer dynamics [Fre02], and finance [Shr04], to name a few. While the author's primary interest is in plasma physical applications, the methods presented in this thesis are of more general applicability. As such, the presentation here will be more mathematical in nature, and various applications will be mentioned but not dwelled upon. For a more detailed discussion of the plasma applications of multilevel Monte Carlo, see [RRD13].

A prototypical class of problems appearing in many of the applications above may be characterized as follows: let $\mathbf{S}(t) \in \mathbb{R}^d$ satisfy the system of SDEs

$$dS_i = a_i(\mathbf{S}, t)\, dt + \sum_{j=1}^{D} b_{ij}(\mathbf{S}, t)\, dW_j, \qquad \mathbf{S}(0) = \mathbf{S}_0 \tag{3.1}$$

for $t \in [0, T]$ and some given $\mathbf{S}_0$, where S_i is the i^{th} component of $\mathbf{S}$, $W(t) \in \mathbb{R}^D$ is a D dimensional Brownian motion, $a_i : \mathbb{R}^d \to \mathbb{R}$ for each $i \in \{1, 2, ..., d\}$, and similarly for b_{ij}. Then, for some given $P : \mathbb{R}^d \to \mathbb{R}$, evaluate $\mathbb{E}[P(\mathbf{S}(T))]$. That is, we wish to find the mean value of some functional of the solution of an SDE.

Since exact solutions are available for only the simplest of SDEs, finite difference methods are frequently used to approximate their solutions. The expectation is then evaluated via a Monte Carlo method. The purpose of the present chapter is to present three improvements

to the class of multilevel Monte Carlo (MLMC) methods - introduced in [Gil08b] - which are the current state of the art.

The MLMC methods themselves improve upon the most straightforward numerical method for the archetypal SDE problem above. That method is to approximate the SDE's solution by the well-known Euler-Maruyama discretization with time step h, given by

$$S_{i,n+1} = S_{i,n} + a_i(\mathbf{S}_n, t_n)h + \sum_{j=1}^{D} b_{ij}(\mathbf{S}_n, t_n)\Delta W_{j,n}, \tag{3.2}$$

where $\mathbf{S}_n$ approximates $\mathbf{S}(t_n)$, with $t_n = nh$, and the $\Delta W_{j,n}$ are independent normal random variables with mean zero and variance h. We may then generate N independent samples of $\mathbf{S}_{T/h}$ by generating different $\Delta W_{j,n}$ for each sample, and estimate the desired expectation by

$$\mathbb{E}[P(\mathbf{S}(T))] \approx \frac{1}{N}\sum_{r=1}^{N} P\left(\mathbf{S}_{T/h}^{(r)}\right), \tag{3.3}$$

where r indexes the N samples.

One desires to approximate the true expectation to within an RMS error ε, which will scale as $O(N^{-1/2})$ and $O(h)$. The computational cost of the scheme is proportional to the total number of time steps taken, which scales as $O(N/h)$. Thus, we see that the computational cost of achieving an RMS error[1] ε - which we henceforth denote by K - is $O(\varepsilon^{-3})$.

In many contexts, such a scaling is prohibitive, so a number of methods which improve upon it have been developed. To understand them, we must define the notions of strong and weak errors for SDE approximations. Let $\mathbf{S}_h$ be an approximate solution of (3.1) obtained by some discretization with time-step h. We say that discretization has *weak error* of order p if

$$|\mathbb{E}[g(\mathbf{S}_h)] - \mathbb{E}[g(\mathbf{S})]| = O(h^p) \tag{3.4}$$

for some broad class of functions $g : \mathbb{R}^d \to \mathbb{R}$ (in particular, that class should include P). We say that discretization has *strong error* of order q if

$$\mathbb{E}\left[|\mathbf{S}_h - \mathbf{S}|\right] = O(h^q). \tag{3.5}$$

[1]Root Mean Square (RMS) error is defined in the usual way - $\sqrt{\mathbb{E}[(S_{true} - S_{approx})^2]}$

We note that the Euler discretization has $p = 1$ and $q = 1/2$ [KP11].

It is straightforward to see that if we modify the naive scheme presented above to use a discretization of weak order p, we have

$$K = O\left(\varepsilon^{-(2+1/p)}\right), \tag{3.6}$$

independent of q. In contrast, the multilevel Monte Carlo (MLMC) methods introduced in [Gil08b] and expanded in [Gil08a, GS12a] achieve

$$K = \begin{cases} O\left(\varepsilon^{-2}(\log \varepsilon)^2\right) & : q = 1/2 \\ O\left(\varepsilon^{-2}\right) & : q > 1/2 \end{cases} \tag{3.7}$$

so long as $p > 0$. The proof of this fact may be found in [Gil08b], and we sketch the argument in section 2.

We thus see that the multilevel method scales better than the naive method outlined above for *any* discretization with finite weak order p. Moreover, the larger the weak order of a discretization, the more regularity we require of P to achieve that order [KP11], further limiting the use of high-order weak schemes. Multilevel schemes are thus a great improvement over simple schemes of the type outlined above.

The MLMC schemes achieve their improved cost scaling by approximating the SDE's solution with many different time-steps (called 'levels') and taking advantage of the discretization's strong convergence to get low variance estimates of the difference in the payoff at adjacent levels. The remaining high variance quantity - the payoff's expectation at the lowest level - is relatively cheap to compute because of the large time-step. However, the algorithm could be further improved by also applying a variance reduction at this lowest level. The first contribution of the present work is to show that, when the payoff function is twice continuously differentiable, we can reduce the variance at the lowest level to zero by finding the payoff using Ito's lemma instead of direct evaluation.

Our second contribution is to again make use of Ito's lemma to derive a variant of the MLMC method that achieves the cost scaling $O(\varepsilon^{-2})$ in spite of having $q = 1/2$. This is a

desirable result because discretizations with $q > 1/2$ require the simulation of Lévy areas when $D > 1$, and Lévy areas are notoriously difficult to sample. Indeed, no suitable algorithm has been implemented for $D > 2$. A method achieving $O(\varepsilon^{-2})$ scaling without Lévy area simulation was also derived in [GS12a]. However, the method we propose, while similar in some respects, is simpler to derive and slightly faster for twice differentiable payoffs.

Thirdly, we make use of our analysis to generalize the antithetic method in [GS12a] to arbitrary refinement factor - that is, the ratio between the time-steps at adjacent levels. The method was originally derived for the case of refinement factor $M = 2$, but we show that $M \approx 4$ to 5 is optimal. Importantly, the generalization to arbitrary M still requires the sampling of only one antithetic path, so the generalization introduces no extra computational complexity. The key lemma in this development - Lemma 3.5 in the present work - was originally proved in [GS12b] toward a different end. Given this lemma, the result is straightforward, but does not appear elsewhere in the literature to the author's knowledge.

The remainder of the chapter is structured as follows. Section 2 reviews the details of MLMC methods and the difficulty in implementing SDE solvers with $q > 1/2$, focusing in particular on the Milstein discretization. In section 3, we show how Ito's lemma can be used to eliminate the lowest level variance in MLMC methods. In section 4, we use the results of the previous section to derive an 'approximate Milstein' version of the MLMC method that achieves the $O(\varepsilon^{-2})$ cost scaling. In section 5, we leverage results from the previous section to generalize the antithetic method of [GS12a]. In section 6, we summarize results and present pseudocode for the algorithms proposed in previous sections. In section 7, we present and discuss numerical results. We conclude in section 8.

3.2 Background

The first portion of this section reviews the derivation and basic properties of MLMC methods, while the second reviews the Milstein discretization, the difficulties inherent in its implementation, and some previous efforts to negotiate those difficulties. For more details on ele-

mentary MLMC, see [Gil08b]. For more information on Milstein, see [GL94, KPW92, Wik01].

3.2.1 MLMC Review

The MLMC schemes are constructed in the following way: for some integer $M > 1$, let $h_l = TM^{-l}$ for $l = 0, 1, 2, ..., L$. Setting $P_l = P(\mathbf{S}_{h_l}(T))$, the following identity holds:

$$\mathbb{E}\left[P_L\right] = \mathbb{E}\left[P_0\right] + \sum_{l=1}^{L} \mathbb{E}\left[P_l - P_{l-1}\right]. \tag{3.8}$$

The weak convergence of the discretization guarantees that $\mathbb{E}[P_L]$ differs from the true expectation by $O(h_L^p)$, and (3.8) shows that it can be estimated by estimating the $L+1$ expectations on the right side. The first term is relatively cheap to compute, since the time-step $h_0 = T$ is much larger than h_L. Meanwhile, the quantities $P_l - P_{l-1}$ have variances controlled by the strong convergence of the discretization, so that their expectations can be estimated accurately with a relatively small number of samples.

We make this more concrete by defining

$$V_l = \mathrm{Var}\left[P_l - P_{l-1}\right], \tag{3.9}$$

for $l > 0$, where $\mathrm{Var}[\cdot]$ denotes the variance of a random variable, and assuming P has a global Lipschitz bound. Then, if P_l and P_{l-1} are sampled using the same Brownian paths, we have

$$\begin{aligned} V_l &= \mathbb{E}\left[(P_l - P_{l-1})^2\right] - \mathbb{E}\left[P_l - P_{l-1}\right]^2 \\ &\lesssim \mathbb{E}\left[|\mathbf{S}_{h_l} - \mathbf{S}_{h_{l-1}}|^2\right] + O\left(h_l^{2p}\right) \\ &= O\left(h_l^{2q}\right) + O\left(h_l^{2p}\right). \end{aligned} \tag{3.10}$$

It is a general feature of SDE finite difference methods that $p \geq q$ [KP11], so we will write

$$V_l = O\left(h_l^{2q}\right) \tag{3.11}$$

henceforth.

If we estimate $\mathbb{E}\left[P_l - P_{l-1}\right]$ with N_l samples - that is

$$\mathbb{E}\left[P_l - P_{l-1}\right] \approx \hat{Y}_l \equiv \frac{1}{N_l}\sum_{r=1}^{N_l}\left(P_l^{(r)} - P_{l-1}^{(r)}\right), \tag{3.12}$$

where r again indexes the N_l samples - then the variance in this estimate is V_l/N_l. Similarly, define $V_0 = \mathrm{Var}[P_0]$ and let

$$\hat{Y}_0 = \frac{1}{N_0}\sum_{r=1}^{N_0} P_0^{(r)}. \tag{3.13}$$

Then, let $\hat{P}_L$ be our estimate of $\mathbb{E}[P_L]$ defined by

$$\hat{P}_L = \sum_{l=0}^{L} \hat{Y}_l. \tag{3.14}$$

This estimate has variance

$$\mathrm{Var}\left[\hat{P}_L\right] = \sum_{l=0}^{L}\frac{V_l}{N_l}. \tag{3.15}$$

The desired RMS error bound of ε may thus be written as

$$(c_1 h_L)^2 + \sum_{l=0}^{L}\frac{V_l}{N_l} \leq \varepsilon^2, \tag{3.16}$$

where c_1 is the constant of proportionality in the weak error estimate of the SDE scheme. That is,

$$|\mathbb{E}[P(\mathbf{S}(T)) - \mathbb{E}[P_L]| \approx c_1 h_L \tag{3.17}$$

for sufficiently small h_L. Note that we assume the scheme is first order in the weak sense ($p = 1$), a quality shared by all the schemes considered in this chapter. We call the first term in (3.16) the *bias error*; it is deterministic and arises from the finite time-step approximation of the SDE's solution. We call the second term - the sum - the *sampling error*; it arises from the estimation of expectations using a finite number of samples.

In the analysis of Giles, (3.16) is satisfied by setting each of the two mean squared errors to $\varepsilon^2/2$. The bias error constraint then immediately gives a formula for L, the total number of levels to be used:

$$L = \left\lceil \frac{\log\left(\sqrt{2}c_1 T/\varepsilon\right)}{\log M} \right\rceil. \tag{3.18}$$

The sampling error constraint gives rise to a constrained optimization problem: one wishes to minimize the computational cost - modeled by the total number of time steps taken -

$$K \propto \sum_{l=0}^{L} N_l(h_l^{-1} + h_{l-1}^{-1}) = \left(1 + \frac{1}{M}\right) \sum_{l=0}^{L} \frac{N_l}{h_l}, \tag{3.19}$$

subject to the constraint $\sum_{l=0}^{L}(V_l/N_l) \leq \varepsilon^2/2$. A Lagrange multiplier argument shows that the optimal choice is

$$N_l = \frac{2}{\varepsilon^2}\sqrt{V_l h_l}\left(\sum_{l=0}^{L}\sqrt{V_l/h_l}\right), \tag{3.20}$$

which in turn gives the cost

$$K \propto \frac{2}{\varepsilon^2}\left(1 + \frac{1}{M}\right)\left(\sum_{l=0}^{L}\sqrt{V_l/h_l}\right)^2. \tag{3.21}$$

When $q = 1/2$, we have $V_l = O(h_l)$, so that each term in the sum is $O(1)$, making the sum $O(L)$. Since L scales like $\log \varepsilon$, we see that $K = O(\varepsilon^{-2}(\log \varepsilon)^2)$, as stated in the introduction. When $q > 1/2$, the terms in the sum decrease geometrically, so that the sum to L is bounded by a convergent infinite sum, giving $K = O(\varepsilon^{-2})$.

In practice, the constant c_1 is not known, so L cannot be specified at the start of the simulation. One typically performs the necessary steps for $L = 1$, estimates the bias error by looking at $\hat{Y}_L$, and increments L while the bias error is estimated to be more that $\varepsilon/\sqrt{2}$. More details can be found in [Gil08b] and in section 6 of this chapter.

3.2.2 Milstein and Lévy Areas

The simplest finite difference scheme for SDEs achieving $q > 1/2$ - and thus yielding the optimal MLMC scaling - is the Milstein scheme, written as

$$S_{i,n+1} = S_{i,n} + a_{i,n}\Delta t + \sum_{j=1}^{D} b_{ij,n}\Delta W_{j,n} + \sum_{j,k=1}^{D} h_{ijk,n}(\Delta W_{j,n}\Delta W_{k,n} - \Omega_{jk}\Delta t - A_{jk,n}), \tag{3.22}$$

where we've abbreviated $a_i(\mathbf{S}_n, t_n) = a_{i,n}$ and similarly for $b_{ij,n}$ and $h_{ijk,n}$, Ω_{jk} is the correlation matrix associated with W, and h and A are defined by

$$h_{ijk} = \frac{1}{2}\sum_{l=1}^{d} b_{lk}\frac{\partial b_{ij}}{\partial x_l}, \tag{3.23}$$

$$A_{jk,n} = \int_{t_n}^{t_{n+1}} \int_{t_n}^{s} \left[dW_j(u) dW_k(s) - dW_k(u) dW_j(s) \right]. \tag{3.24}$$

The $A_{jk,n}$ are known as Lévy areas. When $D = 1$, they vanish, since $A_{jj,n} = 0$, and Milstein is straightforward to implement. When $D = 2$, there is effectively only one non-zero Lévy area, since $A_{jk,n} = -A_{kj,n}$. Recently, an efficient method has been developed for sampling a single Lévy area [DCC13], making Milstein implementation feasible when $D = 2$. Sampling multiple Lévy areas is a more challenging problem because they are not independent. A method for jointly sampling multiple Lévy areas was also proposed in [DCC13, GL94] that builds upon the methods therein and involves sampling a random orthogonal matrix, techniques for which are available in [Mez07]. However, this method has not been implemented or tested with MLMC. As a result, implementing the Milstein discretization and thus achieving the $O(\varepsilon^{-2})$ scaling for MLMC methods is quite challenging when $D > 2$, except in special cases.

Fortunately, in [GS12a] it was observed that while $q > 1/2$ is sufficient to achieve the optimal scaling, it is not necessary. The necessary condition is

$$\mathrm{Var}[P_l - P_{l-1}] = O\left(h_l^\beta\right) \tag{3.25}$$

for some $\beta > 1$. We can see from (3.10) that if P has a global Lipschitz bound, this necessary condition is achieved if

$$\mathbb{E}\left[|\mathbf{S}_{h_l} - \mathbf{S}_{h_{l-1}}|^2\right] = O\left(h_l^\beta\right). \tag{3.26}$$

This resembles a strong scaling requirement (3.5), but there is a key difference. Here, we require two approximate solutions to be within $O(h_l^\beta)$ of each other in the mean square sense. It is not necessary that *either one* of these approximate solutions be within $O(h_l^\beta)$ of the *true* solution, as would be the case if we were relying on strong convergence.

In [GS12a], the Milstein scheme (3.22) with the Lévy areas set to zero, along with an antithetic path sampling method, is used in order to achieve (3.26) with $\beta > 1$, and thus achieve the $O(\varepsilon^{-2})$ cost scaling for SDE systems with arbitrary D. For the moment, we refer the reader to that paper for its detailed derivation and implementation. We will discuss some

key aspects of the antithetic method as they become relevant in the course of our discussion here.

In section 4 of this chapter, we derive an alternative method to that in [GS12a]. We also achieve the $O(\varepsilon^{-2})$ cost scaling for arbitrary D without simulating Lévy areas. Our method requires more regularity of the payoff function, but is slightly cheaper and simpler to derive. In section 5, we generalize the results of [GS12a] to $M > 2$. Since much of the analysis from [GS12a] carries over directly, we simply cite several results without reprinting proofs.

3.3 Variance Reduction via Ito's Lemma

We begin with a simple observation. Suppose that $P(\mathbf{S}) = S_m$, for some $1 \leq m \leq d$. That is, P simply picks out one of the components of $\mathbf{S}$. Such a payoff function is useful in chemical kinetics, for example, in which each component of the SDE represents the concentration of a particular species and we may desire to compute the mean concentration of some key compound.

Then, we may write a simple analytic expression for P_0 - the payoff when the time-step is T - when the Euler discretization is used:

$$P_0 = S_{m,0} + a_m(\mathbf{S}_0)T + \sum_{j=1}^{D} b_{mj}(\mathbf{S}_0)W_j(T), \tag{3.27}$$

where $\mathbf{S}_0$ is the initial data and $S_{m,0}$ is its m^{th} component. The expectation of this expression is simple to evaluate:

$$\mathbb{E}[P_0] = S_{m,0} + a_m(\mathbf{S}_0)T. \tag{3.28}$$

The same result applies to the Milstein scheme, since the additional term has zero expectation. Thus, when P has this simple form (or, indeed, is any linear function of $\mathbf{S}$), the base payoff can be evaluated exactly in terms of the initial condition. There is no need to sample any random variables at all. In effect, $V_0 = 0$ and $N_0 = 1$.

This can represent a great computational saving for MLMC because, as already noted, the lowest level is the only level at which no variance reduction is gained. That is, with the

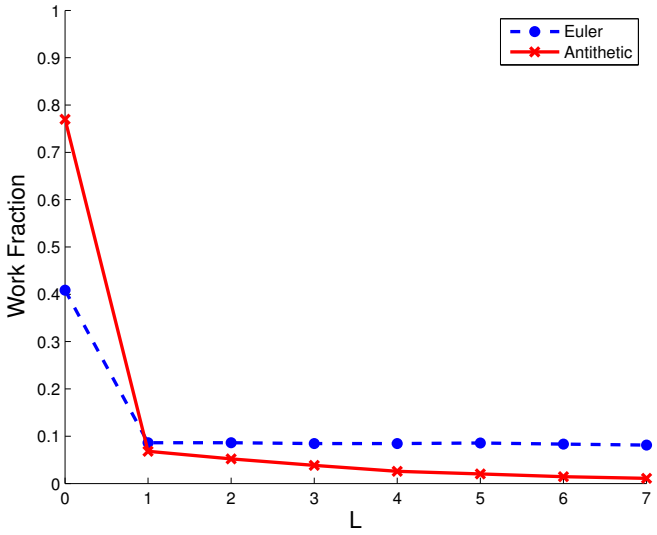

Figure 3.1: The fraction of the computational work exerted at each level in a sample MLMC computation. The Heston model - see (3.84) and proceeding text for specification - is solved with a sinusoidal payoff function, and $M = 2$.

standard approach, V_0 need not obey the same scaling as the other V_l, and may very well be disproportionately large, thus causing the cost of computing P_0 to dominate other costs.

To illustrate this point, we show in fig. 1 the fraction of the computational work at each level in a sample MLMC computation, using both the Euler and antithetic methods. We see that, for each method, the base level (zero) is the most expensive. The base level represents an even larger fraction of the work in the antithetic method. This is a result of the improved variance scaling, which reduces the cost of the higher levels.

There is thus a motivation to investigate whether the technique of eliminating the cost of computing the base level payoff can be generalized to less trivial payoff functions. Toward that end, assume P is twice continuously differentiable. Then, Ito's lemma gives an SDE for P:

$$dP = \left(\sum_{i=1}^{d} a_i P_{x_i} + \frac{1}{2} \sum_{j=1}^{D} \sum_{i,k=1}^{d} b_{ij} b_{kj} P_{x_i x_k} \right) dt + \sum_{j=1}^{D} \sum_{i=1}^{d} b_{ij} P_{x_i} \, dW_j, \tag{3.29}$$

where subscripts on P denote partial derivatives, and all functions are evaluated at $\mathbf{S}(t)$.

With this in mind, construct a vector $\mathcal{S} \in \mathbb{R}^{d+1}$ as follows: for $1 \leq k \leq d$, set $\mathcal{S}_k = S_k$, and set $\mathcal{S}_{d+1} = P(\mathbf{S})$. Then, $\mathcal{S}$ solves

$$d\mathcal{S}_i = \alpha_i \, dt + \sum_{j=1}^{D} \beta_{ij} \, dW_j \tag{3.30}$$

where $\alpha_i(\mathcal{S}) = a_i(\mathbf{S})$ and $\beta_{ij}(\mathcal{S}) = b_{ij}(\mathbf{S})$ for $i \leq d$, and

$$\alpha_{d+1}(\mathcal{S}) = \sum_{i=1}^{d} a_i P_{x_i} + \frac{1}{2} \sum_{j=1}^{D} \sum_{i,k=1}^{d} b_{ij} b_{kj} P_{x_i x_k}, \qquad \beta_{(d+1)j}(\mathcal{S}) = \sum_{i=1}^{d} b_{ij} P_{x_i}. \tag{3.31}$$

This is a system of SDEs in the usual sense. Consider further the "payoff" function $\tilde{P}(\mathcal{S}) = \mathcal{S}_{d+1}$, which is equal to $P(\mathbf{S})$. We now have two distinct formulations of the same problem. The first is to find $\mathbb{E}[P(\mathbf{S}(T))]$ when $\mathbf{S}$ solves (3.1). The second is to find $\mathbb{E}[\tilde{P}(\mathcal{S}(T))] = \mathbb{E}[\mathcal{S}_{d+1}(T)]$ when $\mathcal{S}$ solves (3.30).

The second, new formulation has the considerable advantage that its payoff function is linear, and in particular is of the form considered above, so that $\mathbb{E}[P_0]$ may be immediately evaluated using (3.28) with $m = d+1$. The MLMC method may be applied to (3.30) with $\tilde{P}$ using any discretization available. This approach will not change the resulting cost scaling, but will reduce the cost by a constant factor that may be significant. We demonstrate in section 7 via numerical experiments that these savings are frequently considerable.

This method of using Ito's lemma to linearize the payoff function - we refer to this henceforth as the *Ito linearization technique* - does have two drawbacks. The first, and most serious, is that two continuous derivatives are required of P for Ito's lemma to apply. In finance the payoff frequently has a discontinuity in the first derivative - e.g. European options - or even in the function itself - e.g. digital options. Ito linearization in its present form is not useful for these problems.

In many applications though, there are many natural payoffs with sufficient regularity. We have already noted that in chemical kinetics a simple linear payoff function is of interest. One may also wish to compute the covariances of the chemical concentrations, which may be computed from the means and the payoffs $P(\mathbf{S}) = S_i S_j$ for each i, j, which of course have the necessary smoothness.

The second drawback is that (3.30) is a $(d+1)$-dimensional system, while (3.1) is only d-dimensional. Each time-step of (3.30) is thus slightly more expensive - by a factor of roughly $(d+1)/d$ - than a corresponding time-step of (3.1). In numerical tests, we find that the savings at the base level more than compensate for this added expense.

3.4 Approximate Milstein for MLMC

We now turn to the derivation of an approximate version of the Milstein discretization that achieves $O(\varepsilon^{-2})$ cost scaling in arbitrary dimension. There are several observations that make this possible, the first of which is that when estimating $\mathbb{E}[P_l - P_{l-1}]$, the discretizations used to compute P_l and P_{l-1} need not be identical for the reformulated problem (3.30).

To clarify this point, let us assume we have two discretizations. Given the same h and ΔW, the 'fine' discretization yields the payoff P^f while the 'coarse' one yields P^c. We have the following generalization of (3.8):

$$\mathbb{E}\left[P_L^f\right] = \mathbb{E}\left[P_0^f\right] + \sum_{l=1}^{L} \left\{ \mathbb{E}\left[P_l^f - P_l^c\right] + \mathbb{E}\left[P_l^c - P_{l-1}^f\right] \right\}. \tag{3.32}$$

In the methods of Giles, it is required that

$$\mathbb{E}\left[P_l^c\right] = \mathbb{E}[P_{l-1}^f] \tag{3.33}$$

for some large class of functions P, so that the second term in the sum in (3.32) is identically zero and (3.32) reduces to (3.8). This requires that $\mathbf{S}_{h_l}^f(T)$ and $\mathbf{S}_{h_l}^c(T)$ be *identically distributed*, which in turn requires that the discretizations used at the fine and coarse levels be at least very nearly identical.

However, when solving the reformulation afforded by Ito's lemma in the previous section, we may rewrite (3.32) as

$$\mathbb{E}\left[\mathcal{S}_{d+1}^{f,L}\right] = \mathbb{E}\left[\mathcal{S}_{d+1}^{f,0}\right] + \sum_{l=1}^{L} \left\{ \mathbb{E}\left[\mathcal{S}_{d+1}^{f,l} - \mathcal{S}_{d+1}^{c,l}\right] + \mathbb{E}\left[\mathcal{S}_{d+1}^{c,l} - \mathcal{S}_{d+1}^{f,l-1}\right] \right\}, \tag{3.34}$$

where $\mathcal{S}^{f,l}$ is the result of the 'fine' discretization with time-step h_l, and similarly for $\mathcal{S}^{c,l}$.

This now reduces to the analogue of (3.8) if

$$\mathbb{E}[\mathcal{S}^{c,l}] = \mathbb{E}[\mathcal{S}^{f,l-1}]. \tag{3.35}$$

This condition is actually more than is necessary - we only need the expectations of the last components to match - but there will be no additional difficulty in enforcing this condition. Being constrained by (3.35) instead of (3.33) creates considerable freedom in choosing different fine and coarse discretizations. We leverage this freedom extensively in the remainder of this section.

In what follows, we develop an 'approximate Milstein' method, whose intended application is MLMC methods applied to the modified SDE (3.30), as it takes advantage of this system's linear payoff function. We will, however, denote the solution of the SDE by $\mathbf{S}$ - rather than $\mathcal{S}$ - to emphasize the generality of the specific results. It is only their application to MLMC that requires the modified SDE.

We begin by establishing some notation: define

$$D_i^f(\mathbf{S}, t, h, \Delta W_n) \equiv a_i(\mathbf{S}, t)h + \sum_{j=1}^{D} b_{ij}(\mathbf{S}, t)\Delta W_{j,n} + \sum_{j,k=1}^{D} h_{ijk}(\mathbf{S}, t)(\Delta W_{j,n}\Delta W_{k,n} - \Omega_{jk}h), \tag{3.36}$$

$$\begin{aligned} D_i^c(\mathbf{S}_1, \mathbf{S}_2, t, h, \delta W_n, \delta W_{n+\frac{1}{2}}) &\equiv a_i(\mathbf{S}_1, t)\Delta t + \sum_{j=1}^{D} b_{ij}(\mathbf{S}_2, t)\Delta W_{j,n} \\ &+ \sum_{j,k=1}^{D} h_{ijk}(\mathbf{S}_2, t)(\Delta W_{j,n}\Delta W_{k,n} - \Omega_{jk}\Delta t - \delta W_{j,n}\delta W_{k,n+\frac{1}{2}} + \delta W_{j,n+\frac{1}{2}}\delta W_{k,n}), \end{aligned} \tag{3.37}$$

where ΔW_n is a vector in $\mathbb{R}^D$ whose j^{th} component is $\Delta W_{j,n} = \delta W_{j,n} + \delta W_{j,n+\frac{1}{2}}$. The analysis is simpler when $M = 2$, so we proceed with that case initially and generalize to arbitrary M in section 4.3. Fix l and set $\delta t = h_l$, $\Delta t = 2\delta t = h_{l-1}$, $t_n = n\Delta t$.

3.4.1 Review of Antithetic Method

Because the method we develop here is closely related to the antithetic method of [GS12a], we first state and review that algorithm. In our notation, the antithetic scheme may be

written as

$$\begin{aligned}\mathbf{S}^{f,l}_{n+1} &= \mathbf{S}^{f,l}_{n+\frac{1}{2}} + \mathbf{D}^f(\mathbf{S}^{f,l}_{n+\frac{1}{2}}, t_{n+\frac{1}{2}}, \delta t, \delta W_{n+\frac{1}{2}}), \quad \mathbf{S}^{f,l}_{n+\frac{1}{2}} = \mathbf{S}^{f,l}_n + \mathbf{D}^f(\mathbf{S}^{f,l}_n, t_n, \delta t, \delta W_n) \\ \mathbf{S}^{a,l}_{n+1} &= \mathbf{S}^{a,l}_{n+\frac{1}{2}} + \mathbf{D}^f(\mathbf{S}^{a,l}_{n+\frac{1}{2}}, t_{n+\frac{1}{2}}, \delta t, \delta W_n), \quad \mathbf{S}^{a,l}_{n+\frac{1}{2}} = \mathbf{S}^{a,l}_n + \mathbf{D}^f(\mathbf{S}^{a,l}_n, t_n, \delta t, \delta W_{n+\frac{1}{2}})\end{aligned} \tag{3.38}$$

where $\mathbf{D}^f$ is the vector whose i^{th} component is D^f_i, and the fine payoff is set to

$$P^f_l = \frac{1}{2}\left(P(\mathbf{S}^f_l) + P\left(\mathbf{S}^a_l\right)\right). \tag{3.39}$$

Meanwhile, the coarse evolution is given by

$$\mathbf{S}^{c,l}_{n+1} = \mathbf{S}^{c,l}_n + \mathbf{D}^f(\mathbf{S}^{c,l}_n, t_n, \Delta t, \Delta W_n), \tag{3.40}$$

with the coarse payoff set to $P^c_l = P(\mathbf{S}^c_l)$.

Notice that the evolution equations for $\mathbf{S}^f_l$ and $\mathbf{S}^a_l$ are identical except that the Brownian steps δW_n and $\delta W_{n+\frac{1}{2}}$ have been switched. This has the effect of canceling the leading order contribution of the Lévy areas when the two are averaged, as in (3.39). This cancellation makes the V_l scale like $O(h_l^2)$ for twice differentiable payoffs and like $O(h_l^{3/2-\delta})$ for any $\delta > 0$ when the payoff is Lipschitz, only non-differentiable on a set of measure zero, and the solution is unlikely to be near this set in a certain sense (see [GS12a] for details). The scheme thus achieves the $O(\varepsilon^{-2})$ cost scaling in both cases.

The scheme has two primary drawbacks: 1) it requires twice as much effort to generate P^f_l - due to the need to evolve the antithetic variable $\mathbf{S}^a_l$ - as an Euler based multilevel scheme, and 2) its derivation in [GS12a] is restricted to $M = 2$. In our development, we offer a slight improvement to 1) by moving the doubled effort to the coarse level, which is cheaper by a factor of M. Moreover, we generalize both our method and the antithetic method to $M > 2$ in sections 4.3 and 5.

3.4.2 Approximate Milstein for $M = 2$

We consider the following pair of schemes for $\mathbf{S}^f$ and $\mathbf{S}^c$:

$$\mathbf{S}^{f,l}_{n+\frac{1}{2}} = \mathbf{S}^{f,l}_n + \mathbf{D}^f(\mathbf{S}^{f,l}_n, t_n, \delta t, \delta W_n), \tag{3.41}$$

$$\mathbf{S}_{n+1}^{c,l} = \mathbf{S}_n^{c,l} + \mathbf{D}^c(\mathbf{S}_n^{*,l}, \mathbf{S}_n^{c,l}, t_n, \Delta t, \delta W_n, \delta W_{n+\frac{1}{2}}), \tag{3.42}$$

where $\mathbf{S}^{*,l}$ is given by

$$\mathbf{S}_{n+1}^{*,l} = \mathbf{S}_n^{*,l} + \mathbf{D}^f(\mathbf{S}_n^{*,l}, t_n, \Delta t, \Delta W). \tag{3.43}$$

We set $P_l^f = P(\mathbf{S}_l^f)$ and $P_l^c = P(\mathbf{S}_l^c)$.

It is worth clarifying that in this description the number n always indexes the number of level-l *coarse* time steps taken. This is equal to the number of level-$(l-1)$ *fine* time steps taken, so that number is also indexed by n. By writing (3.41) the way we have, we ensure that $\mathbf{S}_n^{f,l}$, $\mathbf{S}_n^{c,l}$, and $\mathbf{S}_n^{f,l-1}$ are all approximations to $\mathbf{S}(n\Delta t)$ for each whole number n. In addition to $n = 0, 1, 2, 3, ...$, we have definitions of $\mathbf{S}_n^{f,l}$ at $n = 1/2, 3/2, 5/2, ...$, but this fact will not concern us.

In the remainder of this section, we state and prove results that establish first (3.35) and then (3.26) with $\beta = 2$ for this pair of discretizations. The more technical proofs are confined to appendices.

3.4.2.1 Equal Expectations

Theorem 3.1 (Equal Expectations)**.** *For $\mathbf{S}^f$ and $\mathbf{S}^c$ as defined in (3.41)-(3.43), we have*

$$\mathbb{E}\left[\mathbf{S}_n^{f,l-1}\right] = \mathbb{E}\left[\mathbf{S}_n^{c,l}\right] \tag{3.44}$$

for each $n = 0, 1, 2, 3, ...$

Proof. At the $(l-1)^{\text{st}}$ level, we have

$$\mathbf{S}_{n+1}^{f,l-1} = \mathbf{S}_n^{f,l-1} + \mathbf{D}^f(\mathbf{S}_n^{f,l-1}, t_n, \Delta t, \Delta W). \tag{3.45}$$

If we subtract (3.42) from (3.45), we find

$$\begin{aligned}\mathbf{S}_{n+1}^{f,l-1} - \mathbf{S}_{n+1}^{c,l} = \mathbf{S}_n^{f,l-1} - \mathbf{S}_n^{c,l} \\ &+ \left\{a\left(\mathbf{S}_n^{f,l-1}\right) - a\left(\mathbf{S}_n^{*,l}\right)\right\}\Delta t \\ &+ \sum_{j=1}^{D}\left\{b_j\left(\mathbf{S}_n^{f,l-1}\right) - b_j\left(\mathbf{S}_n^{c,l}\right)\right\}\left[\Delta W_{j,n}\right] \\ &+ \sum_{j,k=1}^{D}\left\{h_{jk}\left(\mathbf{S}_n^{f,l-1}\right) - h_{jk}\left(S_n^{c,l}\right)\right\}\left[\Delta W_{j,n}\Delta W_{k,n} - \Omega_{jk}\Delta t\right] \\ &- \sum_{j,k=1}^{D}\left\{h_{jk}\left(\mathbf{S}_n^{c,l}\right)\right\}\left[\delta W_{j,n}\delta W_{k,n+\frac{1}{2}} - \delta W_{j,n+\frac{1}{2}}\delta W_{k,n}\right],\end{aligned} \tag{3.46}$$

where a is the vector whose i^{th} component is a_i, and analogously for b_j and h_{jk}.

We look at (3.46) term by term. In the last three lines, the term in square brackets has zero expectation and is independent of the term in curly braces - this follows from the fact that each Brownian increment is independent of all those before it. Therefore, each of these lines has vanishing expectation. In the second line, $S_n^{*,l}$ and $S_n^{f,l-1}$ are identically distributed for each n because they are approximated by exactly the same method - compare (3.45) and (3.43) - so the term in curly braces has zero expectation. Therefore, if we take the expectation of (3.46), everything vanishes except the first line. Thus, we have

$$\mathbb{E}\left[\mathbf{S}_{n+1}^{f,l-1}\right] - \mathbb{E}\left[\mathbf{S}_{n+1}^{c,l}\right] = \mathbb{E}\left[\mathbf{S}_n^{f,l-1}\right] - \mathbb{E}\left[\mathbf{S}_n^{c,l}\right]. \tag{3.47}$$

Since the coarse and fine approximations start at the same initial condition, the difference in expectation is zero for $n = 0$, and (3.47) guarantees that this remains the case for all integer $n > 0$. □

Corollary 3.1. *With the same definitions as in Theorem 3.1,*

$$\mathbb{E}\left[\mathbf{S}_n^{*,l}\right] = \mathbb{E}\left[\mathbf{S}_n^{c,l}\right]. \tag{3.48}$$

Proof. Since $\mathbf{S}^{*,l}$ and $\mathbf{S}^{f,l-1}$ are identically distributed, they have the same expectation, so this follows directly from Theorem 3.1. □

3.4.2.2 Variance Scaling

Before establishing the variance scaling (3.26) required for the ε^{-2} cost scaling, we need three lemmas. The first establishes that the weak difference between coarse and starred approximations is $O(\Delta t)$, while the last two are convenient rewritings of the fine and coarse discretizations.

Lemma 3.1. *The weak difference between* $\mathbf{S}^{c,l}$ *and* $\mathbf{S}^{*,l}$ *is* $O(\Delta t)$*. That is, for sufficiently differentiable* $f : \mathbb{R}^d \to \mathbb{R}$*, we have*

$$\left|\mathbb{E}\left[f(\mathbf{S}_n^{c,l})\right] - \mathbb{E}\left[f(\mathbf{S}_n^{*,l})\right]\right| = O(\Delta t) \tag{3.49}$$

for all $n \leq T/\Delta t$*.*

Proof. See appendix A. □

In the proof of lemma 3.1 above, we require that f have four continuous and bounded derivatives. Elsewhere in our development, the payoff and SDE coefficients are only required to possess two derivatives, and in practice the scaling predicted by lemma 3.1 is observed in these cases as well. It seems likely that by following [KP11], lemma 3.1 could be reestablished for f merely Hölder continuous, but such an exercise is beyond the scope of this thesis.

Lemma 3.2. *The fine discretization (3.41) can be rewritten as*

$$S_{i,n+1}^{f,l} = S_{i,n}^{f,l} + D_i^c(\mathbf{S}_n^{f,l}, \mathbf{S}_n^{f,l}, t_n, \Delta t, \delta W_n, \delta W_{n+\frac{1}{2}}) + M_{i,n}^f + N_{i,n}^f \tag{3.50}$$

where $\mathbb{E}[M_{i,n}^f] = 0$ *and*

$$\mathbb{E}\left[\max_{n\leq N} \left\|M_n^f\right\|^p\right] = O\left(\Delta t^{3p/2}\right), \qquad \mathbb{E}\left[\max_{n\leq N} \left\|N_n^f\right\|^p\right] = O\left(\Delta t^{2p}\right) \tag{3.51}$$

for any integer $p \geq 2$*.*

Proof. The lemma and proof are identical to Lemma 4.7 and its proof in [GS12a]. □

Lemma 3.3. *The coarse discretization (3.42) may be rewritten as*

$$S^{c,l}_{i,n+1} = S^{c,l}_{i,n} + D^c_i(\mathbf{S}^{c,l}_n, \mathbf{S}^{c,l}_n, t_n, \Delta t, \delta W_n, \delta W_{n+\frac{1}{2}}) + M^c_{i,n} + N^c_{i,n} \tag{3.52}$$

where $\mathbb{E}[M^c_{i,n}] = 0$ *and*

$$\mathbb{E}\left[\max_{n\leq N} \|M^c_n\|^p\right] = O\left(\Delta t^{3p/2}\right), \qquad \mathbb{E}\left[\max_{n\leq N} \|N^c_n\|^p\right] = O\left(\Delta t^{2p}\right). \tag{3.53}$$

Proof. Simple algebra shows that

$$\begin{aligned} S^{c,l}_{i,n+1} = S^{c,l}_{i,n} &+ D^c_i(\mathbf{S}^{c,l}_n, \mathbf{S}^{c,l}_n, t_n, \Delta t, \delta W_n, \delta W_{n+\frac{1}{2}}) \\ &+ \left[a_i\left(\mathbf{S}^{*,l}_n\right) - a_i\left(\mathbf{S}^{c,l}_n\right)\right]\Delta t, \end{aligned} \tag{3.54}$$

so the lemma reduces to analyzing the second line of this expression. Define $\Delta a_{i,n} = a_i\left(\mathbf{S}^{*,l}_n\right) - a_i\left(\mathbf{S}^{c,l}_n\right)$, and write the term in question as

$$\Delta a_{i,n}\Delta t = \mathbb{E}\left[\Delta a_{i,n}\right]\Delta t + \left\{\Delta a_{i,n} - \mathbb{E}\left[\Delta a_{i,n}\right]\right\}\Delta t. \tag{3.55}$$

By Lemma 3.1 above (which we again note uses four derivatives), we have $\mathbb{E}[\Delta a_{i,n}] = O(\Delta t)$, so that the first term is $O(\Delta t^2)$. Thus, we define $N^c_{i,n} = \mathbb{E}[\Delta a_{i,n}]\Delta t$.

The second term on the right of (3.55) clearly has zero expectation. The first term in the curly braces is $O(\sqrt{\Delta t})$ by strong convergence of both schemes (3.42) and (3.43), and the second term in the curly braces is $O(\Delta t)$ as before, so their difference is $O(\sqrt{\Delta t})$. Thus, the second term on the right of (3.55) is $O(\Delta t^{3/2})$, so we define it to be $M^c_{i,n}$. □

Finally, we are ready to prove the desired scaling of the variances:

Theorem 3.2 (Variance Scaling)**.** *Assume the a_i have four continuous bounded derivatives, b_{ij} are twice continuously differentiable with both derivatives uniformly bounded, and that the h_{ijk} have uniformly bounded first derivative. Then, for the pair of fine and coarse discretizations (3.41)-(3.43), we have (3.26) with $\beta = 2$. In fact, we have the stronger statement*

$$\mathbb{E}\left[\max_{n\leq N} \left\|\mathbf{S}^{f,l}_n - \mathbf{S}^{c,l}_n\right\|^2\right] = O\left(\Delta t^2\right), \tag{3.56}$$

where $N = T/\Delta t$.

Proof. See appendix B. □

3.4.3 Generalization to $M > 2$

Thus far, we've developed the approximate Milstein method assuming that the difference in time step at adjacent levels (refinement factor) M is equal to two. This assumption is also made in Giles' development of the antithetic method. However, in [Gil08b] Giles argues that the optimal refinement factor is near seven for an Euler-based multilevel scheme, and a similar argument for Milstein shows the optimal choice to be near four.

Following [Gil08b], the latter argument proceeds as follows: Noting that $P_l^f - P_l^c = (P_l^f - P) - (P_l^c - P)$, where P is the exact mean payoff, we infer that

$$(M-1)^2 k h_l^2 \leq V_l \leq (M+1)^2 k h_l^2, \tag{3.57}$$

for some constant k, where the lower and upper bounds correspond to perfect correlation and anti-correlation between $P_l^f - P$ and $P_l^c - P$. Supposing for simplicity that the actual variance is approximately the geometric mean of the two extremes, we have

$$V_l \approx (M^2 - 1) k h_l^2. \tag{3.58}$$

Substituting this expression into the cost formula (3.21), we have (ignoring for clarity the fact that V_0 need not obey any scaling law)

$$K \propto \varepsilon^{-2} \frac{(M^2-1)(1+M^{-1})}{\left(\sqrt{M}-1\right)^2}, \tag{3.59}$$

which for fixed ε has its minimum for M between 4 and 5. There is thus motivation to study arbitrary M.

Notationally, moving to arbitrary M changes (3.41) to read

$$\mathbf{S}_{n+\frac{1}{M}}^{f,l} = \mathbf{S}_n^{f,l} + \mathbf{D}^f(\mathbf{S}_n^{f,l}, t_n, \delta t, \delta W_{j,n}), \tag{3.60}$$

and we set

$$\Delta t = M \delta t, \qquad \Delta W_{j,n} = \sum_{m=0}^{M-1} \delta W_{j,n+\frac{m}{M}}. \tag{3.61}$$

To see how to change (3.42), we present the following generalization of Lemma 3.2:

Lemma 3.4. *The fine discretization (3.60) can be rewritten as*

$$\begin{aligned} S_{i,n+1}^{f,l} &= S_{i,n}^{f,l} + D_i^f(\mathbf{S}_n^{f,l}, t_n, \Delta t, \Delta W_n,) \\ &\quad - \sum_{j,k=1}^{D} h_{ijk}\left(\mathbf{S}_n^{f,l}\right)\left(\mathcal{A}_{jk,n} - \mathcal{A}_{kj,n}\right) \\ &\quad + M_{i,n}^f + N_{i,n}^f, \end{aligned} \tag{3.62}$$

where $\mathbb{E}[M_{i,n}^f] = 0$ *and*

$$\mathbb{E}\left[\max_{n\leq N} \left\|M_n^f\right\|^p\right] = O\left(\Delta t^{3p/2}\right), \qquad \mathbb{E}\left[\max_{n\leq N} \left\|N_n^f\right\|^p\right] = O\left(\Delta t^{2p}\right), \tag{3.63}$$

and $\mathcal{A}_{jk,n}$ *is defined by*

$$\mathcal{A}_{jk,n} \equiv \sum_{m=1}^{M-1}\left(\delta W_{k,n+\frac{m}{M}} \sum_{q=0}^{m-1} \delta W_{j,n+\frac{q}{M}}\right). \tag{3.64}$$

Proof. See appendix C. □

We note that, as described in [DCC13], $(\mathcal{A}_{jk,n} - \mathcal{A}_{kj,n})$ is a quadrature scheme for the Levy area $A_{jk,n}$ obtained by dividing up the time step Δt into M equal parts. As noted in [DCC13], computing the $\mathcal{A}_{jk,n}$ as written can be done in $O(M)$ operations, even though the double sum contains $O(M^2)$ terms.

With Lemma 3.4 in hand, we can generalize the coarse discretization to arbitrary M. We define

$$\begin{aligned} D_i^{c,M}\left(\mathbf{S}_1, \mathbf{S}_2, t, \Delta t, \delta W_{j,n+\frac{m}{M}}\right) &\equiv a_i(\mathbf{S}_1, t)\Delta t + \sum_{j=1}^{D} b_{ij}(\mathbf{S}_2, t)\Delta W_{j,n} \\ + \sum_{j,k=1}^{D} h_{ijk}(\mathbf{S}_2, t)(\Delta W_{j,n}\Delta W_{k,n} - \Omega_{jk}\Delta t - \mathcal{A}_{jk,n} + \mathcal{A}_{kj,n}). \end{aligned} \tag{3.65}$$

Meanwhile, the starred discretization (3.43) remains unchanged. With these definitions and Lemma 3.4 in place of Lemma 3.2, the proofs of Theorems 3.1 and 3.2 generalize to arbitrary M with only straightforward notational changes.

3.5 Generalization of Antithetic Method to $M > 2$

In this section, we demonstrate that the antithetic method (3.38) may be straightforwardly generalized to arbitrary M. In particular, the same variance scaling can be achieved by using an antithetic variable for which the order of the M Brownian fine sub-steps of each coarse Brownian step is completely reversed.

More explicitly, set $\bar{m} = (M-1) - m$, then we rewrite (3.38) as

$$\begin{aligned} \mathbf{S}^{f,l}_{n+\frac{m+1}{M}} &= \mathbf{S}^{f,l}_{n+\frac{m}{M}} + \mathbf{D}^f(\mathbf{S}^{f,l}_{n+\frac{m}{M}}, t_{n+\frac{m}{M}}, \delta t, \delta W_{n+m/M}), \\ \mathbf{S}^{a,l}_{n+\frac{m+1}{M}} &= \mathbf{S}^{a,l}_{n+\frac{m}{M}} + \mathbf{D}^f(\mathbf{S}^{a,l}_{n+\frac{m}{M}}, t_{n+\frac{m}{M}}, \delta t, \delta W_{n+\bar{m}/M}), \end{aligned} \tag{3.66}$$

for each $m = 0, 1, 2, ..., M-1$. As before, $\mathbf{S}^{f,l}$ and $\mathbf{S}^{a,l}$ are identical except that the Brownian motions are indexed by $\bar{m}$ rather than m for the antithetic variable. By applying Lemma 3.4 to the antithetic variable $\mathbf{S}^{a,l}$, we find that its discretization can be rewritten as

$$\begin{aligned} S^{a,l}_{i,n+1} = S^{a,l}_{i,n} &+ D^f_i(\mathbf{S}^{a,l}_n, t_n, \Delta t, \Delta W_n,) \\ &- \sum_{j,k=1}^{D} h_{ijk}\left(\mathbf{S}^{a,l}_n\right)\left(\bar{\mathcal{A}}_{jk,n} - \bar{\mathcal{A}}_{kj,n}\right) \\ &+ M^a_{i,n} + N^a_{i,n}, \end{aligned} \tag{3.67}$$

where $M^a_{i,n}$ and $N^a_{i,n}$ obey the same scalings as $M^f_{i,n}$ and $N^f_{i,n}$. The quantity $\bar{\mathcal{A}}_{jk,n}$ is defined by

$$\bar{\mathcal{A}}_{jk,n} \equiv \sum_{m=1}^{M-1}\left(\delta W_{k,n+\bar{m}/M} \sum_{q=0}^{m-1} \delta W_{j,n+\bar{q}/M}\right), \tag{3.68}$$

with $\bar{m}$ as defined before and $\bar{q} = (M-1)-q$. The improved variance scaling then results from the following lemma, originally published in [GS12b] with different notation and reprinted here for clarity.

Lemma 3.5.

$$\bar{\mathcal{A}}_{jk,n} = \mathcal{A}_{kj,n}. \tag{3.69}$$

Proof. The proof amounts to a computation:

$$\bar{\mathcal{A}}_{jk,n} = \sum_{m=1}^{M-1} \sum_{q=0}^{m-1} \delta W_{k,n+\bar{m}/M} \delta W_{j,n+\bar{q}/M} \tag{3.70}$$

$$= \sum_{q=0}^{M-2} \sum_{m=q+1}^{M-1} \delta W_{k,n+\bar{m}/M} \delta W_{j,n+\bar{q}/M} \tag{3.71}$$

$$= \sum_{\bar{q}=1}^{M-1} \sum_{\bar{m}=0}^{\bar{q}-1} \delta W_{k,n+\bar{m}/M} \delta W_{j,n+\bar{q}/M} \tag{3.72}$$

$$= \mathcal{A}_{kj,n}. \tag{3.73}$$

Notice that (3.71) comes from simply switching the order of summation, while (3.72) results from rewriting the sums in terms of $\bar{m}$ and $\bar{q}$. □

This lemma implies that, if we define $\bar{\mathbf{S}}^{f,l} = \frac{1}{2}(\mathbf{S}^{f,l} + \mathbf{S}^{a,l})$, we can write

$$\begin{aligned} \bar{S}^{f,l}_{i,n+1} = \bar{S}^{f,l}_{i,n} + D^f_i(\bar{\mathbf{S}}^{f,l}_n, t_n, \Delta t, \Delta W_n,) \\ + M_{i,n} + N_{i,n}, \end{aligned} \tag{3.74}$$

where $M_{i,n}$ and $N_{i,n}$ obey the same scalings as usual. This is in direct analogue to Lemma 4.9 in [GS12a], and its proof is identical, so we omit it. This, in turn, allows one to show the analogue of Theorem 4.10 in [GS12a] and Theorem 3.2 in the present work:

$$\mathbb{E}\left[\max_{n \le N} \left\|\bar{\mathbf{S}}^{f,l}_n - \mathbf{S}^{c,l}_n\right\|^p\right] = O\left(\Delta t^p\right) \tag{3.75}$$

for each $p \ge 2$. The desired variance scaling finally follows directly from Lemma 2.2 in [GS12a], which we restate without proof here:

$$\mathbb{E}\left[\left(\frac{1}{2}\left(P(\mathbf{S}^f) + P(\mathbf{S}^a)\right) - P(\mathbf{S}^c)\right)^p\right] \lesssim \mathbb{E}\left[\left\|\bar{\mathbf{S}}^f - \mathbf{S}^c\right\|^p\right] + \mathbb{E}\left[\left\|\mathbf{S}^f - \mathbf{S}^a\right\|^{2p}\right], \tag{3.76}$$

where we've omitted the l superscripts and assumed that P had two continuous and bounded derivatives. The first term on the right is $O(\Delta t^p)$ by (3.75), and the second term has the same scaling by strong convergence: indeed, $\mathbf{S}^f - \mathbf{S}^a = (\mathbf{S}^f - \mathbf{S}^c) - (\mathbf{S}^a - \mathbf{S}^c)$, and each of the latter two terms is $O(\Delta t^{1/2})$ by the strong convergence of the discretization.

Finally, we note that Theorem 5.2 in [GS12a] may be applied - unchanged - to these results, demonstrating that $V_l = O(h_l^{3/2-\delta})$ for any $\delta > 0$ when P is merely Lipschitz - so long as the set A on which P is non-differentiable is measure zero and

$$\mathbb{P}\left(\min_{y\in A} \|\mathbf{S}(T) - y\| \leq \varepsilon\right) \leq c\,\varepsilon \tag{3.77}$$

for some $c > 0$ and for all $\varepsilon > 0$.

This completes the generalization of the antithetic method to arbitrary M.

3.6 Summary and Implementation

We present an outline of the modified MLMC method including the Ito linearization at the lowest level. This is to be compared to the analogous algorithm in [Gil08b]. This may be used with any discretization we choose - including the approximate Milstein method introduced in section 4 and the generalized antithetic method in section 5 - so long as the discretization is first order in the weak sense. We denote by β the expected scaling of the V_l. That is, $\beta = 2$ for approximate Milstein or generalized antithetic (assuming P has the necessary regularity), and $\beta = 1$ for Euler.

1. Set

$$\mathbb{E}[P_0] = P(\mathbf{S}_0) + \alpha_{d+1}(\mathbf{S}_0)T, \tag{3.78}$$

   where α_{d+1} is as defined in (3.31).

2. Begin with $L = 1$.

3. Estimate V_L and $\hat{Y}_L$ using an initial N_L^i samples, defined by

$$N_L^i = \begin{cases} 400 & : L = 1 \\ M^{-(\beta+1)/2} N_{L-1} & : L > 1 \end{cases} \tag{3.79}$$

4. Set N_l according to

$$N_l = \left\lceil \frac{2}{\varepsilon^2}\sqrt{V_l h_l}\left(\sum_{l=1}^{L}\sqrt{V_l/h_l}\right)\right\rceil \tag{3.80}$$

   for each $l = 1, 2, ..., L$, as per (3.20).

5. Generate additional samples at each level as needed for new N_l, using discretization of your choice to generate approximate solutions of (3.30). Use these samples to update the estimates of the V_l and $\hat{Y}_l$.

6. If $L < 2$ or

$$\max\left\{\left|\hat{Y}_L\right|, M^{-1}\left|\hat{Y}_{L-1}\right|\right\} > \frac{\varepsilon}{\sqrt{2}}, \tag{3.81}$$

let $L \to L+1$ and go to step 3. Else, end with payoff estimate of

$$\hat{P}_L = \mathbb{E}[P_0] + \sum_{l=1}^{L} \hat{Y}_l. \tag{3.82}$$

The inequality (3.81) is the convergence criterion used in [Gil08b]. It determines the algorithm to be converged if the bias error is estimated to be at most $\varepsilon/\sqrt{2}$ when using either of the two finest levels in the estimation.

Equation (3.79) in step 3 is worthy of elaboration. When $L = 1$, we have no information about how many samples we might expect to need, so we pick an arbitrary large number - we find that 400 works well in our test cases, but the number will be problem dependent. However, for $L > 1$, the expected scaling of the V_l allows us to estimate the number of samples needed at the L^{th} level, using

$$N_L \propto \sqrt{V_L h_L} = M^{-(\beta+1)/2}\sqrt{V_{L-1}h_{L-1}} \propto M^{-(\beta+1)/2} N_{L-1}. \tag{3.83}$$

Particularly at large L, when there is relatively little change to the sum in (3.80) as a result of incrementing L, (3.79) is thus a good estimate of N_L as it will be set in step 4. This is preferable to the technique used in [Gil08b] - where $N_L^i = 10^4$, regardless of L - because we avoid wasteful sampling at the high levels where it may be the case that $N_l \ll 10^4$.

3.7 Numerical Results

For our numerical tests, we apply our methods to the Heston model - a financial stochastic volatility model [Hes93] - given by

$$\begin{aligned} dS_1 &= \kappa(\theta - S_1)\,dt + \xi\sqrt{S_1}\,dW_1, \\ dS_2 &= \mu S_2\,dt + \eta\sqrt{S_1}S_2\,dW_2, \end{aligned} \tag{3.84}$$

where S_1 represents the volatility and S_2 the asset price. Throughout our tests, we set the constants $\theta = \mu = \xi = \kappa = 1$ and $\eta = 1/4$. We find that this choice of constants allows us to conduct tests with relatively large L, where the benefits of MLMC are most obvious. We set $\mathbf{S}_0 = (0.5, 1)$, $\Omega_{jk} = \delta_{jk}$, and $T = 0.125$ - a short time simulation allows us to push the limits of the accuracy of the method. Notice that, for this system, $h_{221} = \eta S_2/4$, so that the Milstein discretization does in fact feature Lévy areas.

Notice also that the coefficients of this SDE system do not have uniformly bounded derivatives - namely, the b's have divergent derivative at $S_1 = 0$ - so the assumptions for all of the foregoing results do not hold (see e.g. theorem 3.2), nor do those for standard weak convergence results. However, we have constructed the system so that S_1 is extremely unlikely to approach zero, so that in practice all derivatives are essentially bounded. Indeed, we find excellent agreement between the theory and numerical results.

We test several distinct new MLMC variants:

1. Generalized antithetic method for a payoff with discontinuous derivative
2. Ito linearization technique for smooth payoff using:
   (a) Euler discretization
   (b) Approximate Milstein discretization
   (c) Generalized antithetic discretization

Each of these is compared to the original Euler-based MLMC method introduced in [Gil08b] and the original antithetic method proposed in [GS12a].

In all tests, the computational cost is estimated by the total number of time steps taken, weighted by the dimension of the system being solved. That is, for the standard Euler MLMC method, we set

$$K^e = \sum_{l=0}^{L} N_l(h_l^{-1} + h_{l-1}^{-1}), \tag{3.85}$$

while for the antithetic and generalized antithetic methods (without Ito linearization), we set

$$K^a = \sum_{l=0}^{L} N_l(2h_l^{-1} + h_{l-1}^{-1}) \tag{3.86}$$

to account for the added computation of the antithetic variable $\mathbf{S}^{a,l}$. For the approximate Milstein method, we set

$$K^m = \frac{d+1}{d} \sum_{l=0}^{L} N_l(h_l^{-1} + 2h_{l-1}^{-1}), \tag{3.87}$$

accounting both for the added cost of computing $\mathbf{S}^{*,l}$ and the extra dimension. When Ito linearization is applied to Euler and antithetic methods, we simply scale (3.85) and (3.86) by the factor $(d+1)/d$ and note that $N_0 = 1$.

The counting of time steps is the standard method of estimating computational complexity in the MLMC literature - it is used in [Gil08b, GS12a], among others. However, we note in our discussion at the end of this section that there are other relevant considerations as well.

3.7.1 Generalized antithetic test

We use a standard European option as the payoff function:

$$P(\mathbf{S}) = \max\left\{0, S_2(T) - S_2(0)\right\}. \tag{3.88}$$

Figure 2 demonstrates both the improved variance scaling (left) and corresponding reduction in computational cost (right) afforded by antithetic methods. As predicted in section 4.3, M equal to 4 or 5 minimizes the computational cost. The reduction in cost gained by the generalization to arbitrary M is comparable to that gained by moving from Euler to the

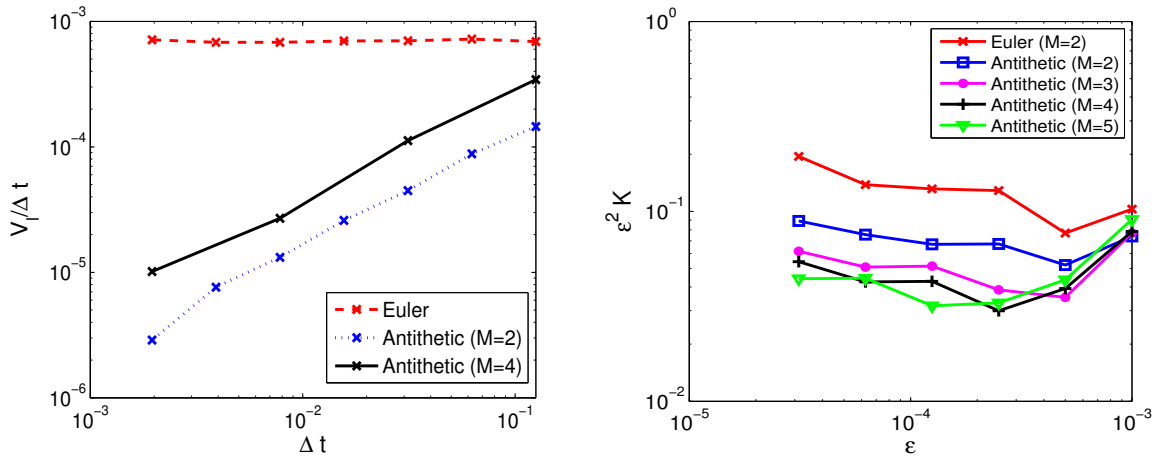

Figure 3.2: Left: A plot of $V_l/\Delta t$ against Δt for the Euler, standard antithetic, and generalized antithetic methods. As expected, the Euler curve is constant, while both antithetic methods demonstrate the same scaling. Right: A comparison of the computational cost of the Euler method to the antithetic method for various refinement factors M as a function of the error tolerance ε. As expected, an M of 4 or 5 is optimal.

original antithetic method. We note that the cost is reduced for larger M in spite of the fact that increasing M actually increases the individual V_l. This because at large M, we need fewer levels, so the sum of the variances is smaller because there are fewer terms in the sum.

3.7.2 Ito linearization and approximate Milstein test

We again use the Heston model with the same parameters but change the payoff function to

$$P(\mathbf{S}) = \sin S_2, \tag{3.89}$$

which of course has the requisite regularity. Figure 3 shows the results, plotting computational cost against error tolerance ε. The Euler, antithetic, and approximate Milstein discretizations are all plotted, each with and without Ito linearization.

For each discretization, Ito linearization improves the efficiency of the scheme, by an order of magnitude in some cases. Note that in the case of approximate Milstein, the use of

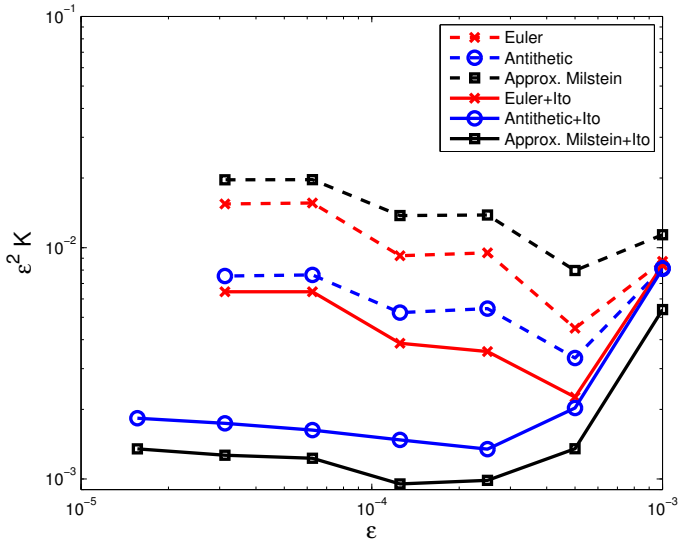

Figure 3.3: Computational cost of MLMC variants with sinusoidal payoff as a function of error tolerance. Euler (red), antithetic (blue), and approximate Milstein (black) discretizations are shown, each with Ito linearization (solid) and without (dashed). All results in this plot use $M = 4$.

Ito's lemma is required for the expectations at adjacent levels to match - see the beginning of section 4 for details - so that the exclusion of Ito linearization is somewhat artificial. This accounts for the disproportionately large expense when Ito linearization is excluded, since the use of Ito's lemma increases the dimension of the system we solve.

The most efficient scheme of those tested is approximate Milstein with Ito linearization, although the advantage over generalized antithetic with Ito linearization is relatively small. As expected based on fig. 1, the approximate Milstein and antithetic methods benefit more from Ito linearization than does Euler because a larger fraction of the work is concentrated at the base level.

We note that neither the approximate Milstein nor the antithetic method produces a completely flat curve when we plot $\varepsilon^2 K$ against ε, as would be predicted by the asymptotic analysis. However, the observations are perfectly consistent with (3.21): the finite sum is bounded by an infinite sum, but is not itself constant in ε. We in fact only expect a flat

curve as $L \to \infty$, and all of the tests conducted here have $L \leq 7$.

Finally, we note that in many cases we get a better-than-expected cost scaling for large ε. This is a result of setting a fixed number of initial samples for $L = 1$ in (3.79) - and for $L = 0$ when Ito linearization is not used - which can turn out to be more than is actually necessary for large ε, making the cost artificially large. We leave this effect in the plots because it is a practical reality of MLMC.

3.7.3 Discussion

The techniques introduced in the present work have the common aim of optimizing MLMC simulations of SDEs. Since the standard MLMC algorithm with the Euler discretization already achieves a nearly optimal cost-to-error scaling, the savings are relatively modest - we rarely save more than a single order of magnitude. While these improvements are hardly negligible, they are small enough that some care in analyzing all sources of computational cost and coding optimization is justified.

In particular, the estimation of computational cost by the total number of time steps taken ignores the fact that not all time steps have identical complexity. In the antithetic and approximate Milstein discretizations, there is an additional term to be computed at each time step. The dominant cost turns out to be the computation of the rank-3 tensor h_{ijk}, which requires $O(d^2D^2)$ operations - the tensor has dD^2 elements, and the computation of each requires a sum of d terms. In contrast, the dominant computation in an Euler time step is the matrix-vector product $\sum_j b_{ij}W_j$, which is $O(dD)$.

With this in mind, a fairer estimate of the computational cost for each method is

$$K = \begin{cases} O\left(\varepsilon^{-2}(\log\varepsilon)^2 dD\right) & : \text{Euler} \\ O\left(\varepsilon^{-2}d^2D^2\right) & : \text{Anithetic \& Approx. Milst.} \end{cases} \tag{3.90}$$

Thus, the optimal discretization is problem dependent - for any fixed ε, Euler with be optimal for some sufficiently large value of dD, while antithetic/approximate Milstein is optimal for smaller values of dD. In financial and chemical kinetic applications, d and D are frequently

large - very possibly exceeding $\log \varepsilon$. Thus, the optimal method is problem dependent, and one should be discouraged from the naive notion that the Milstein and antithetic methods are uniformly more efficient simply because of their more favorable scaling with ε.

This situation is, however, the worst case. Often, b_{ij} and/or h_{ijk} exhibit some form of sparsity, which the code may be written to exploit. It may be possible to leverage the relationship between b_{ij} and h_{ijk} to further accelerate their computation. This is an interesting area of future research.

3.8 Conclusions

In this chapter we have introduced three related improvements to MLMC methods for SDEs. First, we have introduced the idea of Ito linearization, which makes the computation of the base level payoff essentially free, at the price of increasing the dimension of the SDE by one. Secondly, we have introduced an approximate Milstein discretization which, in conjunction with Ito linearization, achieves an $O(\varepsilon^{-2})$ cost scaling with slightly reduced cost compared to the antithetic method. Finally, we demonstrated that the antithetic method can be generalized to arbitrary M without introducing any additional antithetic paths.

The first two techniques are applicable only to payoff functions with two continuous derivatives. As such, they are of very limited use in financial applications, but are expected to be applicable to other fields - examples from chemical kinetics have been cited in the text. The generalized antithetic method, however, requires only a Lipschitz, piecewise smooth payoff, and may thus find applications in finance as well as other disciplines.

Each new method has been tested on a simple SDE system, and we find excellent agreement between the analysis and the numerical results. In the cases in which they are applicable, our new methods consistently outperform the present state-of-the-art.

CHAPTER 4

Conclusions and Future Work

In this thesis, we have addressed the simulation of collisional plasma dynamics, which is a computationally intensive process of importance in many applications. In particular, we have presented two approaches that accelerate Monte Carlo simulation of Coulomb collisions.

The first is a hybrid fluid-Monte Carlo method that leverages the efficiency of fluid schemes to accelerate the simulation by representing some particles using fluid equations. The key insight here is the use of relative entropy as a metric for determining which particles should be part of the fluid representation at any given time. We found that the scheme could be accelerated by a factor of 30 while incurring a relatively small error.

The second uses a Langevin/SDE formulation of the problem and applies the Multilevel Monte Carlo (MLMC) method. The value of the present work is the improvements to MLMC, which take three forms. Firstly, we used Ito's lemma to eliminate the computational cost associated with the base level in the multilevel scheme. It was shown that this could accelerate computations by an order of magnitude when the payoff function is twice differentiable. Secondly, we presented a so-called *approximate Milstein* scheme that achieves the optimal computational complexity. Thirdly, we generalized the antithetic scheme of Giles and Szpruch to arbitrary refinement factors. Each of these latter two represents an incremental, but still noticeable, improvement to the present state of the art.

All of the work presented in this thesis is focused on the spatially homogeneous case. Of obvious interest is the extension of these methods to spatially varying systems. In this final chapter, we discuss some of the challenges inherent in this extension and some avenues forward. We conclude by discussing the implications of this and future work.

4.1 Hybrid Fluid-Monte Carlo Scheme

In our discussion of the hybrid fluid-Monte Carlo scheme, we dealt with one potentially dethermalizing agent - collisions between the fluid and kinetic components of the scheme. In spatially inhomogeneous systems, there are two additional drivers of dethermalization - spatial gradients and electromagnetic fields. We will discuss the difficulties inherent in spatial gradients, which capture the spirit of the challenges associates with electromagnetic fields as well.

In a typical particle-based plasma simulation (PIC), particle positions are updated by

$$\mathbf{x}_{j,n+1} = \mathbf{x}_{j,n} + \Delta t\, \mathbf{v}_{j,n}, \tag{4.1}$$

where $\mathbf{x}_{j,n}$ denotes the position of the j^{th} particle at the n^{th} time step, $\mathbf{v}_{j,n}$ the corresponding velocity, and Δt is the size of the time step. In the hybrid scheme, the issue arises that each simulated particle now has two velocities associated with it - $\mathbf{v}_j$ and $\mathbf{u}_j$. Which is the more appropriate to use in the convection step (4.1)?

Recall that we conceptualize $\mathbf{v}_j$ as being a sample from a distribution of possible velocities for the j^{th} particle, and that $\mathbf{u}_j$ is the mean of this distribution. By the very fact of introducing a distribution in velocity, we generate a distribution in position at the next time step as well, for a particle with uncertain velocity cannot have known position in the future. Thus, the answer to the question above regarding the appropriate velocity for convection is, strictly speaking, neither.

We must instead introduce a distribution in position as well as velocity space. A natural choice is a Maxwellian distribution in space. This approach was taken in [Hew03, Lar03], but in an *ad hoc* manner. Some mathematical backing can be leant to the idea by noticing that if $f_m(\mathbf{x}, \mathbf{v}; \rho, \mathbf{u}, T)$ is a Maxwellian in both velocity and position, with the moments constant in space, then

$$f(\mathbf{x}, \mathbf{v}, t) = f_m(\mathbf{x} - \mathbf{v}t, \mathbf{v}; \rho, \mathbf{u}, T) \tag{4.2}$$

is an *exact solution* of

$$f_t + \mathbf{v} \cdot \nabla_x f = \mathcal{C}(f, f) \tag{4.3}$$

for any collision operator that vanishes on local Maxwellians [Cer88]. It is thus promising to investigate a scheme which evolves particle distributions in this way. The challenge is to maintain a sense in which particles can remain localized within a single cell.

4.2 Multilevel Monte Carlo

At first glance, the extension of MLMC to spatially inhomogeneous problems appears simple. One can simply write down an SDE associated with the full LFP equation:

$$\begin{aligned} d\mathbf{x} &= \mathbf{v}\, dt, \\ d\mathbf{v} &= \frac{e}{m}\left\{\mathbf{E}[f] + \frac{\mathbf{v} \times \mathbf{B}[f]}{c} + \mathbf{F}[f]\right\} dt + \mathbf{D}[f] \cdot dW. \end{aligned} \tag{4.4}$$

Here, $\mathbf{D}$ and $\mathbf{F}$ are the drift and diffusion coefficients associated with the Fokker-Planck collision operator as before, $\mathbf{E}$ and $\mathbf{B}$ are the electric and magnetic fields, respectively, e is the particle charge and m its mass.

The difficulty here is that, unlike in standards SDEs, the coefficients depend not only on the pathwise variables $\mathbf{x}$ and $\mathbf{v}$, but on their distribution f, as indicated by the square bracket notation. Equations of this type are often called McKean-Vlasov equations, after [McK66]. Monte Carlo methods and their convergence for such equations have been studied [AK02, BT97, Oga92].

A multilevel version of these methods, though, faces some difficulties. First of all, to compute $\mathbf{E}$, $\mathbf{B}$, $\mathbf{F}$ and $\mathbf{D}$ at accurately at each time step, we require information about the distribution f at the corresponding time steps. However, at the finest level in MLMC, there are many time steps which have no partner at coarser levels, making it unclear how to obtain the variance reduction that makes MLMC so effective.

Secondly, because the coefficients of the SDE can't be computed exactly for any given path, the errors in the coefficients propagate through to errors in any payoff functions. An

analysis of this propagation in the multilevel context is necessary to determine the accuracy of any extension of MLMC to such equations.

4.3 Concluding Remarks

Each portion of this thesis holds the promise of increasing the efficiency of collisional plasma simulations, with additional applications in rarefied gas dynamics and chemical kinetics. In each context, computer simulations play a crucial role in experimental design and interpretation of results. The acceleration of complex, time-consuming simulations through novel numerical methods like those considered here can dramatically increase their utility for practitioners.

We hope that the methods laid out and tested in this thesis will be useful in their present form, and will also lead to further research. We have discussed some prospects for future work in this concluding chapter, but there is no doubt that more exist. Additionally, we hope that the findings presented here have provided insight into the nature collisions in plasmas, and perhaps sparked new interests in plasma physics and Monte Carlo methods.

APPENDIX A

Proof of Relative Entropy Theorem

In 4.1, we state a theorem about decay of relative entropy:

$$\int_{\mathbb{R}^3} C(f, f_m) \log\left(\frac{f}{\hat{f}_m}\right) d\mathbf{v} \leq 0. \tag{A.1}$$

Here, we provide a proof for the case of the Boltzmann collision operator, given by

$$C(f, g) = \int_{\mathbb{R}^3}\int_{S^2}\left(\frac{d\sigma}{d\Omega}\right)|\mathbf{v} - \mathbf{v}_*|(f'g'_* - fg_*)\, d\Omega\, d\mathbf{v}_*, \tag{A.2}$$

where $d\sigma/d\Omega$ is the differential cross section of the inter-particle force mediating the collisions, the pre-collision velocities are $\mathbf{v}$, $\mathbf{v}_*$, the post-collision velocities $\mathbf{v}'$, $\mathbf{v}'_*$ obey particle momentum and energy conservation, $f' = f(\mathbf{v}')$, and similarly for the other evaluations of f and g.

Because it adds little in the way of complication here, we treat the general case of species with distinct mass. This does require some additional notation: let the two species have distributions f and g, with f_M and g_M being Maxwellian distributions for each respective species having identical mean velocity and temperature.

We initially proceed as in the proof of the H-theorem. Let $\phi(\mathbf{v})$ be an arbitrary function of $\mathbf{v}$. Writing out $C(f, g)$,

$$\int_{\mathbb{R}^3} C(f, g_M)\phi(\mathbf{v})\, d\mathbf{v} = \int B(\theta, |\mathbf{v} - \mathbf{v}_*|)(f'g'_{M*} - fg_{M*})\phi(\mathbf{v})\, d\Omega d\mathbf{v}_* d\mathbf{v}, \tag{A.3}$$

where $B = |\mathbf{v} - \mathbf{v}_*|d\sigma/d\Omega$. Conservation implies

$$m_f\mathbf{v} + m_g\mathbf{v}_* = m_f\mathbf{v}' + m_g\mathbf{v}'_*, \tag{A.4}$$

$$m_f v^2 + m_g v_*^2 = m_f v'^2 + m_g v_*'^2. \tag{A.5}$$

We see that the operator in (A.3) features one of the two symmetries exploited in proving the H-theorem: It is anti-symmetric with respect to exchange of the primed and un-primed velocities. Thus, we can write

$$\int_{\mathbb{R}^3} C(f, g_M)\phi(\mathbf{v})\, d\mathbf{v} = \frac{1}{2}\int B(\theta, |\mathbf{v} - \mathbf{v}_*|)(f'g'_{M*} - fg_{M*})(\phi - \phi')\, d\Omega d\mathbf{v}_* d\mathbf{v}. \tag{A.6}$$

Straightforward algebraic manipulation can be used to show that $|\mathbf{v} - \mathbf{v}_*| = |\mathbf{v}' - \mathbf{v}'_*|$, even when $m_f \neq m_g$. A shorter argument can be made by appealing to the time symmetry of binary collisions.

Now set $\phi = \log(f/f_M)$, so that

$$\phi - \phi' = \log(f/f') - \log(f_M/f'_M). \tag{A.7}$$

Now, note that a simple calculation and observation of (A.4) and (A.5) implies that

$$\log(f_M) + \log(g_{M*}) = \log(f'_M) + \log(g'_{M*}). \tag{A.8}$$

This arises because each side is a linear combination of quantities that are invariant under collisions (total momentum, energy, and mass). As a result, we have $\log(f_M/f'_M) = \log(g'_{M*}/g_{M*})$. Plugging this into the formula for $\phi - \phi'$, and then putting that in (A.6), we have

$$\int_{\mathbb{R}^3} \log\left(\frac{f}{f_M}\right) C(f, g_M)\, d\mathbf{v} = \frac{1}{2}\int B(f'g'_{M*} - fg_{M*}) \log\left(\frac{fg_{M*}}{f'g'_{M*}}\right) d\Omega d\mathbf{v}_* d\mathbf{v}, \tag{A.9}$$

where we've now omitted the arguments on B. Now, since B is non-negative, it doesn't affect the sign of the integrand, and the rest is of the form $(x - y)\log(y/x)$, which is non-positive and zero just in case $x = y$. Thus, the entire integral is at most zero.

It just remains to show when equality is achieved. As already noted, $(x - y)\log(y/x)$ is zero just in case $x = y$, so the right side of (A.9) vanishes if and only if $fg_{M*} = f'g'_{M*}$. Taking the logarithm of both sides gives

$$\log(f) + \log(g_{M*}) = \log(f') + \log(g'_{M*}). \tag{A.10}$$

By (A.8), $f = f_M$ satisfies this equation. If we write $h = f/f_M$, (A.10) reduces to $h = h'$. Fixing $\mathbf{v}$, we can pick $\mathbf{v}_*$ and $\mathbf{v}'_*$ such that $\mathbf{v}'$ has any value we like. Thus, the only solution to $h = h'$ is $h = c(\mathbf{x})$, independent of velocity. Since we assume $\langle f \rangle = \langle f_M \rangle$, we must have $c = 1$.

APPENDIX B

Results on Collisional Moments

To compute the integrals in (2.24) and (2.25), we begin by adopting the notation of [HW04] for the LFP collision operator. We write

$$C_{FP}(f_j, f_M) = -\frac{\partial}{\partial \mathbf{v}} \cdot \left(\frac{f_j}{m} \mathbf{R} - \mathbf{D} \cdot \frac{\partial f_j}{\partial \mathbf{v}} \right), \tag{B.1}$$

where

$$\mathbf{R} = \frac{2\gamma}{m} \frac{\partial H}{\partial \mathbf{v}}, \qquad \mathbf{D} = \frac{\gamma}{m^2} \frac{\partial^2 G}{\partial \mathbf{v} \partial \mathbf{v}}, \tag{B.2}$$

and

$$\gamma = \frac{e^4 \log \Lambda}{8\pi \varepsilon_0^2}. \tag{B.3}$$

We've assumed all the particles under consideration have common mass m and charge e. All subsequent results can be straightforwardly generalized to the case where these quantities differ between species.

Moreover, both here and in appendix C, we find it convenient to work in the rest frame of f_M, so that $\mathbf{u}_M = \mathbf{0}$ and $\mathbf{u}_{jM} = \mathbf{u}_j$.

B.1 Approximating $\mathbf{u}_j$

We define

$$\mathbf{F}_{jM} \equiv \int_{\mathbb{R}^3} \mathbf{v} C_{FP}(\bar{f}_j, f_M) \, d\mathbf{v}, \tag{B.4}$$

so that $(\partial_t \mathbf{u}_j)_M = \mathbf{F}_{jM}$. Using (B.1), we may integrate by parts and use properties relating $\mathbf{R}$ and $\mathbf{D}$ (see [HW04] for more detail) to find

$$\mathbf{F}_{jM} = \frac{2}{m} \int_{\mathbb{R}^3} \bar{f}_j \mathbf{R} \, d\mathbf{v}. \tag{B.5}$$

Then, using (B.2) and (**??**), we can write an explicit expression for $\mathbf{R}$.

$$\mathbf{R} = \frac{2\gamma n_M}{m}\frac{\mathbf{v}}{v^3}\left[x\frac{d\ \mathrm{erf}(x)}{dx} - \mathrm{erf}(x)\right], \tag{B.6}$$

where n_M is the number density associated f_M, and $\mathbf{x} = \mathbf{v}/v_{tM}$. Under the assumption that f_j is Maxwellian, the integral in (B.5) can now be evaluated numerically in general, and analytically in two important limits.

Firstly, as mentioned earlier, near the beginning of a hybrid simulation, f_j is well approximated by a δ-function at the particle's actual velocity, which now coincides with its mean velocity $\mathbf{u}_j$. Making this approximation, we easily find that

$$\mathbf{F}_{jM} \approx \frac{4\gamma n_M}{m^2 v_{tM}^2}\frac{\mathbf{U}_{jM}}{U_{jM}^3}\left[U_{jM}\frac{d\ \mathrm{erf}(U_{jM})}{dx} - \mathrm{erf}(U_{jM})\right], \tag{B.7}$$

where $\mathbf{U}_{jM} = \mathbf{u}_{jM}/v_{tM}$. We'll refer to this expression for $\mathbf{F}_{jM}$ as $\mathbf{F}_{jM}^{\delta}$, which is valid when $v_{tj} \ll v_{tM}$ (i.e. $T_j \ll T_M$).

Secondly, at late times in the simulation, we expect that $u_{jM} \ll v_{tj}$, so that we may approximate $\bar{f}_j = f_m(\mathbf{v}; 1, \mathbf{u}_j, T_j)$ by

$$\bar{f}_j \approx f_m\left(\mathbf{v}; 1, \mathbf{0}, T_j\right)\left(1 + \frac{2\mathbf{v}\cdot\mathbf{u_{jM}}}{v_{tj}^2}\right). \tag{B.8}$$

Plugging this approximation into (B.5) gives (see [HW04] for more detail)

$$\mathbf{F}_{jM} \approx -\frac{1}{\tau_{jM}}\mathbf{u}_{jM}, \tag{B.9}$$

where

$$\tau_{jM} = \frac{3\sqrt{\pi}m^2}{16}\frac{\left(v_{tj}^2 + v_{tM}^2\right)^{3/2}}{\gamma n_M}. \tag{B.10}$$

This expression for $\mathbf{F}_{jM}$ will be called $\mathbf{F}_{jM}^{m}$ and is valid when $u_{jM} \ll v_{tj}$.

B.2 Approximating T

We define

$$W_{jM} \equiv \frac{1}{2}m\int_{\mathbb{R}^3}|\mathbf{v} - \mathbf{u}_j|^2 C_{FP}(\bar{f}_j, f_M)\, d\mathbf{v}, \tag{B.11}$$

so that $(\partial_t T_j)_M = 2W_{jM}/3$. By expanding the squared term in W_{jM}, we find

$$W_{jM} = \frac{1}{2} m \int_{\mathbb{R}^3} v^2 C_{FP}(\bar{f}_j, f_M)\, d\mathbf{v} - m\mathbf{u}_j \cdot \mathbf{F}_{jM}. \tag{B.12}$$

Having already computed expressions for $\mathbf{F}$, it suffices to compute what we'll call W', defined by

$$W'_{jM} \equiv \frac{1}{2} m \int_{\mathbb{R}^3} v^2 C_{FP}(\bar{f}_j, f_M)\, d\mathbf{v}. \tag{B.13}$$

Again, by plugging in the definition of C_{FP} into (B.13) and integrating by parts - twice this time - then using the definitions of $\mathbf{R}$ and $\mathbf{D}$, we find

$$W'_{jM} = \kappa \int_{\mathbb{R}^3} \left[2\frac{d\ \mathrm{erf}(x)}{dx} - \frac{\mathrm{erf}(x)}{x} \right] \bar{f}_j\, d\mathbf{v}, \tag{B.14}$$

where

$$\kappa = \frac{2\gamma n_M}{m v_{tM}} \tag{B.15}$$

and $x = v/v_{tM}$. Again, the integral in (B.14) can be evaluated numerically for a general Maxwellian f, and analytically in two important limits.

We again treat the case in which $v_{tj} \ll v_{tM}$. As before, we approximate f_j by $\delta^3(\mathbf{v} - \mathbf{u}_j)$. The integral for W'_{jM} is now easily evaluated, and when combined with (B.7) and (B.12) gives

$$W_{jM} = \kappa \frac{\mathrm{erf}(U_{jM})}{U_{jM}} = \frac{2\gamma n_M}{m v_{tM}} \frac{\mathrm{erf}(U_{jM})}{U_{jM}}. \tag{B.16}$$

In analogue to the previous subsection, this expression for W_{jM} will be referred to as W^{δ}_{jM} and is valid when $v_{tj} \ll v_{tM}$.

Finally, we consider the $u_{jM} \ll v_{tj}$ limit, just as we did when approximating $\mathbf{F}_{jM}$. As before, we approximate $\bar{f}_j$ by a Taylor series expansion, this time keeping

$$\bar{f}_j \approx f_m\left(\mathbf{v}; 1, \mathbf{0}, T_j\right) \left(1 + \frac{2\mathbf{v} \cdot \mathbf{u}_{jM}}{v_{tj}^2} - \frac{u_{jM}^2}{v_{tj}^2} \right) \tag{B.17}$$

(we ignored the last term before because it gave no contribution to the previous integral). Using this expression for f in (B.14) and integrating gives

$$W_{jM} = \frac{1}{\tau_{jM}} \left[\frac{3}{2} \left(1 - \frac{u_{jM}^2}{v_{tj}^2} \right) (T_M - T_j) + m u_{jM}^2 \right]. \tag{B.18}$$

Again in analogue to the previous subsection, we will denote this expression for W_{jM} by W_{jM}^m and it is valid when $u_{jM} \ll v_{tj}$.

APPENDIX C

Numerical Integration of Collisional Moments

Because of the length of the expressions in this appendix, we abbreviate our notation by dropping the subscripts j and M wherever possible, and again work in coordinates where $\mathbf{u}_M$ vanishes. That is, we let $f_j \to f$, $v_{tj} \to v_t$, $\mathbf{u}_{jM} = \mathbf{u}_j \to \mathbf{u}$, $\mathbf{F}_{jM} \to \mathbf{F}$, and $W_{jM} \to W$.

In appendix B, we derived integral expressions for $\mathbf{F}$ and W', the collisional rates of change of the first and second moments of f, respectively:

$$\mathbf{F} = \frac{2}{m} \int_{\mathbb{R}^3} \bar{f} \mathbf{R} \, d\mathbf{v} \tag{C.1}$$

$$W' = \kappa \int_{\mathbb{R}^3} \left[2 \frac{d \, \mathrm{erf}(x)}{dx} - \frac{\mathrm{erf}(x)}{x} \right] \bar{f} \, d\mathbf{v}, \tag{C.2}$$

where expressions for $\mathbf{R}$ and κ are given in (B.6) and (B.15), respectively, and x is as defined in appendix B. We then derived asymptotically valid analytic expressions for the case when f is Maxwellian with either $v_t \ll v_{tM}$ or $u \ll v_t$. In this appendix, we further demonstrate that the above expressions for $\mathbf{F}$ and W' can expressed in terms of easily computable, one dimensional integrals depending on only two non-dimensional parameters and physical constants for a *general Maxwellian* f.

C.1 Simplifying W'

Let us work in spherical coordinates with the z-axis aligned with $\mathbf{u}$, the mean velocity of f. Then, a Maxwellian $\bar{f}$ may be written as

$$\bar{f} = \frac{1}{\pi^{3/2} v_t^3} \exp\left(-\frac{|\mathbf{v} - \mathbf{u}|^2}{v_t^2} \right) = \frac{1}{\pi^{3/2} v_t^3} \exp\left(-\frac{v^2 + u^2}{v_t^2} \right) \exp\left(\frac{2uv \cos\phi}{v_t^2} \right). \tag{C.3}$$

We observe that every term in (C.2) is spherically symmetric except for the right-most term in (C.3). The angular integration is thus easily performed, giving

$$\int_0^{2\pi}\int_0^{\pi} \exp\left(\frac{2uv\cos\varphi}{v_t^2}\right)\sin\varphi\, d\varphi\, d\theta = \frac{2\pi v_t^2}{uv}\sinh\left(\frac{2uv}{v_t^2}\right). \tag{C.4}$$

Next, we define $\Gamma = v_{tM}/v_t$, so that $v/v_t = \Gamma x$ and $u/v_t = \Gamma U$, with U as defined in appendix B. We can now rewrite

$$W' = \frac{\kappa}{\sqrt{\pi}}\frac{\Gamma}{U}\int_0^{\infty} xG(x;\, U,\Gamma)\left[2\frac{d\mathrm{erf}(x)}{dx} - \frac{\mathrm{erf}(x)}{x}\right] dx, \tag{C.5}$$

where

$$G(x;\, U,\Gamma) \equiv \exp\left(-\Gamma^2(x-U)^2\right) - \exp\left(-\Gamma^2(x+U)^2\right). \tag{C.6}$$

The expression for W' in (C.5) is now a one dimensional integral that is straightforward to evaluate numerically.

C.2 Simplifying F

We work in the same coordinates, and the expression (C.3) for $\bar{f}$ still applies. However, the vector $\mathbf{R}$ contributes to the angular integrals. We write $\mathbf{R} = (\mathbf{v}/v)R(x)$, where

$$R(x) = \frac{2\gamma n_M}{m v_{tM}^2}\frac{1}{x^2}\left[x\frac{d\ \mathrm{erf}(x)}{dx} - \mathrm{erf}(x)\right]. \tag{C.7}$$

The angular portion of the integral for $\mathbf{F}$ now reads

$$\int_0^{2\pi}\int_0^{\pi} \left(\frac{\mathbf{v}}{v}\right)\exp\left(\frac{2uv\cos\varphi}{v_t^2}\right)\sin\varphi\, d\varphi\, d\theta. \tag{C.8}$$

All the components of this vector vanish except for that aligned with $\mathbf{u}$, because the integration against θ yields zero in the other cases. The component along $\mathbf{u}$ may be evaluated, giving

$$\int_0^{2\pi}\int_0^{\pi} \left(\frac{\mathbf{v}}{v}\right)\exp\left(\frac{2uv\cos\varphi}{v_t^2}\right)\sin\varphi\, d\varphi\, d\theta = \frac{2\pi\mathbf{U}}{\Gamma^2U^2x}\left(\cosh(\psi) - \frac{\sinh(\psi)}{\psi}\right), \tag{C.9}$$

where

$$\psi \equiv 2\Gamma^2 Ux. \tag{C.10}$$

We then write $\mathbf{F}$ as

$$\mathbf{F} = \frac{4}{\sqrt{\pi}m}\frac{\Gamma}{U}\left(\frac{\mathbf{U}}{U}\right)\int_0^\infty xR(x)\exp\left(-\Gamma^2\left(x^2+U^2\right)\right)\left(\cosh(\psi)-\frac{\sinh(\psi)}{\psi}\right)dx. \qquad \text{(C.11)}$$

Again, this integral is now easily evaluated numerically.

The expressions (C.5) and (C.11) are used to generate the black curves in fig. 1 and may in theory be used to generate two dimensional (Γ, U) lookup tables which can then govern the evolution of the particle temperatures and mean velocities.

APPENDIX D

Proof of Lemma 3.1

The argument here follows that in [Mil79]. It proceeds in two stages: first, we express the total error as a sum of various local truncation errors, totaling $O(\Delta t^{-1})$ in number. Second, we show that each local truncation error is $O(\Delta t^2)$.

Toward the first end, we introduce some notation for this proof not used elsewhere: Denote by $\mathbf{S}_n^{c,l}[\mathbf{x}]$ that solution of the recursion equation (3.42) at time t_n which starts at $\mathbf{x}$ at time zero, and similarly for $\mathbf{S}_n^{*,l}[\mathbf{x}]$. For this proof we will assume that the system is autonomous, so that

$$\mathbf{S}_{n+1}^{c,l}[\mathbf{x}] = \mathbf{S}_1^{c,l}\left[\mathbf{S}_n^{c,l}[\mathbf{x}]\right], \tag{D.1}$$

and similarly for $\mathbf{S}_{n+1}^{*,l}[\mathbf{x}]$. All of the arguments presented here generalize to the non-autonomous case, but the notation is much cleaner if autonomy is assumed. Define $g_n^c(\mathbf{x}) = \mathbb{E}f(\mathbf{S}_n^{c,l}[\mathbf{x}])$ and similarly for $g_n^*(\mathbf{x})$. Then, leveraging (D.1), we have

$$\begin{aligned} g_{n+1}^c(\mathbf{x}) - g_{n+1}^*(\mathbf{x}) &= \mathbb{E}f\left(\mathbf{S}_1^{c,l}\left[\mathbf{S}_n^{c,l}[\mathbf{x}]\right]\right) - \mathbb{E}f\left(\mathbf{S}_1^{*,l}\left[\mathbf{S}_n^{*,l}[\mathbf{x}]\right]\right) \\ &= \mathbb{E}g_1^c\left(\mathbf{S}_n^{c,l}[\mathbf{x}]\right) - \mathbb{E}g_1^*\left(\mathbf{S}_n^{*,l}[\mathbf{x}]\right) \\ &= \mathbb{E}\left\{g_1^c\left(\mathbf{S}_n^{c,l}[\mathbf{x}]\right) - g_1^*\left(\mathbf{S}_n^{c,l}[\mathbf{x}]\right)\right\} + \mathbb{E}\left\{g_1^*\left(\mathbf{S}_n^{c,l}[\mathbf{x}]\right) - g_1^*\left(\mathbf{S}_n^{*,l}[\mathbf{x}]\right)\right\}. \end{aligned} \tag{D.2}$$

The first expectation in the third line is a local truncation error: it's the difference in f evaluated at the coarse and starred discretizations after one time step, when both started at the same place; namely, $\mathbf{S}_n^{c,l}[\mathbf{x}]$. Due to the nature of the coarse and starred discretizations, the function g_1^* is as smooth as f, so the second expectation is of the same sort we're trying to bound, but one time step earlier than where we started.

If we define $\varepsilon_n[f] = \mathbb{E}f(\mathbf{S}_n^{c,l}[\mathbf{x}]) - \mathbb{E}f(\mathbf{S}_n^{*,l}[\mathbf{x}])$, then (D.2) reads

$$\varepsilon_{n+1}[f] = \mathbb{E}\left\{g_1^c\left(\mathbf{S}_n^{c,l}[\mathbf{x}]\right) - g_1^*\left(\mathbf{S}_n^{c,l}[\mathbf{x}]\right)\right\} + \varepsilon_n[g_1^*]. \tag{D.3}$$

In the same way, we may go on to derive

$$\varepsilon_n[g_1^*] = \mathbb{E}\left\{h_1^c\left(\mathbf{S}_n^{c,l}[\mathbf{x}]\right) - h_1^*\left(\mathbf{S}_n^{c,l}[\mathbf{x}]\right)\right\} + \varepsilon_{n-1}[h_1^*] \tag{D.4}$$

for appropriate definitions of h_n^c and h_n^*. Iterating this process, we find

$$\varepsilon_n[f] = \sum_{k=1}^{n-1}\mathbb{E}\left\{h_1^{k,c}\left(\mathbf{S}_k^{c,l}[\mathbf{x}]\right) - h_1^{k,*}\left(\mathbf{S}_k^{c,l}[\mathbf{x}]\right)\right\} \tag{D.5}$$

for some sequences of functions $\{h_1^{k,c}\}$ and $\{h_1^{*,c}\}$, each of which is as smooth as f and represents the error in the given function after a single time step (we've used the fact that $\mathbf{S}_0^{c,l} = \mathbf{S}_0^{*,l}$). This completes the first step of expressing the total error in terms of local truncation errors.

It just remains to show that each of these errors is $O(\Delta t^2)$. We do this by Taylor expansion of f. Suppose f has four continuous derivatives, so that we can write out its fourth order Taylor series:

$$\begin{aligned} f\left(\mathbf{S}_1^{c,l}[\mathbf{x}]\right) &= f(\mathbf{x}) + \nabla f(\mathbf{x})\cdot\mathbf{D}^c(\mathbf{x},\mathbf{x},t_0,\Delta t,\delta W_0,\delta W_{\frac{1}{2}}) \\ &\quad + \frac{1}{2!}\nabla^2 f(\mathbf{x}) : \mathbf{D}^c\mathbf{D}^c + \frac{1}{3!}\nabla^3 f(\mathbf{x})(\mathbf{D}^c)^3 + \frac{1}{4!}\nabla^4 f(\xi)(\mathbf{D}^c)^4 \end{aligned} \tag{D.6}$$

for some ξ on the line between $\mathbf{x}$ and $\mathbf{S}_1^{c,l}$, and $\mathbf{D}^c$ has the same arguments in all instances. A similar expression holds for $f(\mathbf{S}_1^{*,l}[\mathbf{x}])$. Subtracting the two expressions and taking expectations, we have

$$\begin{aligned} \mathbb{E}f\left(\mathbf{S}_1^{c,l}[\mathbf{x}]\right) - \mathbb{E}f\left(\mathbf{S}_1^{*,l}[\mathbf{x}]\right) &= \frac{1}{2!}\nabla^2 f(\mathbf{x}) : \mathbb{E}\left\{\mathbf{D}^c\mathbf{D}^c - \mathbf{D}^f\mathbf{D}^f\right\} \\ &\quad + \frac{1}{3!}\nabla^3 f(\mathbf{x})\mathbb{E}\left\{(\mathbf{D}^c)^3 - (\mathbf{D}^f)^3\right\} \\ &\quad + \frac{1}{4!}\mathbb{E}\left\{\nabla^4 f(\xi_1)(\mathbf{D}^c)^4\right\} - \mathbb{E}\left\{\nabla^4 f(\xi_2)(\mathbf{D}^f)^4\right\}. \end{aligned} \tag{D.7}$$

Careful but straightforward examination of all the expectations in (D.7) reveals that the lowest order terms that don't vanish in expectation are all $O(\Delta t^2)$. This is true for any function as smooth as f, and so is true of each $h_1^{k,c}$ and $h_1^{k,*}$ in (D.5). The number of terms in the sum in (D.5) is $O(\Delta t^{-1})$, so we have the desired result.

APPENDIX E

Proof of Theorem 3.2

Using Lemmas 3.2 and 3.3, we may write

$$\begin{aligned} S^f_{i,n} - S^c_{i,n} &= \left(S^f_{i,n-1} - S^c_{i,n-1}\right) + \left[a_i(\mathbf{S}^f_{n-1}) - a_i(\mathbf{S}^c_{n-1})\right]\Delta t \\ &+ \sum_{j=1}^{D}\left[b_{ij}(\mathbf{S}^f_{n-1}) - b_{ij}(\mathbf{S}^c_{n-1})\right]\Delta W_{j,n-1} \\ &+ \sum_{j,k=1}^{D}\left[h_{ijk}(\mathbf{S}^f_{n-1}) - h_{ijk}(\mathbf{S}^c_{n-1})\right] L_{jk,n-1} \\ &+ M_{i,n-1} + N_{i,n-1}. \end{aligned} \tag{E.1}$$

where $M_{i,n} = M^f_{i,n} + M^c_{i,n}$ and similarly for $N_{i,n}$, and

$$L_{jk,n} = \Delta W_{j,n}\Delta W_{k,n} - \Omega_{jk}\Delta t. \tag{E.2}$$

If we add up (E.1) all the way back to the initial time and use $\mathbf{S}^f_0 = \mathbf{S}^c_0$, we have

$$\begin{aligned} S^f_{i,n} - S^c_{i,n} &= \sum_{m=0}^{n-1}\left[a_i(\mathbf{S}^f_m) - a_i(\mathbf{S}^c_m)\right]\Delta t \\ &+ \sum_{m=0}^{n-1}\sum_{j=1}^{D}\left[b_{ij}(\mathbf{S}^f_m) - b_{ij}(\mathbf{S}^c_m)\right]\Delta W_{j,m} \\ &+ \sum_{m=0}^{n-1}\sum_{j,k=1}^{D}\left[h_{ijk}(\mathbf{S}^f_m) - h_{ijk}(\mathbf{S}^c_m)\right] L_{jk,m} \\ &+ \sum_{m=0}^{n-1}(M_{i,m} + N_{i,m}). \end{aligned} \tag{E.3}$$

This is conceptually identical to the second equation in the proof of theorem 4.10 (Appendix 4) in [GS12a], and may be treated with exactly the same methods found therein.

In particular, defining

$$R_n = \mathbb{E}\left[\max_{m\leq n} \left\|\mathbf{S}_m^f - \mathbf{S}_m^c\right\|^2\right], \tag{E.4}$$

one can establish the recursive relation

$$R_n \leq C\left(\Delta t^2 + \Delta t \sum_{m=0}^{n-1} R_m\right) \tag{E.5}$$

for some $C > 0$. A discrete version of the Grönwall inequality implies

$$R_n \leq C\left(\Delta t^2 + \sum_{m=0}^{n-1} \Delta t^3 \exp\left\{\sum_{k=m}^{n-1} \Delta t\right\}\right) \leq C\left(\Delta t^2 + n\Delta t^3 \exp(n\Delta t)\right). \tag{E.6}$$

Letting $n \to N$, we have

$$R_N \leq C(1 + T\exp T)\Delta t^2, \tag{E.7}$$

which immediately implies the desired result.

APPENDIX F

Proof of Lemma 3.4

The first step is to reestablish Lemma 3.2 in the case when the fine steps are allowed to have different step sizes. The desired result will follow by induction, in that we will treat the first r time-steps as a single step, and the $(r+1)^{\text{st}}$ as the second step. Let δt_1 be the time step for the first fine step, and δt_2 the time step for the second, with $\delta W_{j,n}$ and $\delta W_{j,n+\frac{1}{2}}$ the corresponding Brownian increments with variances δt_1 and δt_2, respectively. That is,

$$\mathbf{S}^f_{n+\frac{1}{2}} = \mathbf{S}^f_n + \mathbf{D}^f(\mathbf{S}^f_n, t_n, \delta t_1, \delta W_{j,n}), \tag{F.1}$$

$$\mathbf{S}^f_{n+1} = \mathbf{S}^f_{n+\frac{1}{2}} + \mathbf{D}^f(\mathbf{S}^f_{n+\frac{1}{2}}, t_n + \delta t_1, \delta t_2, \delta W_{j,n+\frac{1}{2}}), \tag{F.2}$$

where we've omitted the l superscripts.

Through diligent algebra, we can show that

$$\begin{aligned} S^f_{i,n+1} = {} & S^f_{i,n} + D^f_i(\mathbf{S}^f_n, t_n, \delta t_1 + \delta t_2, \delta W_{j,n} + \delta W_{j,n+\frac{1}{2}}) \\ & - \sum_{j,k=1}^{D} h_{ijk,n}\left(\delta W_{j,n}\delta W_{k,n+\frac{1}{2}} - \delta W_{k,n}\delta W_{j,n+\frac{1}{2}}\right) \\ & + R_{i,n} + M^{(1)}_{i,n} + M^{(2)}_{i,n} \end{aligned} \tag{F.3}$$

where

$$\begin{aligned} R_{i,n} &= \left(a_{i,n+\frac{1}{2}} - a_{i,n}\right)\delta t_2 \\ M^{(1)}_{i,n} &= \sum_{j=1}^{D}\left(b_{ij,n+\frac{1}{2}} - b_{ij,n} - 2\sum_{k=1}^{D} h_{ijk,n}\delta W_{k,n}\right)\delta W_{j,n+\frac{1}{2}} \\ M^{(2)}_{i,n} &= \sum_{j,k=1}^{D}\left(h_{ijk,n+\frac{1}{2}} - h_{ijk,n}\right)\left(\delta W_{j,n+\frac{1}{2}}\delta W_{k,n+\frac{1}{2}} - \Omega_{jk}\delta t_2\right). \end{aligned} \tag{F.4}$$

From here, the argument bounding the remainder terms proceeds exactly as in Lemma 4.7 in [GS12a]. In particular, $M_{i,n}^{(1)}$ and $M_{i,n}^{(2)}$ have vanishing expectation, and may be shown to scale like $\Delta t^{3/2}$ by Taylor expanding $b_{ij,n+\frac{1}{2}}$ and $h_{ijk,n+\frac{1}{2}}$ about t_n. Similarly, $a_{i,n+\frac{1}{2}}$ is Taylor expanded to separate $R_{i,n}$ into two terms, one of which satisfies the appropriate scaling for $M_{i,n}$ while the other satisfies the scaling for $N_{i,n}$. We refer the interested reader to [GS12a] for a thorough treatment.

We now proceed by induction: Suppose that for some $r < M$, we've shown that

$$\begin{aligned} S_{i,n+\frac{r}{M}}^{f,l} &= S_{i,n}^{f,l} + D_i^f \left(\mathbf{S}_n^{f,l}, t_n, r\delta t, \sum_{q=0}^{r-1} \delta W_{j,n+\frac{q}{M}} \right) \\ &\quad - \sum_{j,k=1}^{D} h_{ijk}(\mathbf{S}_n^{f,l}) \left(\mathcal{A}_{jk,n}^{(r)} - \mathcal{A}_{kj,n}^{(r)} \right) \\ &\quad + M_{i,n}^f + N_{i,n}^f \end{aligned} \tag{F.5}$$

where

$$\mathcal{A}_{jk,n}^{(r)} = \sum_{m=1}^{r-1} \left(\delta W_{k,n+\frac{m}{M}} \sum_{q=0}^{m-1} \delta W_{j,n+\frac{q}{M}} \right). \tag{F.6}$$

and $M_{i,n}^f$ and $N_{i,n}^f$ have the scalings stated in the lemma. Note that the base case $r = 1$ is trivial, and that $r = 2$ is given by Lemma 3.2. Then, applying our modified version of Lemma 3.2 to (F.5) and

$$S_{i,n+\frac{r+1}{M}}^{f,l} = S_{i,n+\frac{r}{M}}^{f,l} + D_i^f \left(\mathbf{S}_{n+\frac{r}{M}}^{f,l}, t_n + r\delta t, \delta t, \delta W_{j,n+\frac{r}{M}} \right), \tag{F.7}$$

we have

$$\begin{aligned} S_{i,n+\frac{r+1}{M}}^{f,l} &= S_{i,n}^{f,l} + D_i^f \left(\mathbf{S}_n^{f,l}, t_n, r\delta t, \sum_{q=0}^{r} \delta W_{j,n+\frac{q}{M}} \right) \\ &\quad - \sum_{j,k=1}^{D} h_{ijk}(\mathbf{S}_n^{f,l}) \left[\delta W_{k,n+\frac{r}{M}} \left(\sum_{q=0}^{r-1} \delta W_{j,n+\frac{q}{M}} \right) - \delta W_{j,n+\frac{r}{M}} \left(\sum_{q=0}^{r-1} \delta W_{k,n+\frac{q}{M}} \right) \right] \\ &\quad - \sum_{j,k=1}^{D} h_{ijk}(\mathbf{S}_n^{f,l}) \left(\mathcal{A}_{jk,n}^{(r)} - \mathcal{A}_{kj,n}^{(r)} \right) \\ &\quad + M_{i,n}^f + N_{i,n}^f \end{aligned} \tag{F.8}$$

where the new remainder terms have been absorbed into the $M_{i,n}^f$ and $N_{i,n}^f$. The second and third lines can be combined to obtain

$$\begin{aligned} S_{i,n+\frac{r+1}{M}}^{f,l} &= S_{i,n}^{f,l} + D_i^f \left(\mathbf{S}_n^{f,l}, t_n, r\delta t, \sum_{q=0}^{r} \delta W_{j,n+\frac{q}{M}} \right) \\ &\quad - \sum_{j,k=1}^{D} h_{ijk}(\mathbf{S}_n^{f,l}) \left(\mathcal{A}_{jk,n}^{(r+1)} - \mathcal{A}_{kj,n}^{(r+1)} \right) \\ &\quad + M_{i,n}^f + N_{i,n}^f \end{aligned} \tag{F.9}$$

Letting the induction carry to M, we have the desired result, for $\mathcal{A}_{jk,n}^{(M)} = \mathcal{A}_{jk,n}$ by definition.

References

[ABC08] I.G. Abel, M. Barnes, S.C. Cowley, W. Dorland, and A.A. Schekochihin. "Linearized model Fokker–Planck collision operators for gyrokinetic simulations. I. Theory." *Physics of Plasmas*, **15**:122509, 2008.

[AG97] Francis J. Alexander and Alejandro L. Garcia. "The direct simulation Monte Carlo method." *Computers in Physics*, **11**(6):588, 1997.

[AK02] Fabio Antonelli, Arturo Kohatsu-Higa, et al. "Rate of convergence of a particle method to the solution of the McKean–Vlasov equation." *The Annals of Applied Probability*, **12**(2):423–476, 2002.

[AV94] E.J. Allen and H.D. Victory Jr. "A computational investigation of the random particle method for numerical solution of the kinetic Vlasov-Poisson-Fokker-Planck equations." *Physica A: Statistical Mechanics and its Applications*, **209**(3):318–346, 1994.

[AV04] R. Alexandre and C. Villani. "On the Landau approximation in plasma physics." In *Annales de l'Institut Henri Poincare (C) Non Linear Analysis*, volume 21, pp. 61–95. Elsevier, 2004.

[BBD02] O.V. Batishchev, V. Yu Bychenkov, F. Detering, W. Rozmus, R. Sydora, C.E. Capjack, and V.N. Novikov. "Heat transport and electron distribution function in laser produced plasmas with hot spots." *Physics of Plasmas*, **9**:2302, 2002.

[BBF92] R.A. Bosch, R.L. Berger, B.H. Failor, N.D. Delamater, G. Charatis, and R.L. Kauffman. "Collision and interpenetration of plasmas created by laser-illuminated disks." *Physics of Fluids B: Plasma Physics*, **4**:979, 1992.

[BG46a] Nikolai N. Bogoliubov and K.P. Gurov. "Kinetic equations." *J. Phys.(USSR)*, **10**:265, 1946.

[BG46b] Max Born and H.S. Green. "A general kinetic theory of liquids. I. The molecular distribution functions." *Proceedings of the Royal Society of London. Series A. Mathematical and Physical Sciences*, **188**(1012):10–18, 1946.

[BGK54] Prabhu Lal Bhatnagar, Eugene P. Gross, and Max Krook. "A model for collision processes in gases. I. Small amplitude processes in charged and neutral one-component systems." *Physical review*, **94**(3):511, 1954.

[Bir76] Graeme Austin Bird. "Molecular gas dynamics." *NASA STI/Recon Technical Report A*, **76**:40225, 1976.

[Bir91] Charles K. Birdsall. "Particle-in-cell charged-particle simulations, plus Monte Carlo collisions with neutral atoms, PIC-MCC." *Plasma Science, IEEE Transactions on*, **19**(2):65–85, 1991.

[BN00] A.V. Bobylev and K. Nanbu. "Theory of collision algorithms for gases and plasmas based on the Boltzmann equation and the Landau-Fokker-Planck equation." *Physical Review E*, **61**(4):4576, 2000.

[Bob75] A.V. Bobylev. "On the expansion of the Boltzmann collision integral into Landau series." In *Akademiia Nauk SSSR Doklady*, volume 225, pp. 535–538, 1975.

[BP13] Alexander V. Bobylev and I.F. Potapenko. "Monte Carlo methods and their analysis for Coulomb collisions in multicomponent plasmas." *Journal of Computational Physics*, 2013.

[Bra65] S.I. Braginskii. "Transport processes in a plasma." *Reviews of plasma physics*, **1**:205, 1965.

[BT97] Mireille Bossy and Denis Talay. "A stochastic particle method for the McKean-Vlasov and the Burgers equation." *Mathematics of Computation of the American Mathematical Society*, **66**(217):157–192, 1997.

[Bur06] A.N. Burkitt. "A review of the integrate-and-fire neuron model: I. Homogeneous synaptic input." *Biological cybernetics*, **95**(1):1–19, 2006.

[CC70] Sydney Chapman and Thomas George Cowling. *The mathematical theory of non-uniform gases: an account of the kinetic theory of viscosity, thermal conduction and diffusion in gases*. Cambridge university press, 1970.

[CC91] S. Chapman and T.G. Cowling. *The Mathematical Theory of Non-uniform Gases: An Account of the Kinetic Theory of Viscosity, Thermal Conduction, and Diffusion in Gases*. Cambridge Univ Pr, 1991.

[CDL06] B.I. Cohen, L. Divol, A.B. Langdon, and E.A. Williams. "Effects of ion-ion collisions and inhomogeneity in two-dimensional kinetic ion simulations of stimulated Brillouin backscattering." *Physics of plasmas*, **13**(2):022705–022705, 2006.

[CDW99] Phillip Colella, Milo R. Dorr, and Daniel D. Wake. "A conservative finite difference method for the numerical solution of plasma fluid equations." *Journal of Computational Physics*, **149**(1):168–193, 1999.

[Cer69] Carlo Cercignani. *Mathematical methods in kinetic theory*. Springer, 1969.

[Cer88] Carlo Cercignani. *The Boltzmann equation*. Springer, 1988.

[CFP13] Antoine J. Cerfon, Jeffrey P. Freidberg, Felix I. Parra, and Timothy A. Antaya. "Analytic fluid theory of beam spiraling in high-intensity cyclotrons." *Physical Review Special Topics-Accelerators and Beams*, **16**(2):024202, 2013.

[CL84] Francis F. Chen and M.A. Lieberman. *Introduction to plasma physics and controlled fusion/Francis F.* : Plenum Press, New York, 1984.

[CRG96] Seung J. Choi, Daniel J. Rader, and Anthony S. Geller. "Massively parallel simulations of Brownian dynamics particle transport in low pressure parallel-plate reactors." *Journal of Vacuum Science & Technology A*, **14**(2):660–665, 1996.

[CT06] T.M. Cover and J.A. Thomas. *Elements of Information Theory*. John Wiley & Sons, New Jersey, 2006.

[CW03] J. Candy and R.E. Waltz. "Anomalous transport scaling in the DIII-D tokamak matched by supercomputer simulation." *Physical review letters*, **91**(4):045001, 2003.

[CWD08] Russel Caflisch, Chiaming Wang, Giacomo Dimarco, Bruce Cohen, and Andris Dimits. "A hybrid method for accelerated simulation of Coulomb collisions in a plasma." *Multiscale Modeling & Simulation*, **7**(2):865–887, 2008.

[DCC10] A.M. Dimits, B.I. Cohen, and R.E. Caflisch. "Efficient Hybrid Methods for Coulomb Collisions in a Plasma." *Bulletin of the American Physical Society*, **55**, 2010.

[DCC13] A.M. Dimits, B.I. Cohen, R. Caflisch, M.S. Rosin, and L.F. Ricketson. "Higher-order Time Integration of Coulomb Collisions in a Plasma Using Langevin Equations." *Journal of Computational Physics*, 2013.

[DL93] A.M. Dimits and W.W. Lee. "Partially linearized algorithms in gyrokinetic particle simulation." *Journal of Computational Physics*, **107**(2):309–323, 1993.

[DUX09] B.D. Dudson, M.V. Umansky, X.Q. Xu, P.B. Snyder, and H.R. Wilson. "BOUT++: A framework for parallel plasma fluid simulations." *Computer Physics Communications*, **180**(9):1467–1480, 2009.

[DV05] L. Desvillettes and Cédric Villani. "On the trend to global equilibrium for spatially inhomogeneous kinetic systems: the Boltzmann equation." *Inventiones mathematicae*, **159**(2):245–316, 2005.

[FP02] Francis Filbet and Lorenzo Pareschi. "A numerical method for the accurate solution of the Fokker–Planck–Landau equation in the nonhomogeneous case." *Journal of Computational Physics*, **179**(1):1–26, 2002.

[Fre02] Glenn H. Fredrickson. "Dynamics and rheology of inhomogeneous polymeric fluids: A complex Langevin approach." *The Journal of chemical physics*, **117**(14):6810–6820, 2002.

[Fre07] Jeffrey P. Freidberg. *Plasma physics and fusion energy*. Cambridge University Press, 2007.

[Fri05] Alex Friedman. "Implicit multiscale PIC and related topics." In *Workshop on Multiscale Processes in Fusion Plasmas, IPAM, UCLA*, pp. 10–14, 2005.

[FS01] Jing Fan and Ching Shen. "Statistical simulation of low-speed rarefied gas flows." *Journal of Computational Physics*, **167**(2):393–412, 2001.

[FVF13] Ricardo A. Fonseca, Jorge Vieira, Frederico Fiúza, Asher Davidson, Frank S. Tsung, Warren B. Mori, and Luís O. Silva. "Exploiting multi-scale parallelism for large scale numerical modelling of laser wakefield accelerators." *Plasma Physics and Controlled Fusion*, **55**(12):124011, 2013.

[GH13] Irene M. Gamba and Jeffrey R. Haack. "A conservative spectral method for the Boltzmann equation with anisotropic scattering and the grazing collisions limit." *arXiv preprint arXiv:1306.4625*, 2013.

[Gil00] Daniel T. Gillespie. "The chemical Langevin equation." *The Journal of Chemical Physics*, **113**:297, 2000.

[Gil08a] M.B. Giles. "Improved multilevel Monte Carlo convergence using the Milstein scheme." *Monte Carlo and quasi-Monte Carlo methods 2006*, pp. 343–358, 2008.

[Gil08b] M.B. Giles. "Multilevel Monte Carlo path simulation." *Operations Research*, **56**(3):607–617, 2008.

[GL94] J.G. Gaines and T.J. Lyons. "Random generation of stochastic area integrals." *SIAM Journal on Applied Mathematics*, **54**(4):1132–1146, 1994.

[GPS02] H. Goldstein, C. Poole, and J. Safko. "Classical Mechanics.", 2002.

[GS12a] M.B. Giles and L. Szpruch. "Antithetic multilevel Monte Carlo estimation for multi-dimensional SDEs without Lévy area simulation." *arXiv preprint arXiv:1202.6283*, 2012.

[GS12b] Michael B. Giles and Lukasz Szpruch. "Antithetic multilevel Monte Carlo estimation for multidimensional SDEs." *Monte Carlo and Quasi-Monte Carlo Methods 2012 (submitted)*, 2012.

[Har77] C.J. Harris. "Modelling, simulation and control of stochastic systems with applications in wastewater treatment." *International Journal of Systems Science*, **8**(4):393–411, 1977.

[Hes93] Steven L. Heston. "A closed-form solution for options with stochastic volatility with applications to bond and currency options." *Review of financial studies*, **6**(2):327–343, 1993.

[Hew03] Dennis W. Hewett. "Fragmentation, merging, and internal dynamics for PIC simulation with finite size particles." *Journal of Computational Physics*, **189**(2):390–426, 2003.

[HFU88] F. Haghighat, P. Fazio, and T.E. Unny. "A predictive stochastic model for indoor air quality." *Building and Environment*, **23**(3):195–201, 1988.

[HH07] Thomas M.M. Homolle and Nicolas G. Hadjiconstantinou. "A low-variance deviational simulation Monte Carlo for the Boltzmann equation." *Journal of Computational Physics*, **226**(2):2341–2358, 2007.

[HK94] Genze Hu and John A. Krommes. "Generalized weighting scheme for δf particle-simulation method." *Physics of plasmas*, **1**:863, 1994.

[HR88] Teddy Holt and Sethu Raman. "A review and comparative evaluation of multilevel boundary layer parameterizations for first-order and turbulent kinetic energy closure schemes." *Reviews of geophysics*, **26**(4):761–780, 1988.

[HS76] S.P. Hirshman and D.J. Sigmar. "Approximate Fokker–Planck collision operator for transport theory applications." *Physics of Fluids*, **19**:1532, 1976.

[HW04] R.D. Hazeltine and F.L. Waelbroeck. "The Framework of Plasma Physics (Boulder, CO.", 2004.

[IKV11] M.S. Ivanov, A.V. Kashkovsky, P.V. Vashchenkov, Ye A. Bondar, Deborah A. Levin, Ingrid J. Wysong, and Alejandro L. Garcia. "Parallel object-oriented software system for DSMC modeling of high-altitude aerothermodynamic problems." In *AIP Conference Proceedings-American Institute of Physics*, volume 1333, p. 211, 2011.

[JLM96] M.E. Jones, D.S. Lemons, R.J. Mason, V.A. Thomas, and D. Winske. "A grid-based Coulomb collision model for PIC codes." *Journal of Computational Physics*, **123**:169, 1996.

[JNS06] T. Johzaki, H. Nagatomo, H. Sakagami, Y. Sentoku, T. Nakamura, K. Mima, Y. Nakao, and T. Yokota. "Core heating analysis of fast ignition targets by integrated simulations." In *Journal de Physique IV (Proceedings)*, volume 133, pp. 385–389. EDP sciences, 2006.

[JST81] Antony Jameson, Wolfgang Schmidt, Eli Turkel, et al. "Numerical solutions of the Euler equations by finite volume methods using Runge-Kutta time-stepping schemes." *AIAA paper*, **1259**:1981, 1981.

[KCK12] S. Koh, C.S. Chang, S. Ku, J.E. Menard, H. Weitzner, and W. Choe. "Bootstrap current for the edge pedestal plasma in a diverted tokamak geometry." *Physics of Plasmas*, **19**:072505, 2012.

[KHY02] H.C. Kim, M.S. Hur, S.S. Yang, S.W. Shin, and J.K. Lee. "Three-dimensional fluid simulation of a plasma display panel cell." *Journal of applied physics*, **91**(12):9513–9520, 2002.

[Kir46] John G. Kirkwood. "The statistical mechanical theory of transport processes I. General theory." *The Journal of Chemical Physics*, **14**:180, 1946.

[KK09] Arnold Kritz and David Keyes. "Fusion simulation project workshop report." *Journal of fusion energy*, **28**(1):1–59, 2009.

[KP11] Peter E Kloeden and Eckhard Platen. *Numerical solution of stochastic differential equations*, volume 23. Springer, 2011.

[KPA08] Peter R. Kramer, Charles S. Peskin, and Paul J. Atzberger. "On the foundations of the stochastic immersed boundary method." *Computer Methods in Applied Mechanics and Engineering*, **197**(25):2232–2249, 2008.

[KPV04] Andreas J. Kemp, Robert E.W. Pfund, and Jürgen Meyer-ter Vehn. "Modeling ultrafast laser-driven ionization dynamics with monte carlo collisional particle-in-cell simulations." *Physics of Plasmas*, **11**:5648, 2004.

[KPW92] Peter E. Kloeden, Eckhard Platen, and I.W. Wright. "The approximation of multiple stochastic integrals." *Stochastic analysis and applications*, **10**(4):431–441, 1992.

[Kul67] Solomon Kullback. "A lower bound for discrimination information in terms of variation (corresp.)." *Information Theory, IEEE Transactions on*, **13**(1):126–127, 1967.

[KW87] G. Kallianpur and Robert L. Wolpert. "Weak convergence of stochastic neuronal models." In *Stochastic methods in biology*, pp. 116–145. Springer, 1987.

[Lan36] L.D. Landau. "The transport equation in the case of Coulomb interactions." *Phys. Z. Sowjetunion*, **10**(154), 1936.

[Lar03] David J. Larson. "A Coulomb collision model for PIC plasma simulation." *Journal of Computational Physics*, **188**(1):123–138, 2003.

[Lee94] Sean Lee. "The convergence of complex Langevin simulations." *Nuclear Physics B*, **413**(3):827–848, 1994.

[Lev96] C. David Levermore. "Moment closure hierarchies for kinetic theories." *Journal of Statistical Physics*, **83**(5-6):1021–1065, 1996.

[Lev97] C. David Levermore. "Entropy-based moment closures for kinetic equations." *Transport Theory and Statistical Physics*, **26**(4-5):591–606, 1997.

[LWD09] D.S. Lemons, D. Winske, W. Daughton, and B. Albright. "Small-angle Coulomb collision model for particle-in-cell simulations." *Journal of Computational Physics*, **228**:1391, 2009.

[LWW07] Hongwei Liu, Moran Wang, Jinku Wang, Guoyan Zhang, Huailin Liao, Ru Huang, and Xing Zhang. "Monte Carlo simulations of gas flow and heat transfer in vacuum packaged MEMS devices." *Applied thermal engineering*, **27**(2):323–329, 2007.

[McK66] H.P. McKean Jr. "A class of Markov processes associated with nonlinear parabolic equations." *Proceedings of the National Academy of Sciences of the United States of America*, **56**(6):1907, 1966.

[Mez07] Francesco Mezzadri. "How to generate random matrices from the classical compact groups." *Notices Amer. Math. Soc.*, **54**(5):592–604, 2007.

[Mil79] G.N. Mil'shtein. "A method of second-order accuracy integration of stochastic differential equations." *Theory of Probability & Its Applications*, **23**(2):396–401, 1979.

[MLJ97] W.M. Manheimer, M. Lampe, and G. Joyce. "Langevin representation of Coulomb collisions in PIC simulations." *Journal of Computational Physics*, **138**:563, 1997.

[MT04] Grigori N. Milstein and Michael V. Tretyakov. *Stochastic numerics for mathematical physics.* Springer-Verlag, Berlin, 2004.

[Nan97] K. Nanbu. "Theory of cumulative small-angle collisions in plasmas." *Physical Review E*, **55**(4):4642, 1997.

[NHH98] Robert P. Nance, David B. Hash, and H.A. Hassan. "Role of boundary conditions in Monte Carlo simulation of microelectromechanical systems." *Journal of Thermophysics and Heat Transfer*, **12**(3):447–449, 1998.

[Oga92] Shigeyoshi Ogawa. "Monte Carlo simulation of nonlinear diffusion processes." *Japan journal of industrial and applied mathematics*, **9**(1):25–33, 1992.

[PC99] L. Pareschi and R.E. Caflisch. "An Implicit Monte Carlo Method for Rarefied Gas Dynamics: I. The Space Homogeneous Case." *Journal of Computational Physics*, **154**(1):90, 1999.

[PCJ10] G. Park, C.S. Chang, I. Joseph, and R.A. Moyer. "Plasma transport in stochastic magnetic field caused by vacuum resonant magnetic perturbations at diverted tokamak edge." *Physics of Plasmas*, **17**:102503, 2010.

[PG11] A. Pataki and L. Greengard. "Fast elliptic solvers in cylindrical coordinates and the Coulomb collision operator." *Journal of Computational Physics*, **230**(21):7840–7852, 2011.

[PRT00] L. Pareschi, G. Russo, and G. Toscani. "Fast spectral methods for the Fokker–Planck–Landau collision operator." *Journal of Computational Physics*, **165**(1):216–236, 2000.

[RMJ57] M.N. Rosenbluth, W.M. MacDonald, and D.L. Judd. "Fokker-Planck equation for an inverse-square force." *Physical Review*, **107**:1, 1957.

[Roe86] P.L. Roe. "Characteristic-based schemes for the Euler equations." *Annual review of fluid mechanics*, **18**(1):337–365, 1986.

[RRD13] M.S. Rosin, L.F. Ricketson, A.M. Dimits, R.E. Caflisch, and B.I. Cohen. "Multilevel Monte Carlo simulation of Coulomb collisions." *arXiv preprint arXiv:1310.3591*, 2013.

[SB02] Q. Sun and I.D. Boyd. "A direct simulation method for subsonic, microscale gas flows." *Journal of Computational Physics*, **179**:400, 2002.

[SF03] Hongwei Sun and Mohammad Faghri. "Effect of surface roughness on nitrogen flow in a microchannel using the direct simulation Monte Carlo method." *Numerical Heat Transfer: Part A: Applications*, **43**(1):1–8, 2003.

[She08] M. Sherlock. "A Monte-Carlo method for Coulomb collisions in hybrid plasma models." *Journal of Computational Physics*, **227**:2286, 2008.

[Shr04] Steven E. Shreve. *Stochastic Calculus for Finance II, Continuous Time Models*. springer, 2004.

[SMK00] Yasuhiko Sentoku, Kunioki Mima, Shin-ichi Kojima, and Hartmut Ruhl. "Magnetic instability by the relativistic laser pulses in overdense plasmas." *Physics of Plasmas*, **7**:689, 2000.

[TA77] Tomonor Takizuka and Hirotada Abe. "A binary collision model for plasma simulation with a particle code." *Journal of Computational Physics*, **25**(3):205–219, 1977.

[Tru65] B.A. Trubnikov. "Particle interactions in a fully ionized plasma." *Reviews of plasma physics*, **1**:105, 1965.

[TT99] Eleuterio F Toro and Eleuterio F Toro. *Riemann solvers and numerical methods for fluid dynamics*, volume 16. Springer, 1999.

[TTR12] A.G.R. Thomas, M. Tzoufras, A.P.L. Robinson, R.J. Kingham, C.P. Ridgers, M. Sherlock, and A.R. Bell. "A review of Vlasov–Fokker–Planck numerical modeling of inertial confinement fusion plasma." *Journal of Computational Physics*, **231**(3):1051–1079, 2012.

[TTT13] M. Tzoufras, A. Tableman, F.S. Tsung, W.B. Mori, and A.R. Bell. "A multi-dimensional Vlasov-Fokker-Planck code for arbitrarily anisotropic high-energy-density plasmasa)." *Physics of Plasmas (1994-present)*, **20**(5):056303, 2013.

[Van82] Bram Van Leer. "Flux-vector splitting for the Euler equations." In *Eighth international conference on numerical methods in fluid dynamics*, pp. 507–512. Springer, 1982.

[VKB09] J. Van Dijk, G.M.W. Kroesen, and A. Bogaerts. "Plasma modelling and numerical simulation." *Journal of Physics D: Applied Physics*, **42**(19):190301, 2009.

[Vla68] A.A. Vlasov. "The vibrational properties of an electron gas." *Physics-Uspekhi*, **10**(6):721–733, 1968.

[Wik01] Magnus Wiktorsson. "Joint characteristic function and simultaneous simulation of iterated Itô integrals for multiple independent Brownian motions." *Annals of Applied Probability*, pp. 470–487, 2001.

[WL04] Moran Wang and Zhixin Li. "Simulations for gas flows in microgeometries using the direct simulation Monte Carlo method." *International Journal of Heat and Fluid Flow*, **25**(6):975–985, 2004.

[WLC08] Chiaming Wang, Tungyou Lin, Russel Caflisch, Bruce I. Cohen, and Andris M. Dimits. "Particle simulation of Coulomb collisions: Comparing the methods of Takizuka & Abe and Nanbu." *Journal of Computational Physics*, **227**(9):4308–4329, 2008.

[Yvo35] Jacques Yvon. *La théorie statistique des fluides et l'équation d'état*, volume 203. Hermann & cie, 1935.